Directed Evolution Of Antibodies Against Complex Targets

by

Alec A. Desai

A dissertation submitted in partial fulfillment
of the requirements for the degree of
Doctor of Philosophy
(Chemical Engineering)
in the University of Michigan
2021

Doctoral Committee:

Professor Peter M. Tessier, Chair
Associate Professor Nina Lin
Associate Professor Anna Schwendeman
Associate Professor Greg Thurber

Alec A. Desai

aldesai@umich.edu

ORCID iD: 0000-0002-8322-7096

Dedication

This work is dedicated to my family at home and at work.

Acknowledgements

I would like to thank Dr. Tessier, my dissertation committee members, and members of the Tessier lab for their help with the work. I would also like to thank Scholar Space, UoM Library and Rackham OARD for help in preparing this document.

Table of Contents

List of Figures

Abstract

Antibodies are an emerging class of biotherapeutics that are currently used for treating a myriad of diseases, including cancer, autoimmune disorders and viral infections. Their great success in the clinic is attributable to their many attractive properties, including their high affinity, drug-like biophysical properties (high specificity, stability, solubility), long circulation times *in vivo*, and amenability to protein engineering for further maturing their properties. Nevertheless, there are several outstanding challenges in their generation and engineering against complex targets that we have sought to address in this work. First, we have investigated *in vitro* methods for systematically generating antibodies with high conformational and sequence specificity against protein aggregates that form in neurodegenerative disorders such as Alzheimer's and Parkinson's disease. We have developed novel next-generation sequencing and flow cytometry library sorting methods to identify antibodies with high specificity for aggregates associated with Alzheimer's disease (amyloid β and tau fibrils) and Parkinson's disease (α-synuclein fibrils). Our anti-amyloid Aβ antibodies rival those of the FDA-approved drug, Aducanumab, in terms of their affinity (EC_{50} values of ~1-10 nM) and conformational specificity while displaying much lower levels of off-target binding. We also developed a novel flow cytometry-based selection method by capturing amyloid aggregates on nanoparticles. Using this technique, we have successfully isolated conformational antibodies against tau and α-synuclein aggregates. Our tau antibodies display similar levels of affinity (EC_{50} values of ~0.5 nM) and conformational specificity as a leading clinical antibody, Zagotanemab, while displaying much lower levels of off-target binding. Our α-synuclein antibody shows similar affinity (EC_{50} value of ~10-20 nM) and substantially higher

conformational specificity relative to a leading clinical-stage antibody, Cinpanemab. Moreover, we have also developed novel directed evolution methods for generating small antibodies (nanobodies) that potently neutralize SARS-CoV-2. Unexpectedly, we discovered that systematically swapping the binding loops between low affinity lead nanobodies results in unusually large increases in affinity and neutralization activity. We show that intentionally swapping nanobody binding loops during directed evolution is a powerful method for generating high-affinity nanobodies without the need for multiple rounds of affinity maturation. These approaches result in engineered antibodies and nanobodies that rival best-in-class molecules and hold great potential for advancing the field of antibody engineering to generate the next generation of safe and potent antibody drugs.

Chapter 1 **Introduction**

Antibodies belong to an important class of molecules used by an immune system to bind and neutralize foreign particles. They are 'Y' shaped glycoproteins which consists of four covalently linked polypeptide chains (Fig. 1A). They consist of two identical large chains known as 'heavy chains', each composed for 4 polypeptides domains namely: variable domain (V_H), constant domains one (C_H1), two (C_H2) and three (C_H3). They also consist of two identical small chains known as 'light chain', each composed of two polypeptide domains namely: variable light (V_L) and constant light (C_L) (Fig. 1, (1)). A monoclonal antibody is a bivalent molecule and is divided into three regions; it has two identical antigen binding regions (Fab; fragment antigen binding) composed of V_H, C_H1, V_L and C_L and crystallizable fragment (Fc, fragment crystallizable)

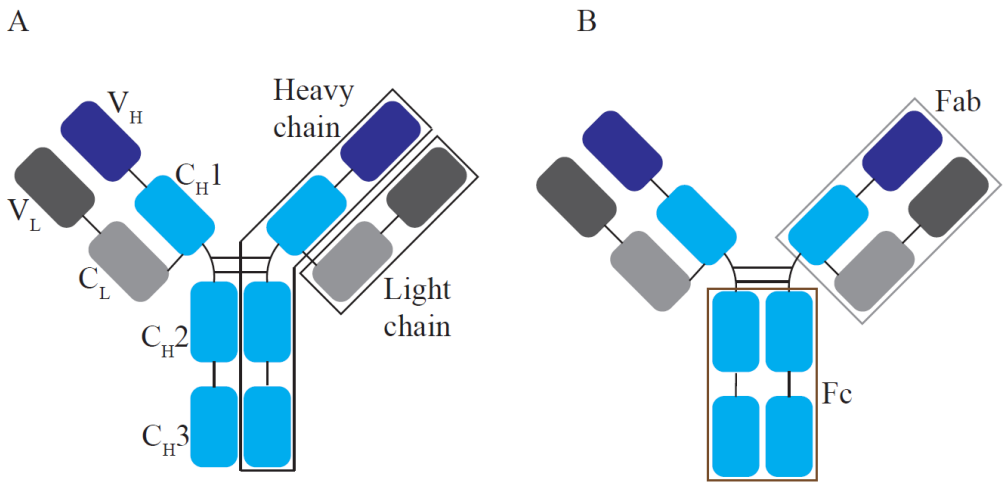

Figure 1-1: Structure of an antibody
(A) Illustration of a monoclonal antibody (IgG1, immunoglobulin 1) showing polypeptide chains (heavy and light chains) and different domains [variable heavy (V_H), constant heavy 1,2,3 (C_H1, C_H2, C_H3,), variable light (V_L) and constant light (C_L)]. (B) Antibody structure is divided into three regions, Fab (fragment antigen binding) and Fc (fragment crystallizable).

consisting of C_H2-C_H3 homo dimer (Fig. 1B, (1)). A full-length monoclonal antibody consists of 12 domains with an average molecular weight of ~150 kDa or ~150 gm/mol.

Although antibodies are natural molecules used by immune systems to fight against foreign particles, they can be re-programmed for several different applications including their use as re-agents for detection, therapeutic and diagnostic applications. They have been used successfully as therapeutics for several diseases like cancers, autoimmunity diseases, inflammatory diseases, infectious diseases like SARS-CoV-2 and drug delivery. Many of the top selling drugs, including the best-selling drug (Humira or Adalimumab), are monoclonal antibodies. Currently, antibodies are the best class of bio-therapeutics with over 100 antibodies approved as drugs and another 20-30 more under review (2).

The grand success of antibodies in clinical trials can be attributed to many of their amazing properties including high affinity and exquisite specificity towards their target antigen (1,3). There are also some properties specific to their structure like effector function, re-formatting them as bi-specific antibodies and antibody drug conjugates which make them very appealing for specific applications. Apart from these, they also have several drug-like properties which make them particular attractive like high stability and solubility, low off-target binding and toxicity, longer circulation times and ease of manufacturing, purification, storage, handling and shipping (1,3).

Antibodies also have the flexibility of reformatting them into smaller fragments (Fig. 2) including nanobodies (Nb, single domain antibodies), single-chain variable fragments (scFv, two domain antibodies) or antigen binding fragments (Fab, four domain antibodies). These are attractive for special applications where larger size is a constraint or binding to cryptic and inaccessible sites or minimizing effector function. Several antibody fragments have also been approved for use as drugs (4,5).

Many of the amazing properties of an antibody or antibody fragment can be attributed to the variable domains: V_H and V_L. Each variable domain consists of three highly flexible and variable polypeptide loops known as complementarity determining regions (CDRs). These loops vary in amino acids chemistry and length giving rise to different binding properties and selectivity for antibodies. Since majority of the antigen binding characteristics of an antibody come from CDRs, the design of CDRs is particularly important and a lot of systematic research has been done for it .(1)

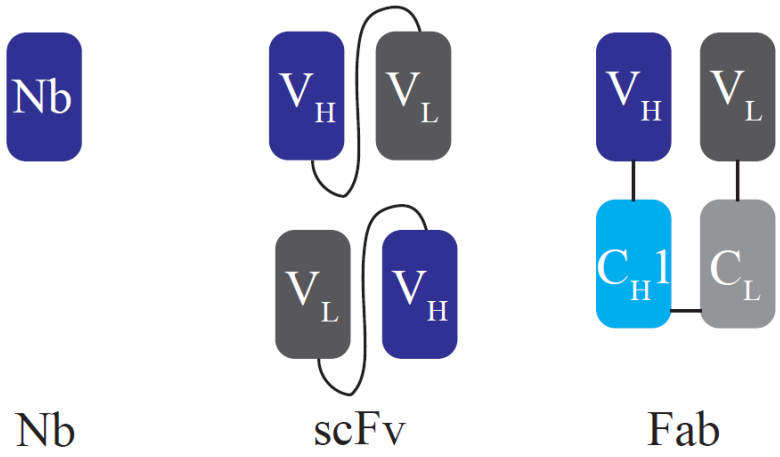

Figure 1-2: Reformatting antibody into antibody fragments.
Antibody can be reformatted into multiple fragments including nanobody (Nb, single domain), single chain variable fragment (scFv, two domains) and antigen binding fragment (Fab, four domains).

In this work, we have mainly focused on designing CDRs for antibody fragments to achieve the desired set of binding properties. We have made antibody libraries, performed high throughput screening, isolation and engineering of antibodies. The design methods include rational design, grafting, error-prone PCR, directed and saturation mutagenesis. Depending on the target antigen and its properties and antibody scaffold some designs might work better compared to other so we have tried multiple strategies and reported the outcomes from the most promising ones.

We have used antibodies to target to proteins involved in multiple devastating neurodegenerative pathologies: tauopathies (6,7) and synucleinopathies (8). In neurodegenerative diseases or pathologies, the neurons lose their structure and functions over time which leads to their death. Diseases belonging to this class have a common mechanism: a healthy protein undergoes conformational change, starts aggregating and becomes toxic to cells. From a therapeutic or diagnostic view, it is very important to design molecules which would selectively bind to toxic fibrillary/aggregated conformers but not the benign monomer. In other words, the molecule of choice should have highest conformational specificity for fibrils over monomeric proteins.

Tauopathies are associated with loss of memory and are characterized by the presence of intercellular tau neurofibrillary tangles (NFTs). Alzheimer's disease is the most common tauopathy which is characterized by the presence of the two protein deposits: intracellular deposits of amyloid beta (Aβ) in addition to intercellular deposits of NFTs (9). Synucleinopathies are associated with loss of movements and Parkinson's disease is the most common synucleinopathy characterized by the presence of α-synuclein fibrils. In this work, we have isolated antibodies with high affinity and high conformational specificity against Aβ, tau and α-synuclein aggregates.

We have also successfully isolated high affinity and high neutralization potency antibodies against SARS-CoV-2 . This coronavirus is the cause of the current pandemic which has affected more than 150 countries with more than 130 million cases and 3 million deaths (10,11).

In this work, we have successfully isolated and engineered antibodies with desired properties against Aβ, tau and α-synuclein amyloid aggregates and SARS-CoV-2 spike protein. Our antibodies rival or are better than best-in-class molecules including clinical and reagent antibodies and approved drugs. Our anti-amyloid Aβ antibodies rival approved drug, Aducanumab

in terms of affinity (~2-12 nM) and conformational specificity but show remarkably lower off-target. We also developed a novel flow cytometry-based selection method by capturing amyloid aggregates on nanoparticles. Using this technique, we have successfully isolated conformational antibodies against tau and α-synuclein aggregates. Our tau antibodies display similar levels of affinity (~0.5 nM) and conformational specificity to clinical antibody Zagotanemab but considerably lower off-target binding. Our α-synuclein antibody show similar affinity (~20 nM) but substantially higher conformational specificity compared to clinical antibody Cinpanemab.

References

1. Tiller, K. E.; Tessier, P. M., Advances in Antibody Design. *Annu Rev Biomed Eng* **2015,** *17*, 191-216.

2. Kaplon, H.; Reichert, J. M., Antibodies to watch in 2021. *MAbs* **2021,** *13* (1), 1860476.

3. Rabia, L. A.; Desai, A. A.; Jhajj, H. S.; Tessier, P. M., Understanding and overcoming trade-offs between antibody affinity, specificity, stability and solubility. *Biochem Eng J* **2018,** *137*, 365-374.

4. Nelson, A. L., Antibody fragments: hope and hype. *MAbs* **2010,** *2* (1), 77-83.

5. Xenaki, K. T.; Oliveira, S.; van Bergen En Henegouwen, P. M. P., Antibody or Antibody Fragments: Implications for Molecular Imaging and Targeted Therapy of Solid Tumors. *Front Immunol* **2017,** *8*, 1287.

6. Murphy, M. P.; LeVine, H., 3rd, Alzheimer's disease and the amyloid-beta peptide. *Journal of Alzheimer's disease : JAD* **2010,** *19* (1), 311-23.

7. Kovacs, G. G., Invited review: Neuropathology of tauopathies: principles and practice. *Neuropathol Appl Neurobiol* **2015,** *41* (1), 3-23.

8. Martí, M. J.; Tolosa, E.; Campdelacreu, J., Clinical overview of the synucleinopathies. *Mov Disord* **2003,** *18 Suppl 6*, S21-7.

9. Long, J. M.; Holtzman, D. M., Alzheimer Disease: An Update on Pathobiology and Treatment Strategies. *Cell* **2019,** *179* (2), 312-339.

10. Haque, S. M.; Ashwaq, O.; Sarief, A.; Mohamed, A. K. A. J., A comprehensive review about SARS-CoV-2. *Future Virology* **2020,** *15* (9), 625-648.

11. Hu, B.; Guo, H.; Zhou, P.; Shi, Z. L., Characteristics of SARS-CoV-2 and COVID-19. *Nat Rev Microbiol* **2021,** *19* (3), 141-154.

Chapter 2 **Rational Affinity Maturation Of Anti-Amyloid Antibodies With High Conformational And Sequence Specificity**

Introduction

Of the many human disorders facing our society today, neurodegenerative diseases such as Alzheimer's and Parkinson's diseases are arguably the most menacing and least treatable (12,13). These diseases – which are linked to the formation of toxic prefibrillar oligomers and amyloid fibrils – are particularly concerning because their frequency of occurrence is linked to age and, thus, the number of cases is expected to increase as life expectancy increases in the coming years due to significant advances in treating other human disorders such as cancer and heart disease.

Conformational antibodies specific for different conformers of amyloid-forming proteins are important for detecting, disrupting and reversing toxic protein aggregation (14,15). Several previous reports have demonstrated creative methods for using immunization (15-23), autoantibody screening (16,24-33), directed evolution (34-37) and rational design methods (38-43) for generating these antibodies. Despite this progress, there are several common problems associated with generating conformational antibodies against amyloid-forming proteins. First, the nature of amyloidogenic antigens is extremely complex and particularly unattractive for typical antibody selection methods due to their insolubility, heterogeneity in terms of size and conformation, hydrophobicity and multivalency. Second, the use of immunization to generate such antibodies is limited due to uncontrolled presentation of aggregated antigens to the immune system and immunodominant epitopes. Third, the use of conventional directed evolution methods such as yeast surface display is limited by the inability to use fluorescence-activated cell sorting due to the lack of soluble antigens.

These and many other challenges typically result in antibodies that recognize protein aggregates with either conformational specificity [e.g., common fibril or oligomer structure (16,17,31)] or sequence specificity (e.g., linear peptide epitopes) but not both. Even in cases where antibodies with strict conformational and sequence specificity have been identified [e.g., (21,27,33,44,45)], these approaches typically require extensive secondary screening to identify such rare variants and are not readily extendable to generate conformational antibodies against

different sites in the same protein or other proteins in a systematic, efficient and predictable manner.

Toward the goal of rational and efficient methods for generating high-quality antibodies with strict conformational and sequence-specificity, we have previously developed directed evolution methods for discovering lead antibodies with high conformational specificity (34). Our approach involves designing single-chain (scFv) antibody libraries with focused mutagenesis in the most important antibody complementarity-determining region (CDR) that typically governs antigen binding (heavy chain CDR3). We sampled combinations of mutations that are most commonly observed in natural antibodies based on tens of thousands of human antibody CDRs (46). From such libraries, we identified an attractive lead antibody (AF1) that recognizes amyloid fibrils of the Aβ42 peptide with high conformational and sequence specificity (34). This antibody displays much weaker affinity for soluble Aβ42 and extremely low levels of non-specific binding even at high antibody concentrations (100 nM). Interestingly, the low level of non-specific binding for AF1 is similar to that of several highly-specific, clinical-stage antibodies (47).

Nevertheless, the affinity of AF1 for Aβ42 fibrils is modest (EC_{50} of ~100 nM) and at least an order of magnitude weaker than other clinical-stage antibodies that target Aβ42 aggregates. Therefore, we sought to affinity mature AF1 against Aβ fibrils to increase affinity while maintaining strict conformational and sequence specificity as well as low levels of non-specific binding.

To accomplish this, there are several challenges that must be addressed. The first and most significant challenge is that most mutations that increase the affinity of such conformational antibodies also increase specific interactions with soluble Aβ (reduced conformational specificity) or non-specific interactions (reduced sequence specificity) or both. A second key challenge is that the multivalent nature of protein aggregates frustrates the selection of affinity-enhancing mutations due to avidity effects. A third challenge is the selection of antibody sites to mutate as well as sets of mutations to sample in order to maximize the likelihood of obtaining matured antibody variants with high specificity and low levels of non-specific interactions. Here we report an integrated approach for affinity maturing conformational antibodies specific for Aβ fibrils and demonstrate that this approach results in antibody variants with favorable combinations of binding properties relative to Aβ clinical-stage antibodies.

Results

Antibody library design and identification of affinity-matured candidates– Our strategy for systematic affinity maturation of a lead Aβ conformational antibody is summarized in Fig. 2-1. The first step in this process is to design an antibody library that preserves the antigen recognition activity of the lead antibody (AF1) while identifying sites in the CDRs for affinity maturation. Given that AF1 was generated by directed mutagenesis in heavy chain CDR3, we sought to identify sites in the other five CDRs for further mutagenesis. However, there are a large number of potential CDR sites to mutate (54 positions in the five CDRs) and a daunting number of theoretically possible antibody variants ($>10^{70}$ variants).

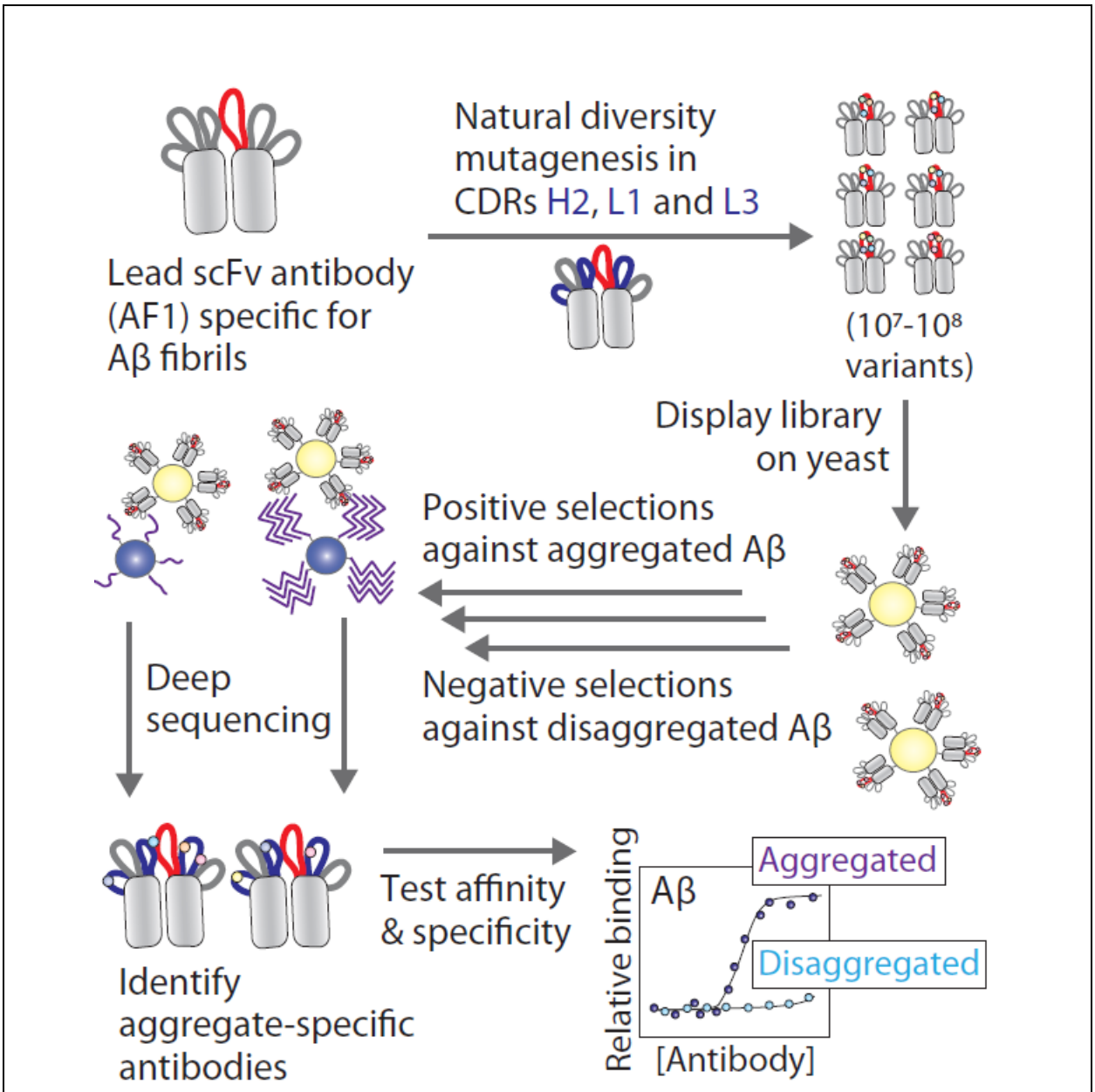

Figure 2-1: Proposed method for systematically maturing the affinity and specificity of Aβ amyloid antibodies.
A lead single-chain antibody fragment (scFv) specific for Aβ fibrils was mutated by targeting solvent-exposed and naturally diverse sites in three complementarity-determining regions (CDRs), including heavy chain CDR2 (H2) and light chain CDRs 1 (L1) and 3 (L3). The library was displayed on yeast and sorted negatively against disaggregated Aβ and positively against aggregated Aβ using magnetic-activated cell sorting. The enriched libraries were subjected to deep sequencing, and clones with mutations predicted to be favorable were evaluated in terms of their affinities and conformational specificities.

To limit the library design to a size that can be evaluated using standard display methods such as yeast surface display (~10^7-10^9 variants), we sought to identify the most attractive subset of CDR sites and subset of residues per site that met a number of design criteria. First, we reasoned that the most naturally diverse sites in human antibodies are the most attractive for mutagenesis

because they are most likely to be solvent exposed and positioned for productive engagement of the antigen while being least likely to adversely impact protein stability (46). We only considered CDR sites in which the most common residue on average in human antibodies, as judged by the AbYsis database of tens of thousands of human antibodies (48), was present at a frequency of <50%.

Next, we prioritized the remaining CDR sites for mutagenesis with the goal of sampling combinations of four to six residues per site that included the wild-type residue and combinations of residues expected to lead to high antibody specificity in addition to high affinity. The lead AF1 clone possessed five Asp and five Tyr residues in heavy chain CDR3, and we previously found that removal of either type of residue from this CDR reduced specificity and increased non-specific binding (49). Therefore, we identified sites in the other CDRs that were compatible with encoding the wild-type residue and at least one of these residues (Asp or Tyr) as well as other residues that are most common in human antibodies using degenerate codons (50). Third, we eliminated degenerate codons that included positively-charged residues (Arg, Lys and His) because we and others have shown that excessive positive charge in the antigen-binding site is linked to increased risk for non-specific interactions (51-57). We also eliminated degenerate codons that encoded stop codons and minimized the number of Cys-encoding codons while not completely eliminating them. The reason for not completely excluding Cys from the library design is because it is encoded by degenerate codons that include combinations of common CDR residues in human antibodies such as Gly, Tyr and Asp. Fourth, we selected degenerate codons that maximized the sum of the average frequencies of each residue in human antibodies to maximize coverage of the natural amino acid diversity of human antibodies.

Our library design is shown in Fig. 2-2. We identified eleven sites for mutagenesis in three CDRs, namely five sites in heavy chain CDR2, four sites in light chain CDR 1, and two sites in light chain CDR3. At each site, the wild-type residue is boxed in red and the three to five mutations included in our designs are highlighted as bolded black font (Fig. 2A). At each site, the residues are listed in order of most common on average in human antibodies (top) to least common (bottom). For example, at position 52 in heavy chain CDR2, we sampled the wild-type residue (Tyr) along with five other residues that included Asp, two residues common in human antibodies at this position (Ser and Asn), and two residues that are less common but required because of the

constraints of degenerate codons. Using a similar strategy at the other ten CDR sites (Fig. 2-2B), the resulting designed library contained $1.1x10^8$ theoretical variants.

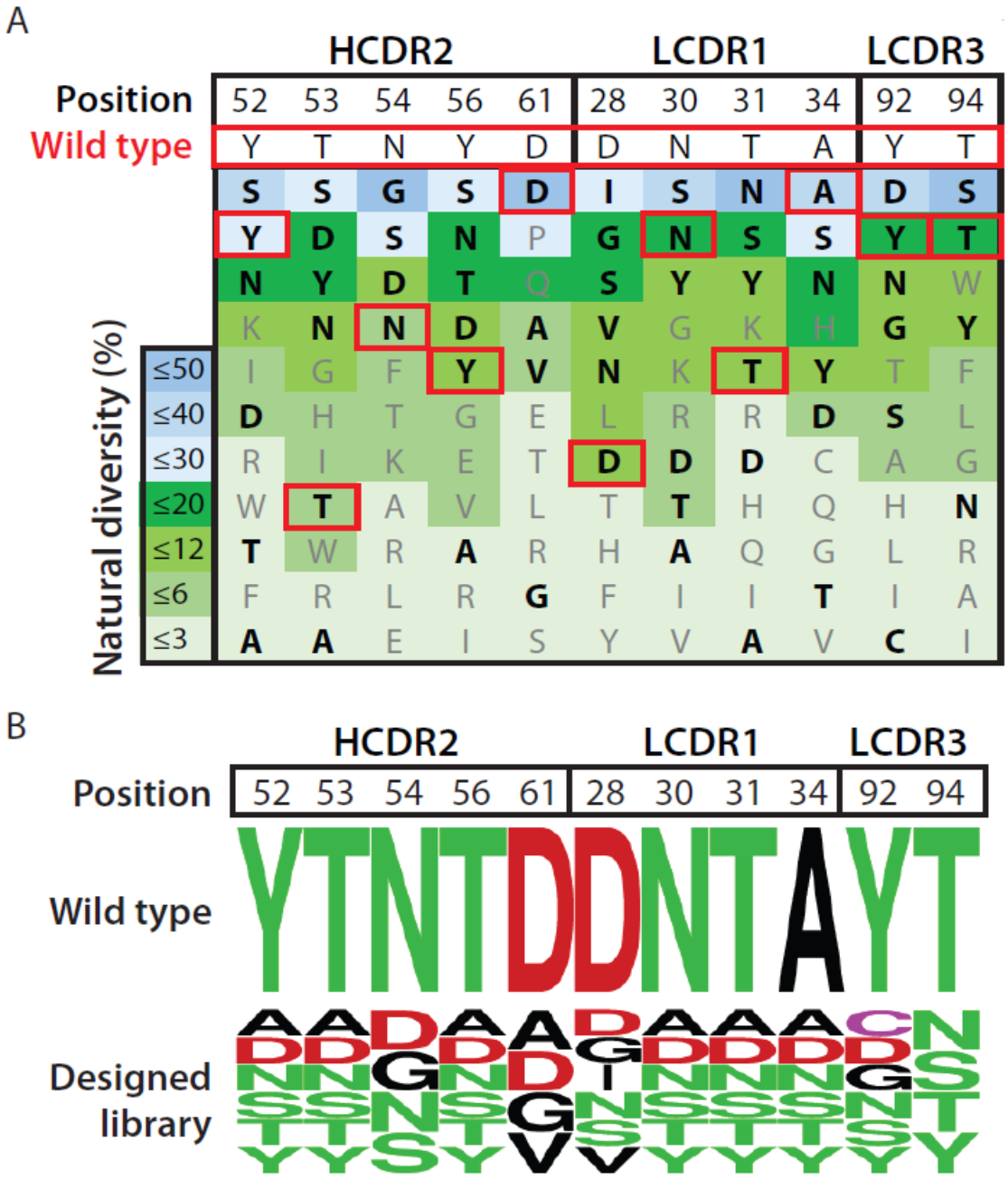

Figure 2-2: Design of AF1 antibody sub-library for affinity maturation that targets naturally diverse and solvent-exposed CDR sites with mutations that are common in human antibodies**.**

(A) Sites in heavy (H2) and light (L1 and L3) chain CDRs were identified based on their solvent exposure, diversity in human antibodies, and compatibility with sets of mutations most commonly observed in human antibodies. The wild-type residues at each site (boxed in red) were included in the library, and the average frequency (%) of each residue observed at each site in human antibodies is color coded. Some of the most common residues in human antibodies were not sampled because they are incompatible with degenerate codons encoding the wild-type residue and other favorable residues. Residues in black and bold text were sampled at each site. (B) Summary of the designed antibody library at eleven CDR sites that includes the wild-type residue and three to five mutations that aim to sample combinations of residues most commonly observed in human antibodies. The color codes are green for polar residues, red for negatively-charged residues, black for hydrophobic residues and purple for cysteine residues.

Next, we generated the antibody library, displayed it on the surface of yeast as C-terminal Aga2 fusion proteins, and sorted the library against Aβ42 fibrils immobilized on magnetic beads (Fig. 2-3). To maximize antibody specificity, we performed three negative selections per round of sorting to remove non-specific antibodies before performing positive selections against Aβ fibrils. In rounds 1 and 2, we performed negative selections against disaggregated (immobilized) Aβ to maximize conformational specificity. In rounds 3-5, we performed negative selections against islet amyloid polypeptide (IAPP) fibrils to maximize sequence specificity. After five rounds of sorting, we observed strong enrichment in terms of the percentage of yeast cells that bound to fibrillar Aβ relative to control selections performed against disaggregated Aβ (Fig. 2-3A). The ratio of the number of yeast cells retained against fibrillar Aβ relative to that for disaggregated Aβ was >100 after five rounds of selection (Fig. 2-3B).

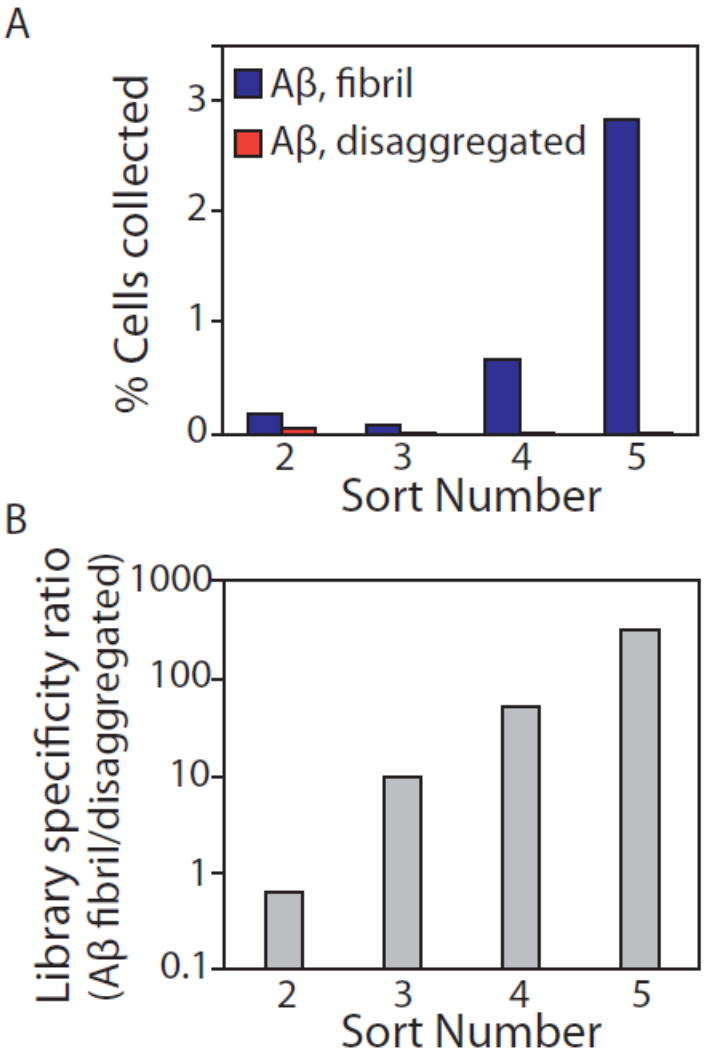

Figure 2-3: Summary of the results for sorting the yeast-displayed antibody library against Aβ fibrils.
(A) The library was subjected to five rounds of selection against Aβ fibrils, and the percentage of retained cells was evaluated for both fibrillar and disaggregated Aβ. (B) The ratio of antibody-displaying yeast cells bound to fibrillar Aβ relative to disaggregated Aβ in each round of selection. In (A) and (B), 10^7 antibody-displaying yeast cells were used in rounds 2-5 of selection relative to 10^9 yeast cells in round 1.

These promising sorting results led us to sequence the sorted antibody libraries before and after rounds 4 and 5 of selection to better understand mutations most strongly correlated with improved antibody binding (Fig. 2-4). We identified 7464 unique antibodies using deep sequencing and evaluated correlations between individual mutations or sets of mutations and enrichment ratios for antibody variants with such mutations. Therefore, we evaluated the Spearman correlation coefficients for all possible single and multiple sets of mutations by comparing the enrichment ratios for all antibody variants with either wild-type or mutant residues at these sites regardless of

the residues at the other sites. While significant sets of mutations were identified when considering as few as one mutation and as many as nine mutations (the maximum we evaluated), we found that sets of five and six mutations led to the best combination of relatively large numbers of mutant (>10) and wild-type (>10) antibodies per set of mutations, high Spearman correlation values ($\rho>0.5$) and high statistical significance (p-value<0.001). Moreover, we found that Spearman correlation coefficients were well correlated between rounds 4 and 5 of sorting, which demonstrates that the deep sequencing results are consistent between multiple rounds of sorting.

For example, we evaluated a set of six mutations (T53A and Y56N in HCDR2, D28N, N30A and T31Y in LCDR1, and T94Y in LCDR3) by identifying all antibody variants that had these mutations (16 variants) or wild-type residues (16 variants) at these positions regardless of their residues at the other five mutated sites (Fig. 2-4A). We found that this set of mutations resulted in large, positive and highly significant Spearman correlation coefficients in both rounds 4 ($\rho=0.83$ and p-value of $8\text{x}10^{-8}$) and 5 ($\rho=0.85$ and p-value of $2\text{x}10^{-9}$). We expected that antibody variants with these mutations would display improved antibody affinity.

A

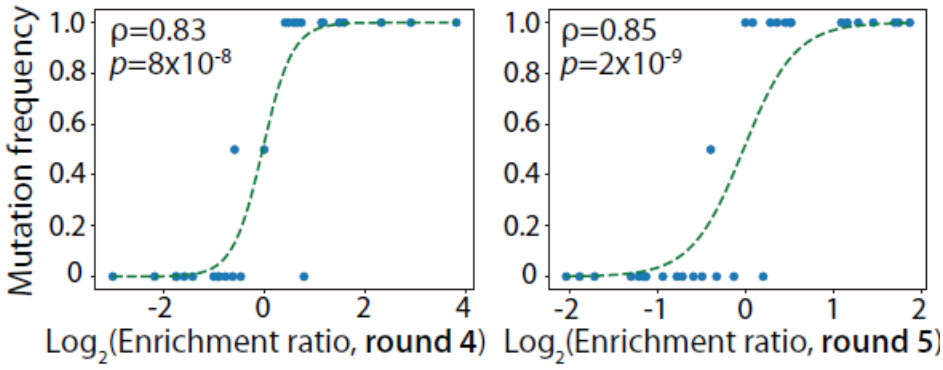

B

	HCDR2					LCDR1				LCDR3		Spearman's correlation			
Antibody	52	53	54	56	61	28	30	31	34	92	94	Round 4		Round 5	
WT	Y	T	N	Y	D	D	N	T	A	Y	T	ρ	p-value	ρ	p-value
99		A		N		N	A	Y			Y	0.83	8E-08	0.85	2E-09
97			S	A		N	A	Y			Y	0.84	2E-11	0.73	3E-08
100			S		A	N	A	Y	S			0.81	2E-18	0.75	1E-15
95			S		A		Y	S	T		S	0.81	7E-08	0.75	9E-08
102			S		A	N	A	S			Y	0.80	3E-08	0.74	2E-07
89		N		A	G	N		S			Y	0.82	3E-06	0.67	9E-05
98					A	N	A	Y	S		Y	0.77	4E-13	0.72	6E-11
96		Y				N	A	A	S		Y	0.80	1E-10	0.66	2E-06
92			S		A	N	Y	S			Y	0.76	4E-07	0.69	7E-06
93		S			G	N		N	T		Y	0.72	5E-05	0.72	2E-05
101			S		G	N		S	T		Y	0.77	2E-07	0.67	2E-06
91		A				N	Y	S		S	Y	0.72	2E-06	0.66	4E-05
88			S		G	N	Y		T		Y	0.70	2E-05	0.64	2E-05
94			S		A	N	A		S		S	0.66	2E-08	0.59	7E-08
90			S			N	Y	S		S	Y	0.71	2E-09	0.52	6E-05

Figure 2-4: Identification of sets of affinity-enhancing mutations using deep sequencing.
Antibody libraries were sequenced before and after sorts 4 and 5 against Aβ fibrils, and sets of six mutations were identified that were strongly correlated with increased enrichment relative to wild-type. (A) Correlation between the frequency of clones with a particular set of six mutations (T53A and Y56N in HCDR2, D28N, N30A and T31Y in LCDR1, and T94Y in LCDR3) and enrichment ratios for clones observed with the corresponding mutations. (B) Antibody variants with sets of six mutations that display strong correlation with improved enrichment for recognizing Aβ fibrils relative to wild-type (AF1). In (A), the lines (logistic regression curves) are guides to the eye. In (A) and (B), the Spearman correlation coefficients were evaluated using antibody variants with wild-type or mutant residues at the specified positions regardless of their residues at the other five mutated positions. There are two to four additional mutations not shown for each antibody variant because they are not one of the six mutations most correlated with improved enrichment ratios. Enrichment ratios were calculated as the ratios of the frequencies of each variant observed in the sequencing results for the fibril selections (output) divided by the corresponding values for the input frequencies. The color codes for the amino acids are described in Fig. 2.

Several other sets of six mutations were observed that also displayed favorable Spearman correlations, and we selected antibody variants with these mutations for further analysis (Fig. 2-4B). We also identified sets of five mutations with favorable Spearman correlation coefficients that correspond to these same antibody variants. The antibodies in Figs. 2-4B had a total of eight

to ten mutations, including the sets of five and six mutations most correlated with improved enrichment ratios, which is why the same antibodies appear in both figures.

Selected antibody variants display increased affinity and high conformational specificity– We next generated the selected antibodies as Fc-fusion proteins and evaluated their affinities and conformational specificities. To critically evaluate our antibodies, we directly compared them to two clinical-stage antibodies specific for Aβ, namely aducanumab and crenezumab. Aducanumab recognizes an N-terminal Aβ epitope (residues 3-7), and selectively recognizes Aβ fibrils and oligomers relative to disaggregated Aβ (26,58). In contrast, crenezumab recognizes a central Aβ epitope (residues 13-24) and binds to both aggregated and disaggregated Aβ (26,58). We grafted the variable domains of each clinical-stage antibody onto an IgG1 scaffold with a human Fc fragment, which resulted in differences in both antibody sequences outside of the variable regions, including in the C_H1, hinge and Fc regions, between the antibodies tested in this study and the actual clinical-stage antibodies (e.g., crenezumab is an IgG4 antibody). Herein we refer to these antibodies as their common names despite these differences. The selected antibody clones and clinical-stage antibodies both expressed well (purification yield of >30 mg/L) and were isolated with high purity.

Given the primary goal of our work to affinity mature our lead Aβ antibody (AF1), we evaluated the apparent affinity of the selected antibody variants relative to AF1 and the clinical-stage antibody controls (Fig. 2-5A and 2-5B). As expected, we observe modest affinity for AF1 binding to Aβ fibrils (EC_{50} of 99±2 nM). Notably, we observed significant (order of magnitude) increases in affinity for all of the selected antibody variants, and the EC_{50} values (4-13 nM) were similar to crenezumab (9±1 nM) and modestly higher than aducanumab (3±0.2 nM).

Nevertheless, we have observed that it is relatively common to lose antibody conformational specificity during *in vitro* affinity maturation. Therefore, we next evaluated if the affinity-matured antibodies retained conformational specificity (Fig. 2-5C and 2-5D). To evaluate this, we pre-incubated the antibodies (30 nM) with various concentrations of disaggregated Aβ and then evaluated their fibril-binding activity. As expected, crenezumab displayed low conformational specificity and its binding to Aβ fibrils was inhibited due to competition with disaggregated Aβ. Conversely, aducanumab binding to fibrils was weakly inhibited by disaggregated Aβ, which is consistent with its high conformational specificity (25). Notably, the binding of our affinity-

matured clones to Aβ fibrils was also weakly inhibited by disaggregated Aβ (82-99% bound antibody at 1000 nM disaggregated Aβ) and behaved similar to the parental antibody (AF1).

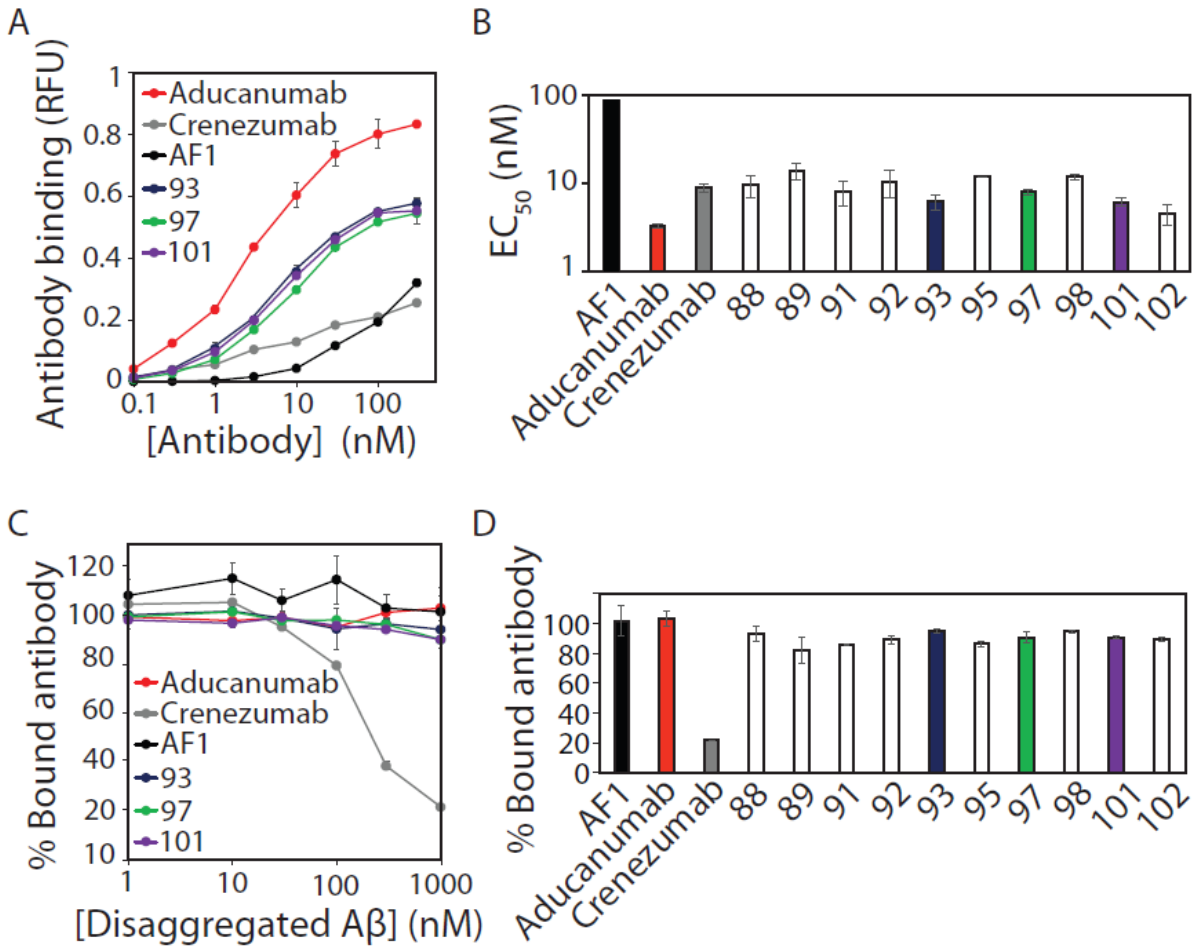

Figure 2-5: Identified antibody variants display increased affinity and high conformational specificity for Aβ fibrils.
(A) Concentration-dependent binding of selected antibody variants to immobilized Aβ fibrils. (B) Apparent affinity (EC_{50}) of selected antibody variants for Aβ fibrils. (C) Binding analysis of antibodies (30 nM) pre-incubated with different concentrations of disaggregated Aβ prior to binding to immobilized Aβ fibrils. (D) Percentage of bound antibody to Aβ fibrils for antibodies (30 nM) pre-incubated with disaggregated Aβ (1000 nM). In (A-D), clinical-stage Aβ antibodies (aducanumab and crenezumab) were used for comparison, the results are average values, and the error bars are standard deviations (two independent repeats).

These encouraging results led us to evaluate conformational specificity of the selected antibodies using immunodot blots (Fig. 2-6). The parental antibody (AF1) displayed weak reactivity at 10 nM and required long exposure times (45 min) to detect signals for Aβ fibrils. Conversely, the clinical-stage antibody controls and the affinity-matured variants at the same concentration developed signals rapidly, as evidenced by their results after a short-time (30 s) exposure (Fig. 2-6). Aducanumab and the selected affinity-matured variants (clones 93, 97 and 101) displayed relatively high conformational specificity. Moreover, crenezumab displayed little

conformational specificity, as expected based on our results in Fig. 2-5. Longer exposures (45 min) for the clinical-stage and affinity-matured variants reveal additional binding to both fibrillar and disaggregated Aβ. The nonlinear nature of the signals generated via immunoblots, especially at long exposure times, are difficult to interpret and caution should be exercised when evaluating them.

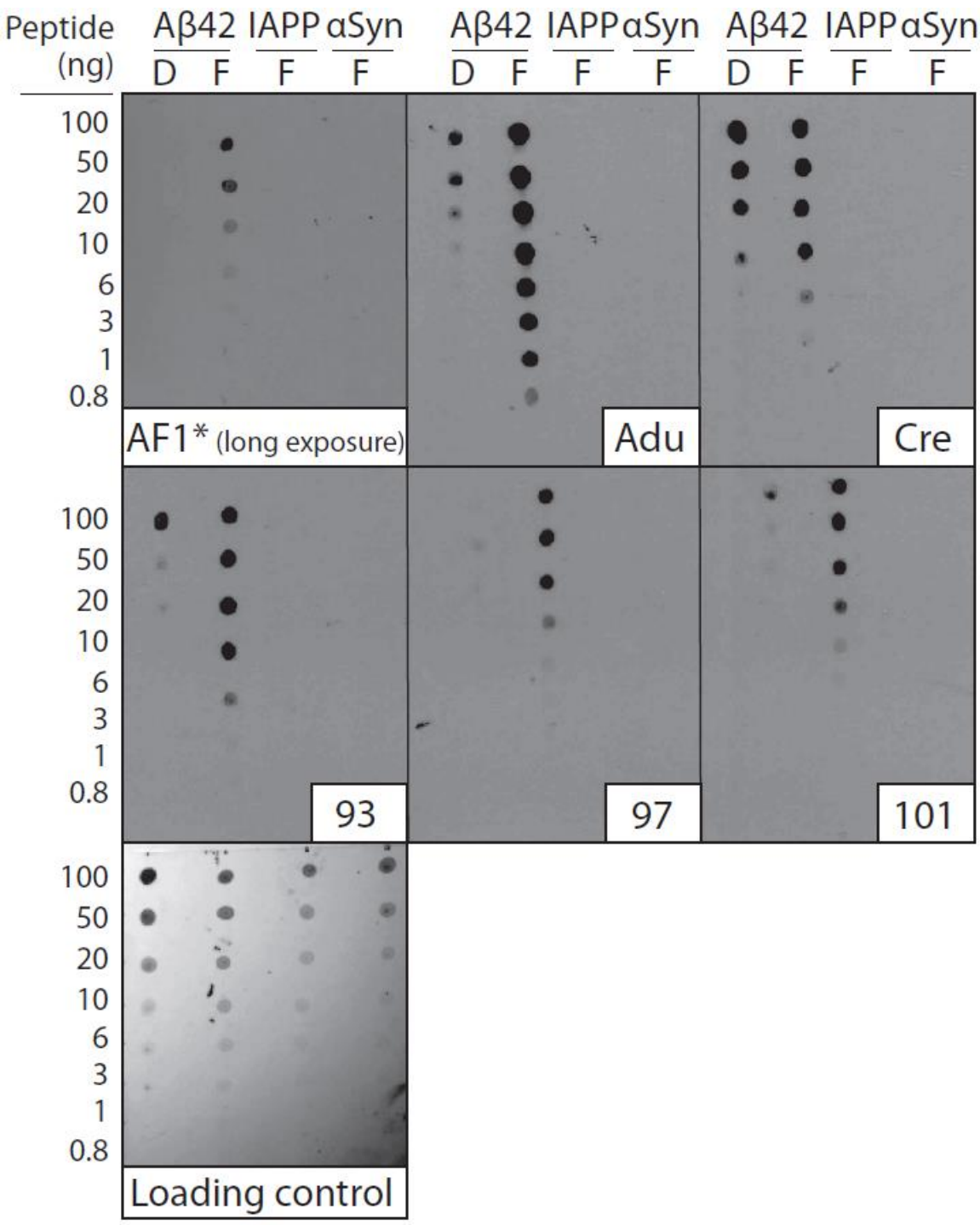

Figure 2-6: Immunoblot analysis of the conformational and sequence specificity of the affinity-matured Aβ antibodies.
Fibrillar (F) Aβ, islet amyloid polypeptide (IAPP), α-synuclein (αSyn) and disaggregated (D) Aβ were immobilized on nitrocellulose membranes and probed with Aβ antibodies (10 nM in PBST with 1% milk), including aducanumab (Adu) and crenezumab (Cre). The blots were imaged after relatively short exposure times (30 s) except for AF1 (45 min exposure). A loading control blot was detected using colloidal silver stain. The experiments were repeated three times and a representative example is shown.

Next, we evaluated the epitope recognized by our affinity-matured antibodies relative to aducanumab and crenezumab (Fig. 2-7). Aβ fibrils that corresponded to full-length Aβ42 or N-terminal truncations were deposited on nitrocellulose blots and probed with various antibodies. AF1 and the affinity-matured clones strongly recognized Aβ1-42 fibrils and weakly recognized fibrils without the first (Aβ2-42) and second (Aβ3-42) residues. Aducanumab also recognized similar Aβ fibril variants, albeit more strongly, and very weakly recognized Aβ4-42 fibrils. This finding is consistent with the N-terminal epitope of aducanumab reported previously (25,59). Conversely, crenezumab recognized fibrils of all of the peptide variants (including Aβ4-42, Aβ5-42 and Aβ11-42) given that its epitope is reported to be Aβ residues 13-24 (59). These findings demonstrate that the affinity-matured antibodies recognize a conformational epitope involving Aβ N-terminus that is similar to the epitope recognized by aducanumab.

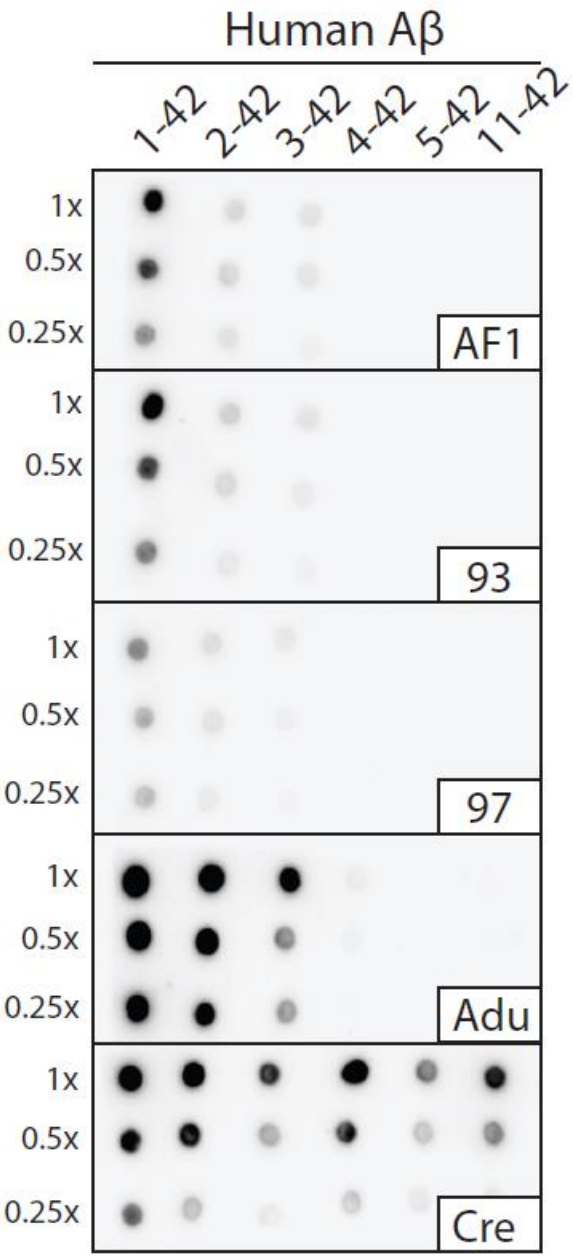

Figure 2-7: Conformational epitope analysis of Aβ antibodies.
Aβ fibrils formed with different Aβ peptides, including several N-terminal truncations, were immobilized on nitrocellulose membranes and probed with different Aβ antibodies. Antibody binding was performed overnight at 10 nM in PBST with 1% milk (4 ˚C). Aducanumab (Adu) and crenezumab (Cre) were included as controls. The image was captured after a 3 min exposure. The experiments were performed three times and a representative image is shown.

We next evaluated if the affinity-matured antibodies recognize aggregated Aβ formed *in vivo* (Fig. 2-8, 2-9). Therefore, we first evaluated the antibodies using immunodot blots of brain homogenates obtained from transgenic mice that overexpress humanized mutant amyloid

precursor protein and presenilin 1 (5xFAD) relative to control (wild-type) mice (Fig. 2-8). The parental antibody (AF1) displayed weak immunoreactivity with the 5xFAD samples, while the selected clones (93, 97 and 101) displayed strong and specific detection of 5xFAD samples from four mouse brains relative to those from four control mouse brains. Interestingly, aducanumab detected the 5xFAD samples and also weakly reacted with the wild-type samples, while crenezumab failed to detect either type of sample. At longer exposures, aducanumab and crenezumab displayed high background while the affinity-matured antibodies displayed strong and specific recognition of 5xFAD samples. Moreover, we confirmed these findings for two affinity-matured antibodies (clones 93 and 97) using western blotting, and detected strong and specific signals for the 5xFAD samples for the PBS insoluble (Fig. 2-9) and PBS soluble fractions. For the latter samples, we did not observe antibody binding to low molecular weight Aβ species for either the affinity-matured antibody (clone 97) or a sequence-specific antibody (NAB 228) that detects both low and high molecular weight Aβ species (34). Finally, we also found that the affinity-matured antibodies recognized Aβ conformers in the human brain-tissue lysates of Alzheimer's patients via immunodot blotting.

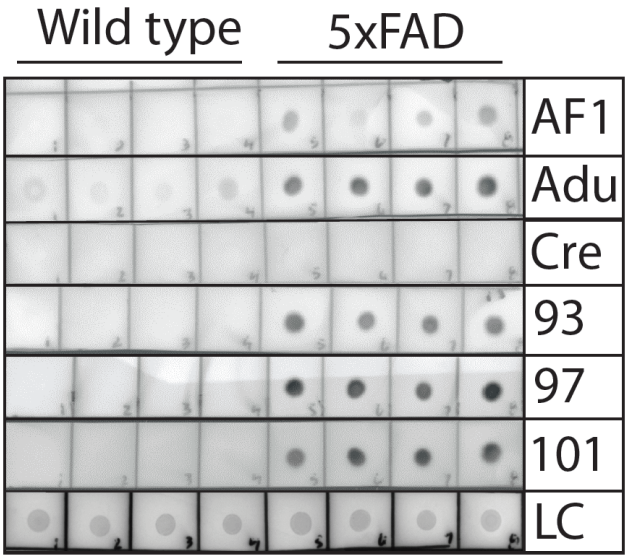

Figure 2-8: Immunoblot analysis of transgenic (5xFAD) and wild-type mouse brain samples using Aβ antibodies.
Brain samples (insoluble fraction) obtained from 5xFAD (22-24 months old) and wild-type mice were immobilized on nitrocellulose membranes and probed with Aβ antibodies (50 nM in TBST with 1% milk), including aducanumab (Adu) and crenezumab (Cre). The blots were imaged after a relatively short exposure (15 s). Ponceau S staining was used as a loading control (LC). The experiments were repeated three times and a representative example is shown.

We also evaluated the ability of the affinity-matured antibodies to stain Aβ aggregates in tissue sections of transgenic (5xFAD) mouse brains relative to wild-type mouse brains (Fig. 2-10). Clone 97 selectively recognized plaques in the frontal cortex of 5xFAD mouse brains, while a sequence-specific Aβ antibody (NAB 228) recognized more diffuse material that surrounded the plaque cores, as observed by the lack of significant overlap of immunostaining for the two antibodies (Fig. 2-10A). Aducanumab displayed similar staining of Aβ plaques and also displayed little overlap in staining with the sequence-specific antibody (Fig. 2-10B). Notably, aducanumab displayed higher levels of non-specific binding to wild-type tissue than clone 97. We observed similar patterns of immunostaining for hippocampus (CA1) tissue samples using clone 97 (Fig. 2-10C) and aducanumab (Fig. 2-10D). Overall, these results demonstrate that our affinity-matured antibodies recognize Aβ aggregates formed *in vitro* and *in vivo* with high affinity and conformational specificity, and compare favorably to clinical-stage Aβ antibodies.

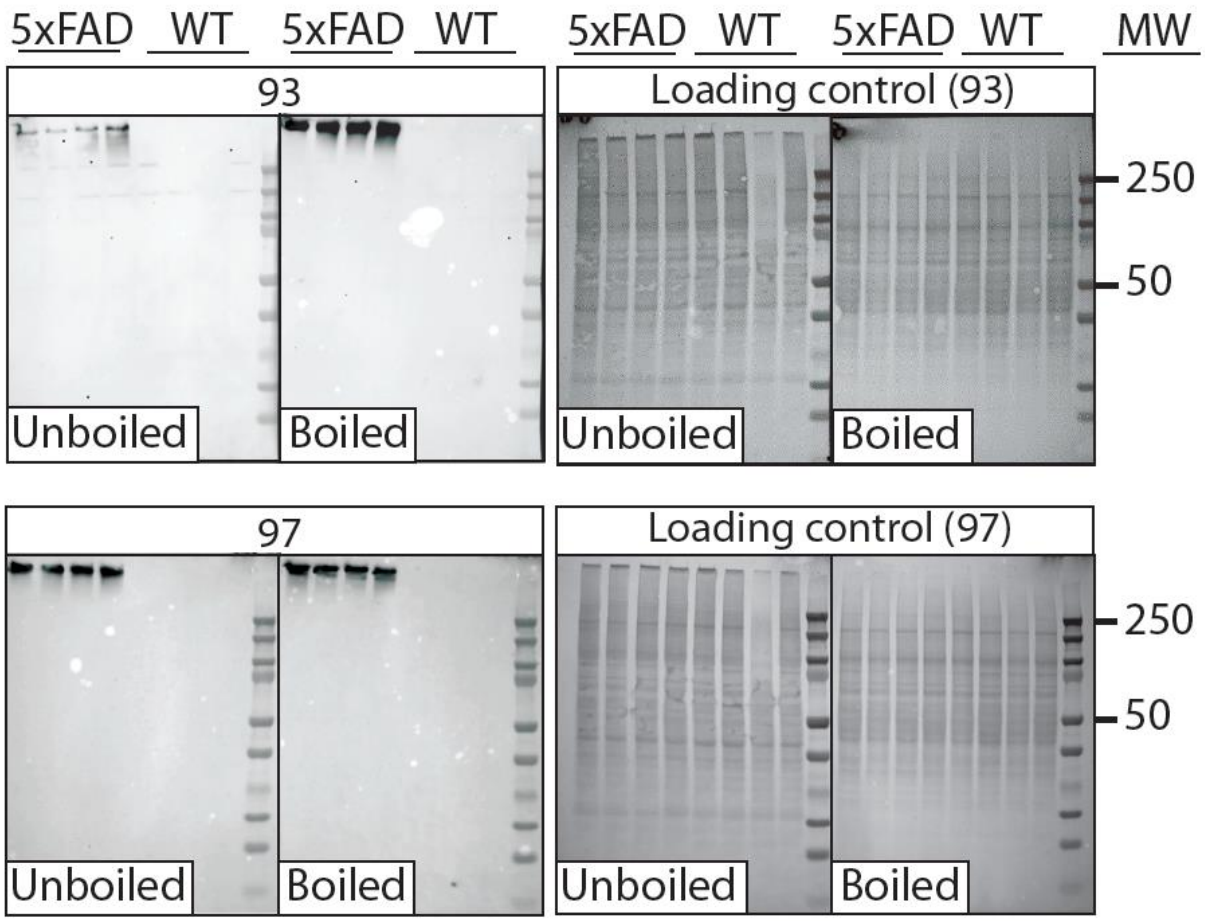

Figure 2-9: Western blot analysis of 5xFAD and wild-type mouse brain samples using affinity-matured Aβ antibodies. Brain samples (PBS insoluble fraction) isolated from 5xFAD (22-24 months old) and wild-type (WT) mice were processed (with or without boiling) via SDS-PAGE, transferred to nitrocellulose membranes, and probed with a subset of Aβ antibodies (100 nM in TBST with 1% milk). The blots were imaged after 6 min of exposure. Ponceau S staining was used as loading control. The experiments were repeated three times and a representative example is shown.

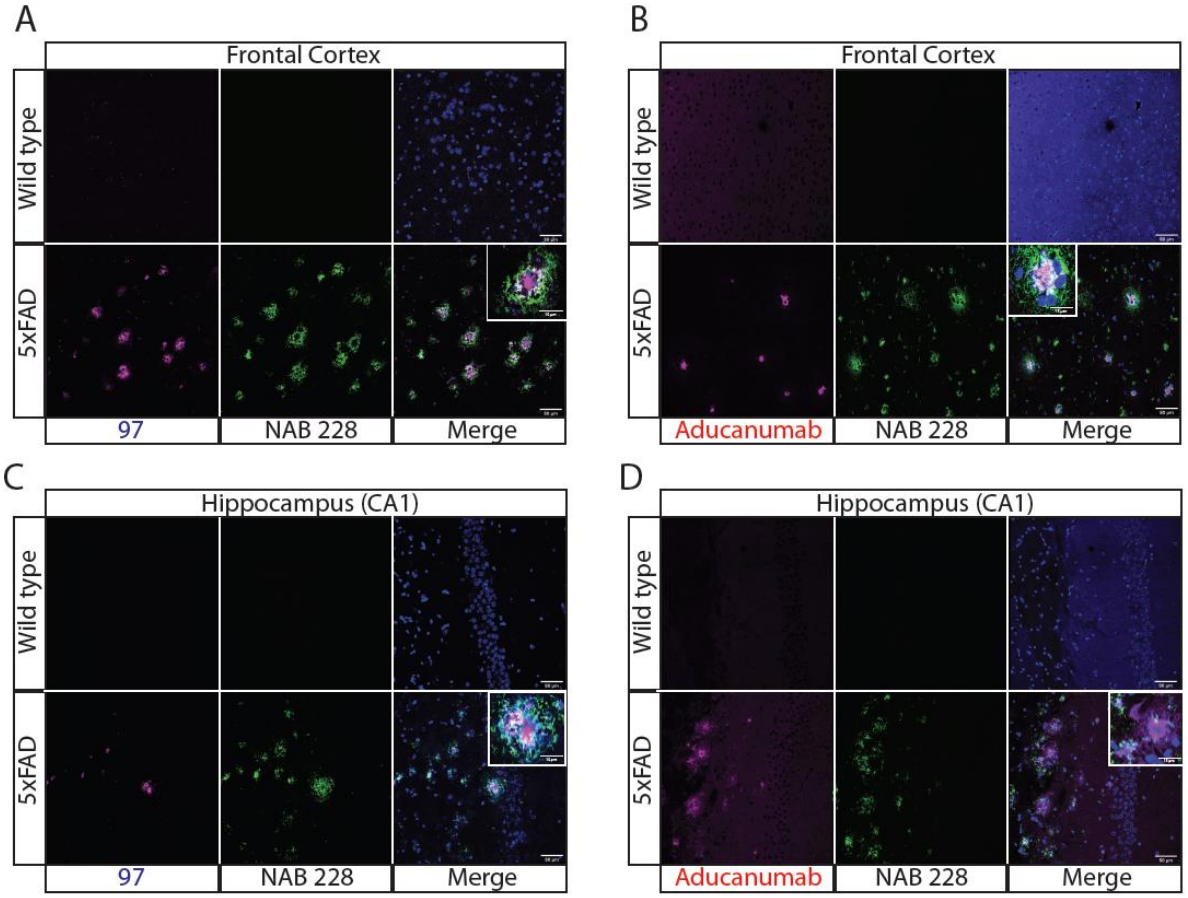

Figure 2-10: Immunofluorescence staining of 5xFAD and wild-type mouse brain sections using Aβ antibodies.
(A-D) Mouse brain sections from the (A, B) frontal cortex and (C, D) hippocampus (CA1) were stained using conformational antibodies [clone 97 in (A) and (C) and aducanumab in (B) and (D)] at 200 nM, a sequence-specific Aβ antibody (NAB 228; recognizes Aβ 1-11) at 1:200x dilution, and DAPI. The 5xFAD mice were 8 months old. Slides were imaged using Leica SP5 confocal microscope. The scale bars are 50 µm for the main images and 15 µm for the inset images.

Affinity-maturated antibodies display favorable biophysical and specificity properties– One of the most common limitations of using *in vitro* antibody discovery and engineering methods is the generation of antibodies with suboptimal biophysical properties – such as low stabilities, solubilities and specificities – relative to antibodies generated by the immune system (47,60-62). Therefore, we next sought to evaluate the biophysical properties of our affinity-matured antibodies to determine if they maintained favorable specificities and stabilities (Fig. 2-11). First, we evaluated non-specific binding for our antibodies using a previously reported polyspecificity reagent (PSR) that is composed of soluble membrane proteins isolated from CHO cells (Fig. 2-11A) (47,63). Antibody binding to this reagent is a strong indicator of the level of antibody specificity and the likelihood of abnormal pharmacokinetics (64). Encouragingly, our affinity-

matured antibodies displayed extremely low levels of non-specific interactions that were similar to their parental antibody (AF1) and a control clinical-stage antibody with high specificity (elotuzumab) (47). Moreover, the matured antibodies were even more specific than crenezumab, which also displayed relatively low levels of non-specific binding. Interestingly, aducanumab displayed much higher levels of non-specific binding that were similar to the control clinical-stage antibodies with high levels of non-specific binding (emibetuzumab and duligotuzumab) (47). Although these results were performed using the affinity-matured antibodies after only one-step purification (Protein A) and the control clinical-stage antibodies after two-step purification (Protein A and size-exclusion chromatography), we obtained similar non-specific binding measurements for the former antibodies after two-step purification.

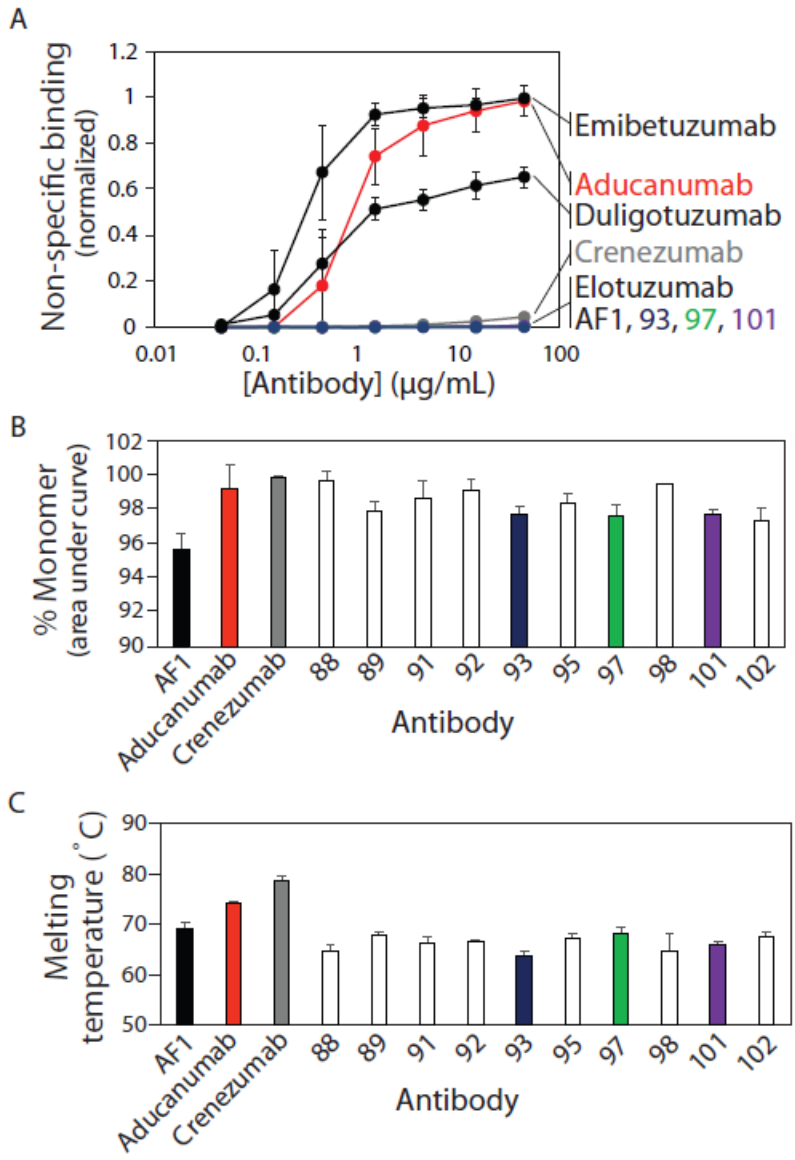

Figure 2-11: Biophysical characterization of Aβ antibodies.
(A) Antibody non-specific binding to soluble membrane proteins. The soluble membrane proteins were biotinylated and their binding to immobilized antibodies was evaluated via flow cytometry. (B) Percentage of monomeric antibody evaluated via size-exclusion chromatography. (C) Antibody melting temperature (midpoint of unfolding) evaluated using dynamic scanning fluorimetry. In (A-C), the values are averages and the error bars are standard deviations (three independent repeats).

We also evaluated the physical stabilities of our antibodies (Fig. 2-11B and 2-11C). Antibodies with poor stability often display aggregation at low pH during elution from Protein A columns (65-70). Therefore, we evaluated the percentage of monomeric antibody after Protein A purification for the affinity-matured antibodies relative to the control clinical-stage antibodies

(Figs. 2-11B and S9). Encouragingly, we observed that the affinity-matured antibodies displayed high levels of monomeric protein (>95%) that were similar to the clinical-stage antibodies. Moreover, we evaluated the melting temperatures of our single-chain antibodies (as scFv-Fc fusion proteins) relative to the clinical-stage IgGs (Figs. 2-11C and S10) to evaluate if affinity maturation reduced stability (3,71,72). Due to the lack of constant (C_H1 and C_L) domains, it is expected that the single-chain antibodies will have lower stabilities than the clinical-stage IgGs. Nevertheless, we find that the affinity-matured antibodies displayed high stabilities (T_m values of 64-69 ^oC) that were comparable to the parental antibody (AF1, T_m of 69 ^oC) and modestly lower than the clinical-stage IgGs (74-79 ^oC). In summary, our affinity-matured antibodies display a combination of biophysical properties that are favorable and unique in comparison to clinical-stage Aβ antibodies.

Additional affinity maturation does not compromise conformational and sequence specificity– We evaluated the feasibility of using our methods to further affinity mature one of the best antibody variants (clone 97) while maintaining high conformational specificity and low non-specific binding. Therefore, we designed and screened a sub-library for clone 97 with mutations in heavy chain CDR1 and light chain CDR2, as these two CDRs were the only ones not mutated during the initial round of discovery (heavy chain CDR3) and the first round of affinity maturation (heavy chain CDR2 and light chains CDRs 1 and 3).

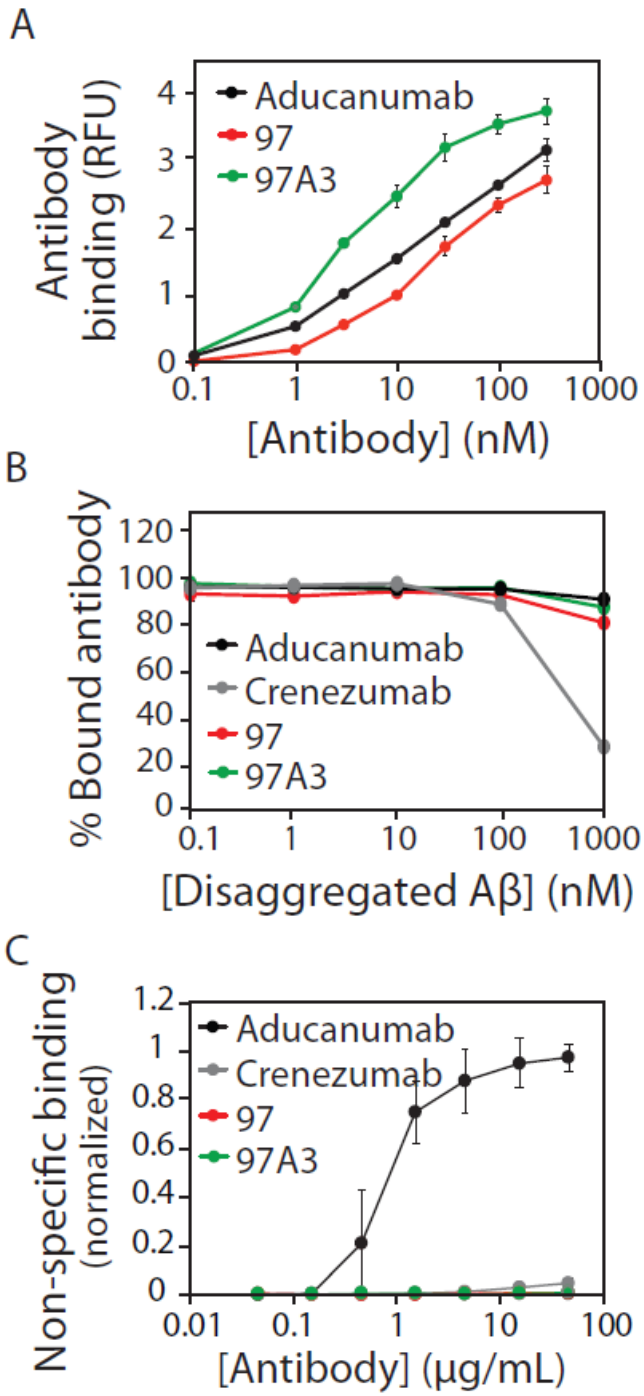

Figure 2-12: Additional affinity maturation results in an Aβ antibody variant (97A3) with improved affinity, high conformational specificity and low non-specific binding.
(A) Concentration-dependent binding of clone 97A3 to Aβ fibrils relative to its parental antibody (clone 97) and aducanumab. (B) Binding analysis of antibodies (30 nM) pre-incubated with different concentrations of disaggregated Aβ prior to binding to immobilized Aβ fibrils. (C) Antibody non-specific binding to soluble membrane proteins. In (A) and (B), the experiments were performed as described in Figure 5. In (C), the experiments were performed as described in Figure 11.

MACS selections against Aβ42 fibrils yielded a single enriched antibody variant with five mutations in light chain CDR2 (97A3; Fig. 2-12). Notably, this clone displayed higher apparent affinity than the parental antibody (~6-fold improvement) and aducanumab (~3-fold improvement; Fig. 2-12A). Given that different batches of fibrils were used to perform the binding experiments in Figs. 5 and 12, the EC_{50} values for clone 97 (8±1 nM in Fig. 2-5 and 18±1 nM in Fig. 2-12) and aducanumab (3±1 nM in Fig. 5 and 10±2 nM in Fig. 2-12) were modestly different. Moreover, the affinity-matured antibody (97A3) displayed high conformational specificity similar to clone 97 and aducanumab (Fig. 2-12B) and low non-specific binding that was similar to clone 97 and much lower than aducanumab (Fig. 2-12C). Moreover, 97A3 was mostly monomeric after one-step Protein A purification (>93%) and displayed high stability (T_m of 69±0.5 °C) that was similar to the parental antibody (97% monomer and T_m of 68±2 °C; Fig. S11). This demonstrates that our affinity maturation methods can be used to generate antibodies with superior affinity and levels of non-specific binding relative to aducanumab while maintaining high conformational specificity and thermal stability.

Discussion

We have demonstrated a rational and systematic approach for affinity maturing conformational antibodies specific for insoluble polypeptide aggregates. Prior to this work, we were skeptical about the feasibility of this process due to the likelihood of strong avidity effects between multivalent yeast-displayed antibodies interacting with multivalent Aβ aggregates immobilized on magnetic beads. In the case of soluble and monovalent antigens, it is much easier to select affinity-matured antibodies using yeast surface display because of the reduced antigen-specific avidity effects and the ability to use FACS. However, in the case of insoluble aggregates, it is not possible to use FACS because of the particulate and insoluble nature of polypeptide aggregates.

While any antibody engineering campaign has the potential to succeed if enough clones are screened, we found a surprisingly high level of success at identifying affinity-matured clones using our reported approach. For example, all 19 of the clones that were identified via our deep sequencing analysis displayed increased affinity during our primary screens performed with immunodot blots. Moreover, all of the 15 clones tested for conformational specificity displayed low levels of binding to disaggregated Aβ in our competition experiments (Fig. 2-5C and 2-5D). Finally, all of the 15 clones tested for Aβ fibril affinity displayed 8- to 20-fold improvements in their EC_{50} values compared to AF1 (Fig. 2-5A and 2-5B).

Given this higher-than-expected success rate, this raises the question of why this approach was successful and what are the most important aspects of this methodology to consider for future studies. One potentially relevant observation is related to how we identified sets of mutations most correlated with improved enrichment ratios using deep sequencing. This process assumes that the sets of mutations (e.g., sets of six mutations) govern the improved behavior and ignores the residues at the other randomized sites. It is logical that introducing these sets of mutations into the parental antibody – without introducing any mutations at the other sites – may improve antibody affinity. However, we found that this approach was much less robust, as <50% (7 out of 15) of the antibody mutants tested using this strategy showed increased affinity (as judged by immunoblots; data not shown). This suggests that mutated residues at sites not considered in a given mutational set (e.g., sites 1 and 2 when evaluating sets of mutations at sites 3-8) contribute to the overall binding activity and were important to our success in identifying affinity-matured variants.

We also suspect that our strategy for designing sub-libraries with particular types of mutations contributed to the success of selecting antibody variants with improved affinity while maintaining both conformational specificity for Aβ aggregates and low levels of off-target binding. Given the

acidic nature of Aβ42 (theoretical pI of 5.3), it is common in our experience to select positively-charged mutations that increase antibody affinity due to attractive electrostatic interactions (51,72). However, over-enrichment in positively-charged residues in antibody CDRs is a key risk factor for off-target binding (49,53,54,56,57,73-76). Therefore, we eliminated positively-charged mutations from our library design. We speculate that this may have reduced (at least partially) the strong avidity effects due to reduction of relatively long-range (attractive) electrostatic interactions during library sorting. While positive charge is obviously not deleterious in all cases for specific and high-affinity binding, it may be that eliminating positively-charged mutations reduces non-specific electrostatic interactions that frustrate selection of antibody clones with intrinsic increases in affinity due to avidity effects.

It is also notable that our parental (AF1) and affinity-matured antibodies display unusually low levels of non-specific binding. The origin of the high non-specific binding for Aβ (aducanumab) and other non-Aβ (emibetuzumab and duligotuzumab) clinical-stage antibodies relative to low non-specific binding for Aβ (crenezumab) and non-Aβ (elotuzumab) clinical-stage antibodies appears linked to the charge properties of the antibody variable regions (Table S1). The three antibodies with high non-specific binding have variable fragments (Fvs) that are either strongly positively-charged (+9.1 for aducanumab and +5.2 for emibetuzumab) or strongly negatively charged (-4.9 for duligotuzumab), as judged by their theoretical net charges at pH 7.4. In contrast, the antibodies with low non-specific binding have near neutrally charged Fvs (+0.2 for crenezumab and -0.9 for elotuzumab at pH 7.4). Moreover, AF1 and the affinity-matured clones with low levels of non-specific interactions have weakly positively-charged Fvs (+0.2 for AF1 and +1.2 to +2.2 for the first-generation affinity-matured variants and +2.2 for the second-generation variant) that are intermediate to the antibodies with high levels of non-specific interactions. This suggests that

near neutrally (or weakly positively) charged Fvs may be optimal for high antibody specificity. This is consistent with the fact that clinical-stage antibodies with low levels of non-specific and self-interactions typically have Fvs with near neutral charges (1.5±2.5 at pH 7.4) (52), which overlaps with the observed Fv charges for the antibodies with high specificity in this study.

It is also notable that several Aβ-specific antibodies have more positively-charged Fv regions (theoretical net charge at pH 7.4) than antibodies in this study with high specificity, including gantenerumab (+6.1), ponezumab (+4.2), BAN2401 (+2.3) and solanezumab (+3.2) in addition to aducanumab (+9.1; Table S1). The acidic nature of Aβ, as noted above, is likely one reason for this bias toward positively-charged antigen-binding sites. However, in the case of Aβ antibodies such as aducanumab that have abnormally positively-charged Fv regions, it is possible that these properties are linked to improved transport across the blood-brain barrier. A key step to adsorptive-mediated transcytosis – which can be specific [receptor-mediated (77-80)] or non-specific [electrostatically mediated (81)] in nature – is antibody binding at the cell surface. Antibodies with positively-charged Fvs are known to interact with negatively-charged cell membranes and display enhanced cellular uptake (73,82,83). Moreover, antibodies that display high levels of non-specific interactions are linked to increased transcytosis in cell culture (80). Therefore, we speculate that the unique positively-charged properties of aducanumab variable regions – while potentially deleterious in terms of off-target binding – may be beneficial in promoting cellular internalization and transcytosis.

However, it is also notable that administration of Aβ antibodies such as aducanumab and bapineuzumab have been linked to amyloid-related imaging abnormalities (ARIA) detected by magnetic resonance imaging (26,59,84-86). ARIA is associated with disruption of the blood-brain barrier (regional vasogenic edema). Interestingly, the effectiveness of aducanumab at reducing

amyloid in the brain is associated with increased frequency of brain edema or ARIA (26). This may suggest that the non-specific mechanism by which antibodies such as aducanumab enter the brain – which likely is enhanced by positively-charged Fv regions – results in a narrow therapeutic index (79). This also suggests that using bispecific antibodies that combine more specific Aβ antibodies – such as those reported in this study – with antibodies that target receptors at the blood-brain barrier (87-90) may enable the use of lower antibody doses, and be a safer and more effective strategy for targeting Aβ aggregates in the brain.

It is also important to consider several other aspects of our methods and findings. First, we evaluated the apparent affinities (EC_{50} values) of the antibodies at relatively low antigen concentrations (1% biotinylated fibrils immobilized on beads at 1 μM), which we found to be important to differentiate between the parental (AF1) and affinity-matured variants. At higher antigen concentrations (10% biotinylated fibrils immobilized on beads at 6 μM), we observed smaller improvements for the affinity-matured variants (data not shown), which is likely due to avidity effects. Second, we evaluated the immunodot blots at different exposure times using X-ray film (Fig. 2-6) and found that the apparent conformational specificities were dependent on exposure time. Caution should be exercised when evaluating antibody conformational specificity using dot blots because the signal for aggregates in some cases can readily saturate while the signal for disaggregated peptide can continue to increase with exposure time, leading to potentially misleading results. Third, our deep sequencing analysis only scratched the surface of the many promising antibody candidates that could be evaluated in the future. Due to errors in our initial evaluation of the deep sequencing data, the reported antibody variants have favorable but not the most favorable sets of mutations and corresponding enrichment ratios. This suggests that there may be additional opportunities to generate even better antibodies using this approach in the future.

Our findings suggest a number of additional future directions. First, our affinity maturation methodology could be readily applied to further increase the affinities of the reported Aβ antibodies in this study. Second, we expect that this approach could be applied to evolve not only the affinity but also the conformational specificity of existing antibodies against diverse types of amyloidogenic aggregates. The ability to control antigen presentation to antibody sub-libraries enables the selection of variants with increased conformational specificity in addition to increased affinity. This is particularly important for aggregates such as prefibrillar oligomers that are challenging to isolate, stabilize and use as antigens for immunization. Moreover, even for conformational antibodies discovered by immunization, it is likely that additional affinity maturation would be beneficial for their use in diagnostic and therapeutic applications. Indeed, we are currently testing the generality of these methods for maturing the affinity and conformational specificity of antibodies specific for a number of different amyloidogenic proteins.

Experimental Procedures

Aβ solubilization and fibril preparation

Aβ fibrils were prepared as described previously (34). Lyophilized Aβ1-42 (Anaspec, AS20276) and biotinylated Aβ1-42 (Anaspec, AS23526-05) peptide were dissolved in hexafluoro-2-isopropanol (HFIP), aliquoted and stored at -80 °C at 1 mg/mL (Aβ1-42) and 0.17 mg/mL (biotinylated Aβ1-42). For fibril preparation, aliquots were thawed and HFIP was evaporated overnight. Peptides were dissolved in 50 mM NaOH and ultracentrifuged at 221000xg at 4 °C for 1 h. The supernatant (typically 45 μL) was collected, transferred to a new tube, and neutralized with nine times the volume (typically 405 μL) of acidified PBS (PBS with 4.7 mM HCl). The peptide concentration was determined by measuring the absorbance at 280 nm.

Unlabeled fibrils were assembled at 37 °C for at least 3 d without agitation by further diluting the soluble peptide in PBS to a final concentration of 12.5 μM along with the addition of 10% fibril seeds (1.25 μM of preformed fibrils). Biotinylated fibrils were assembled in similar manner except that the assemblies were doped with 1 or 10% biotinylated Aβ monomer (final concentration of Aβ monomer was 12.5 μM). After at least 3 d, the assemblies were ultracentrifuged at 221000xg for 1 h (4 °C). The supernatant was discarded and the fibril pellet was re-suspended in fresh PBS (typically ~100 μL for unlabeled fibrils). For biotinylated fibrils, the pellet was resuspended in the same initial volume to achieve a nominal fibril concentration of 12.5 μM. Unlabeled fibrils were briefly sonicated for 30 s (three cycles of 10 s on and 30 s off) on ice and their concentration was determined by the BCA assay. Biotinylated fibrils were sonicated for 2 min (12 cycles of 10 s on, 30 s off) on ice before incubating them with Streptavidin Dynabeads (Invitrogen, A11047). For fibril bead preparation for sorting, 10% biotinylated fibrils (6 μM) were mixed with 10^7 beads in a final volume of 400 μL in PBSB (PBS with 1 mg/mL

BSA). For fibril bead preparation for antibody analysis, 1% biotinylated fibrils (1 μM) were mixed with 10^7 beads in a final volume of 400 μL in PBSB.

Antibody library generation

Antibody library genes (theoretical diversity of $1.1x10^8$) were prepared by PCR. Three degenerate oligos were designed with diversity in LCDR1, LCDR3 and HCDR2. Four individual PCRs were performed for the AF1 scFv gene using the yeast surface display plasmid (34) as a template, three of which used degenerate primers. Overlap PCR was then performed to combine DNA fragments with terminal primers. The PCR product was purified via a 1% agarose gel followed by gel extraction (Qiagen, 28706). The wild-type AF1 scFv plasmid was double digested with NheI-HF (New England Biolabs, R3131L) and XhoI (New England Biolabs, R1046L), treated with alkaline phosphatase (New England Biolabs, M0525L), and purified via a 1% agarose gel. The digested backbone was cut and purified with a gel extraction kit. The scFv gene and digested backbone were ligated by homologous recombination in the EBY100 yeast strain (*Saccharomyces cerevisiae*) via electroporation, as described earlier (34,91). The total number of transformants obtained was ~10^9.

For clone 97 affinity maturation, a library was constructed by diversifying five positions in light chain CDR2 and five positions in heavy chain CDR1 using NNK codons. The antibody genes were prepared by overlap extension PCR. The plasmid backbone was digested with NheI-HF and XhoI, treated with alkaline phosphatase, and purified by 1% agarose gel. The scFv antibody library genes were ligated by homologous recombination in the yeast strain EBY100 via electroporation as described above. The total number transformants obtained was ~$5x10^8$.

Yeast surface display and sorting

Five rounds of magnetic-activated cell sorting (MACS) were performed against Aβ fibrils (10% biotinylated fibrils) immobilized on streptavidin beads. For round 1, yeast cells (10^9) expressing antibodies were sorted first using negative selections (three times) against disaggregated (biotinylated) Aβ immobilized on streptavidin beads (10^7 beads per round) in PBSB, as described previously (34). Next, the remaining yeast cells after negative selections were sorted against 10^7 beads coated with Aβ fibrils in PBSB supplemented with 1% milk for 3 h (room temperature). The yeast cells bound to fibril-coated beads were collected by magnetic separation, washed, and grown in low pH SD-CAA media (20 g/L of dextrose, 6.7 g/L of yeast nitrogen base without amino acids, 5 g/L of casamino acids, 16.75 g/L of sodium citrate trihydrate, 4 g/L citric acid). Dilutions were plated to estimate the number of cells collected for the selections against Aβ fibrils. For round 2, the sorting was performed in similar way except with a reduced number of yeast cells (10^7 cells).

For rounds 3, 4 and 5, the sorting was performed in similar way as round 2 except that the negative selections were performed against IAPP fibrils (10% biotinylated IAPP fibrils immobilized at a peptide concentration of 6 μM). IAPP and biotinylated IAPP peptide were dissolved in HFIP at 1 mg/mL, aliquoted and frozen at -80 ^{o}C. Next, the peptides were thawed followed by snap freezing in liquid nitrogen and lyophilization. The lyophilized peptide was dissolved at pH 7.4 in 20 mM Tris (typically 150 μL) and centrifuged at 21000xg for 10 min to remove aggregates. The supernatant (typically 145 μL) was then transferred to a new tube. The peptide concentration was determined by measuring the absorbance at 280 nm. Fibrils were assembled at 32 μM (10% biotinylated peptide) at 37 ^{o}C and 300 RPM for 3-4 d. Post assembly, fibrils were purified by ultracentrifugation at 221000xg for 1 h at 4 ^{o}C. The fibril pellet was re-suspended to the same final volume to achieve fibrils at 32 μM. For bead preparation, fibrils were

sonicated for 2 min (10 s on, 30 s off) on ice followed by mixing with streptavidin beads (6 μM fibrils with 10^7 beads in a final volume of 400 μL)

For clone 97 affinity maturation, MACS was performed as described above. For round 1, 10^9 yeast cells expressing antibodies were incubated with 10^7 beads coated with Aβ fibrils (1% biotinylated fibrils were immobilized at 1 μM Aβ42) at room temperature for 3 h in PBSB with 1% milk. Yeast cells bound to fibril-coated beads were collected via a magnet, washed once with ice-cold PBSB, and grown in SDCAA media. For rounds 2 and 3, sorting was performed in a similar way except with 10^7 cells. In round 4, a negative selection was performed against biotinylated and disaggregated Aβ monomer (1000 nM) via FACS. Antibody display was detected using mouse anti-myc antibody (Cell Signaling, 2276S) at 1/1000x dilution followed by secondary staining with goat anti-mouse IgG (H+L) AF488 (Invitrogen, A11001) at 200x dilution. Disaggregated Aβ binding was detected using streptavidin AF647 (Invitrogen, S32357) at 1000x dilution. Yeast cells displaying antibody but not binding to disaggregated Aβ were collected and grown in SDCAA media. For rounds, 5, 6, 7 and 8, MACS was performed as described above with 10^7 cells and 10^7 beads. In rounds 6, 7 and 8, after incubating yeast with fibril-coated beads, yeast bound to such beads were washed (3x for 20 min per wash with end-over-end mixing) with PBSB supplemented with 0.05% Tween 20 to select for antibodies with increased affinity and potentially with lower off-rates.

Deep sequencing and data analysis

Yeast plasmids containing scFv genes were extracted after regrowing the sorted antibody libraries from rounds 2-5 using a Zymoprep Yeast Plasmid Miniprep II Kit (Zymo Research, D2004). PCR was used to amplify a portion of the scFv gene containing LCDR1, LCDR3, and HCDR2, and to add Illumina adapter regions as well as DNA barcodes. These PCR products were

run on 1% agarose gels and purified using a QIAquick Gel Extraction Kit (Qiagen, 28704). A second PCR was performed with 2 µL of the purified products using primers that anneal to the Illumina adapter regions. This product was also purified via a gel extraction kit. The samples were sequenced using Illumina MiSeq with 300 bp paired-end sequencing reactions.

To analyze the paired-end output .fastq files, the two .fastq files corresponding to each sample were merged into one .fastq file using BBMerge with the qtrim parameter set to 15 (92). The resulting file was converted to a .fasta file and each line was analyzed. The lines containing a sequence were checked to ensure it was the correct length (540 bp) and that there were not bases called as 'N.' If so, it was translated using BioPython (93). If the resulting translation did not contain stop codons and started with the correct amino acid (T), it was further analyzed. Otherwise, the reverse complement of the sequence was translated and checked for starting amino acid and stop codons. Next, the eleven residues with potential mutations in the sequences were identified and added to a dictionary if they were previously unobserved or increased their count of observation. This process was repeated for every sample and the results were recorded in a .csv file.

To select clones for experimental evaluation, mutational analysis was performed to identify sets of mutations most strongly correlated with improved antibody binding. For example, for a given set of potential mutations (e.g., D61G in HCDR2 and D28N, N30Y and A34T in LCDR1), clones were collected that contain those mutations (potentially among others) as well as all the clones with wild-type residues in those positions (irrespective of other mutations). Next, the Spearman correlation coefficients were calculated for the correlations between the enrichment ratios of the identified clones (x-axis) and the frequencies of mutations (y-axis). Mutational analysis was conducted for one to nine mutations, and at least ten clones were required in each of

the mutant and wild-type sets. Moreover, the Spearman correlation coefficients were required to be statistically significant (p-value <0.05).

Mammalian plasmid cloning, expression and purification

Antibody sequences selected from deep sequencing analysis were ordered as separate V_L and V_H geneblocks. The geneblocks were combined by overlap PCR with primers containing NheI (forward primer) and HindIII (reverse primer) restriction sites. The PCR products were run on 1% agarose gels and purified via a Qiagen gel extraction kit. The purified DNA fragments were then double digested by NheI-HF (New England Biolabs, R3131L) and HindIII-HF (New England Biolabs, R3104L) and further purified using a PCR clean-up kit (Qiagen, 28104). HEK293-6E mammalian expression plasmids were double digested with NheI-HF and HindIII-HF followed by alkaline phosphatase treatment. The digested backbone was then gel purified using a 1% agarose gel. DNA inserts and plasmid backbones were ligated by T4 DNA ligase (New England Biolabs, M0202L), and the ligation mixtures were transformed into competent DH5α cells and plated on LB agar plates supplemented with 100 µg/mL ampicillin. Single colonies were picked, grown in LB supplemented with ampicillin, mini-prepped (Qiagen, 27106), and sequence confirmed.

For antibody expression, plasmids (15 µg) were mixed with PEI (45 µg) in F17 media (Invitrogen, A1383502) and incubated at room temperature for 10-20 min after vortexing briefly. The resulting mixture was then added to cells growing in F17 media supplemented with L-glutamine (Gibco, 25030081), Kolliphor (Fisher, NC0917244) and antibiotic G418 (Gibco, 10131035). Yeastolate (BD Sciences, 292804) was added at 20% w/v after 24-48 h. The expression was continued for 4-5 d, and media was collected by centrifuging cells at 3500xg for 40 min. The media was transferred to a new tube and 1 mL of Protein A resin (Pierce, 20333) was added. Media and beads were rocked gently overnight at 4 ^{o}C. Beads were collected by passing media through a

filter column (Thermo Fisher Scientific, 89898) under vacuum. Beads were washed with 50-100 mL of PBS and protein was eluted from the beads in 0.1 M glycine (pH 3). Protein was then buffer exchanged into 20 mM acetate (pH 5) using Zeba desalting column (Thermo Fisher Scientific, 89894), passed through 0.2 µm filters (EMD Millipore, SLGV004SL), aliquoted, and stored at -80 °C. Protein concentrations were determined by measuring the absorbance at 280 nm, and purity was evaluated by SDS-PAGE (Invitrogen, WG1203BOX).

Analytical size-exclusion chromatography

The purity of antibodies after the first purification step (Protein A) was also evaluated using size-exclusion chromatography (SEC). A Shimadzu Prominence HPLC System was used that was outfitted with a LC-20AT pump, SIL-20AC autosampler and FRC-10A fraction collector. Antibodies in 20 mM acetate (pH 5) were buffer exchanged into PBS (pH 7.4). For analytical SEC, 100 µL of antibodies (diluted to 0.1 mg/mL) were loaded onto a SEC column (Superdex 200 Increase 10/300 GL column; GE, 28990944) and analyzed at 0.75 mL/min using a PBS running buffer supplemented with 200 mM arginine (pH 7.4). Absorbance was monitored at 220 and 280 nm, and the 280 nm signal was primarily used for analysis. The percentage of antibody monomer was evaluated by analyzing the area under the monomeric peak (excluding times before 7 min and after 22 min). In some cases, the antibodies were purified using SEC after Protein A purification. In those cases, the peak times for fraction collection were chosen based on the analytical runs. Antibody fractions were collected, buffer exchanged into PBS (pH 7.4), filtered, aliquoted and stored at -80 °C.

Antibody binding analysis

For affinity analysis, the binding of antibodies [including clinical-stage antibodies whose sequences were obtained from the Therapeutic Antibody (TABS) database] to Aβ fibrils was

evaluated using streptavidin dynabeads and flow cytometry. Beads were immobilized with 1% biotinylated fibrils as described above. The fibril-coated beads were washed twice with PBSB and then blocked with 10% milk in PBS at room temperature for 1 h with end-over-end mixing. Afterward, the beads were washed 2x with PBSB.

Antibodies were thawed and centrifuged at 21000xg for 5 min to remove aggregates. The supernatant was transferred to a new tube and the antibody concentration was determined by measuring absorbance at 280 nm. Antibody dilutions were made in PBSB. Fibril-coated beads ($1.25x10^5$ beads per antibody concentration) were incubated with antibodies in 96-well plates (Greiner, 650261) in 1% milk for 3 h at 25 °C (300 RPM). Next, the plates were centrifuged at 3500 RPM for 5 min, the supernatants were discarded, and the beads were washed once with ice-cold PBSB. After washing, the plates were spun down again and the beads with resuspended with 300x diluted goat anti-human Fc AF647 (Jackson Immunoresearch, 109-605-098) on ice for 4-5 min. Beads were then washed once more with ice-cold PBSB and analyzed via flow cytometry using a BioRad ZE5 Analyzer. For control beads, blank streptavidin beads were also blocked with 10% milk in PBS and treated in the same way as the fibril-coated beads. Two independent repeats were performed with different batches of beads coated with Aβ fibrils.

For antibody conformational specificity analysis, the experiments were performed in the same way as described above except that the antibodies were pre-incubated with disaggregated (non-biotinylated) Aβ. Antibody binding analysis was performed in 1% milk at a fixed antibody concentration (30 nM) and a range of disaggregated Aβ concentrations. The antibody binding results were normalized to the average value obtained without disaggregated Aβ. Two independent repeats were performed with different batches of beads coated with Aβ fibrils.

Antibody epitope analysis

Fibrils were also assembled using Aβ peptides with N-terminal deletions including Aβ2-42 (Bachem, 40306028.0500), Aβ3-42 (Bachem, 4090137.0500), Aβ4-42 (Bachem, 4090138.0500), Aβ5-42 (Bachem, 4041241.0500) and Aβ11-42 (Anaspec, 63317) in addition to Aβ1-42, and purified using ultracentrifugation. Fibrils were then spotted on nitrocellulose membranes at equal Thioflavin T florescence. Membranes were blocked with 5% milk in PBS at room temperature for 1 h followed by 3x washing with PBST (PBS with 0.1% Tween 20). Membranes were then incubated with Aβ antibodies at 10 nM (1% milk) in PBST at room temperature for 2-3 h. Following primary incubation, membranes were washed 3x with PBST followed by incubation with goat anti-human Fc IgG HRP (1/5000x dilution, Invitrogen, A18817) in PBST at room temperature (1 h). Following secondary incubation, the blots were washed 3x with PBST, developed with ECL (Pierce, 32109) and imaged with a Bio-Rad imager.

Polyspecificity analysis

The polyspecificity reagent (PSR) was prepared as previously described (63). CHO cells (10^9, Gibco, A29133) were pelleted, the cell pellets were washed separately with PBSB and Buffer B (50 mM HEPES, 0.15 M NaCl, 2 mM $CaCl_2$, 5 mM KCl, 5 mM $MgCl_2$, 10% Glycerol, pH 7.2), and then pelleted again. The pellets were resuspended in 5 mL of Buffer B supplemented with a protease inhibitor (Sigma Aldrich, 4693159001). Next, the resuspended cells were homogenized for 90 s (three cycles of 30 s) followed by sonication for 90 s (three cycles of 30 s). The cell suspension was then spun down at 40000xg for 1 h and the supernatant was discarded.

The pellet, comprising the enriched membrane fraction, was resuspended in Buffer B with a Dounce homogenizer for 30 strokes. The protein concentration was determined using a detergent compatible protein assay kit (BioRad, 5000116). The enriched membrane fraction was diluted to a theoretical concentration of 1 mg/mL in solubilization buffer (pH 7.2), the latter of which

contained 50 mM HEPES, 0.15 M NaCl, 2 mM $CaCl_2$, 5 mM KCl, 5 mM $MgCl_2$, 1% n-dodecyl-β-D-maltopyranoside (Sigma Aldrich, D4641), and a protease inhibitor (Sigma Aldrich, 11873580001). The solution was then mixed overnight (end-over-end) at 4 °C. The soluble membrane protein fraction was centrifuged at 40000xg for 1 h and the supernatant was collected. The final concentration of supernatant was ~0.8-0.9 mg/mL.

Sulfo-NHS-LC-biotin (Thermo Fisher, PI21335) was dissolved in distilled water at ~11.5 mg/mL. The stock solution of Sulfo-NHS-LC-biotin (150 μL) and the PSR reagent (4.5 mL at 0.8-0.9 mg/mL) were mixed via end-over-end mixing at room temperature (45 min). The reaction was quenched (10 μL of 1.5 M hydroxylamine at pH 7.2), and biotinylated PSR was aliquoted and stored at -80 °C.

Protein A magnetic beads (Invitrogen, 88846) were washed twice and incubated with antibodies in 96-well plates (VWR, 650261) overnight at 4 °C. The antibodies were purified either via one-step (Protein A) or two-step (Protein A followed by SEC) purification methods. Next, the antibody- coated beads were washed by centrifuging the 96-well plates at 3500xg for 4 min and washed twice with PBSB. Afterward, the beads were resuspended with a 10x diluted solution of biotinylated PSR and incubated on ice for 20 min. Beads were washed once with PBSB and incubated with 1000x diluted solution of streptavidin AF-647 (Invitrogen, S32357) and 1000x diluted solution of goat anti-human Fc $F(ab')_2$ AF-488 (Invitrogen, H10120) on ice (4 min). Bead were washed once, resuspended in PBSB, and analyzed via flow cytometry. The antibody binding steps were performed in PBSB, and three independent repeats were performed. The control antibodies used were the variable regions of crenezumab, elotuzumab, duligotuzumab and emibetuzumab grafted onto a common IgG1 framework, which results in differences in the

antibodies we have evaluated and the actual clinical-stage drugs. The control antibodies were two-step purified (Protein A and SEC).

Immunoblotting analysis of synthetic Aβ peptides

For immunoblots using synthetic Aβ peptides, disaggregated Aβ and unlabeled Aβ fibrils were prepared as discussed above. Disaggregated Aβ, and fibrils of Aβ, IAPP and α-synuclein were spotted on nitrocellulose membranes. Membranes were allowed to dry for at least 1 h at room temperature before use. Membranes were blocked with 5% milk in PBS for 1 h at room temperature. Afterward, the membranes were washed 3x using PBST (PBS with 0.1% v/v Tween 20) with rocking (5 min). Antibodies were thawed, centrifuged, and their concentrations were determined via absorbance measurements at 280 nm. Antibody binding was performed at 10 nM in PBST with 1% milk at room temperature (3 h). Next, the membranes were washed 3x with PBST and incubated with a 7500x diluted solution of goat anti-human Fc HRP (Invitrogen, A18817) at room temperature (1 h). Following secondary incubation, the blots were washed 3x with PBST and developed with ECL (Pierce, 32109). The signals were evaluated using X-Ray film (Thermo Scientific, 34090) and the films were developed. Three independent repeats were performed for all experiments.

Mouse models

This study was conducted in a facility approved by the American Association for the Accreditation of Laboratory Animal Care, and all experiments were performed in accordance with the National Institutes of Health Guide for the Care and Use of Laboratory Animals and approved by the Institutional Animal Care and Use Committee of the University of Michigan. Mice were housed at the University of Michigan animal care facility and maintained according to U.S. Department of Agriculture standards (12 h light/dark cycle with food and water available ad

libitum). 5xFAD mice (B6.Cg_Tg(APPSwFlLon,PSEN1*M146L*L286V)6799Vas/Mmjax; The Jackson Laboratory MMRRC stock #034848) expressing human amyloid precursor protein (APP) and presenilin-1 (PSEN1) with five AD mutations: the Swedish (K670N/M671L), Florida (I716V), and London (V717I) APP mutations and the M146L and L286V PSEN1 mutations and non-transgenic littermates (courtesy of Geoffrey Murphy, University of Michigan) were euthanized at 8 months (for immunofluorescence analysis) and 22-24 months (for immunoblots and western blots) for brain collection.

Tissue harvesting

Animals were deeply anesthetized with isofluorane and perfused transcardially with 1x PBS. Brains were divided sagittally. One half was immediately placed on dry ice and stored at -80 °C for biochemical studies while the other half was fixed in 4% paraformaldehyde at 4 °C for 24 h, and cryoprotected in 10% and 30% sucrose solutions in 1xPBS at 4 °C until saturated. Fixed hemispheres were snap frozen in OCT medium and sectioned at 12 μm sagittally using a cryostat and sections were stored at -20 °C for immunofluorescence.

Immunoblotting and western blotting analysis of mouse brain samples

The 5xFAD and non-transgenic littermate forebrain samples were homogenized in PBS with a protease inhibitor cocktail (Sigma Aldrich, 11873580001) using a 1:3 dilution of tissue: PBS (w/v). Samples were centrifuged at 9300xg for 10 min at 4 °C. Supernatants (soluble fraction) were snap frozen and stored at -80°C for Western blot analysis. Pellets were resuspended in PBS with protease inhibitor cocktail (Roche, 11836170001), centrifuged at 9300xg for 10 min (4 °C), and supernatants were discarded. The pellet was resuspended in radioimmunoprecipitation assay (RIPA) buffer with protease inhibitor, vortexed (1 min), and incubated at room temperature (1 h). Samples were sonicated (water bath sonicator) for 5 min and centrifuged for 30 min (16000xg at

4 ºC). RIPA (PBS soluble and insoluble) fractions of brain extracts (7 µg of total protein) were spotted directly onto nitrocellulose membranes and allowed to dry (1 h). Control dot blots (loading controls) were stained with Ponceau S (5 min) and washed 3x with distilled water. The other dot blots were blocked with 10% nonfat dry milk in Tris Buffered Saline with 0.1% Tween 20 (TBST) buffer at room temperature (1 h). Each dot blot was then incubated with antibodies at 50 nM (1% nonfat dry milk in TBST) overnight at 4 ºC. Next, the blots were washed with TBST and incubated with a 5000x diluted solution of HRP-conjugated goat anti-human IgG at room temperature for 1 h. Afterward, the blots were washed with TBST and developed using Ecobright Nano HRP Substrate (Innovative Solutions) and visualized with the Genesys G:Box imaging system (Syngene). Three independent repeats were performed.

For western blotting, 50 µg of total protein was loaded on precast NuPAGE 4-12% Bis-Tris gels (Invitrogen, WG1402A). Gels were subsequently transferred onto nitrocellulose membranes and first stained with Ponceau S and washed 3x with distilled water. After imaging, membranes were destained for 1 min with 0.1 M NaOH and washed 3x with distilled water. Next, membranes were blocked for 1 h at room temperature with 10% nonfat dry milk in TBST buffer. Membranes were probed overnight at 4°C with aducanumab (Adu) and NAB 228 (Sigma-Aldrich, A8354; recognizes Aβ1-11) at 100 nM in TBST with 1% milk or 100 nM antibody (clone 93 or 97) in 1% nonfat dry milk in TBST. HRP-conjugated goat anti-human/mouse IgG (5000x dilution) HRP was used for detection. Ecobright Nano HRP Substrate (Innovative Solutions) was used to visualize bands with the Genesys G:Box imaging system (Syngene). Three independent repeats were performed.

Human disease brain tissue

Frozen brain tissue from the anterior cingulate was obtained from subjects with MSA, and age-matched control subjects from the Michigan Brain Bank (University of Michigan, Ann Arbor, MI, USA). Brain tissue was collected with the informed consent of the patients. Protocols were approved by the Institutional Review Board of the University of Michigan and abide by the Declaration of Helsinki principles. Samples were examined at autopsy by neuropathologists for diagnosis.

Processing of human brain tissues

Lysis buffer (600 µL; 50 mM Na phosphate, pH 7.4, 150 mM NaCl, 2 mM EGTA, 2 mM EDTA, PhosSTOP (Sigma-Aldrich; 4906845001), cOmplete EDTA-free Protease Inhibitor Cocktail mini (Sigma-Aldrich; 11836170001), 6 µL/ml saturated phenylmethylsulfonyl fluoride (PMSF), and 10 mM Na azide) were added to 0.3 g of hippocampal tissue from individuals diagnosed with AD and age-matched controls negative for Aβ, α-synuclein, and tau pathology. Next, tissue samples were homogenized in safe-lock tubes containing 4 zirconium beads per tube for 1 min (speed 4) followed by cooling on ice for 5 min (Nova Advance homogenizer, Next Advance). Homogenization was repeated three more times. For additional homogenization, samples were passaged five times through a 25G needle, followed by centrifugation at 1,000xg for 10 min. After resuspension with 150 µL lysis buffer, pellets were passaged five times through a 25G needle syringe. Then samples were sonicated (PIP 50, DF 10%, and CPB 200) for 100 cycles (1 s ON and 1 s OFF) in M220 Focused-ultrasonicator (Covaris). To digest RNA/DNA, 1 µL benzonase (Sigma; E1014) was added to 50 µL sample (1:50 ratio) supplemented with 2 mM $MgCl_2$ (final concentration). After incubation for 30 min at room temperature, equal volumes of benzonase-treated samples and 1% sarkosyl were incubated for 30 min at 4 ℃. Following

centrifugation at 18,000xg, the total protein concentrations of the pellets was determined by BCA and used for the dot blots.

Immunofluorescence analysis of mouse brain samples

Fixed brain sections were post-fixed for 10 min in methanol at 4 ℃. Sections were washed in 1x PBS three times for 10 min and subjected to heat-induced antigen retrieval in 10 mM citrate buffer (pH 6). Sections were washed in 1x PBS two times for 5 min and permeabilized with 0.5% Triton-X 100, washed for 10 min in 1xPBS, and blocked using the Mouse on Mouse (M.O.M.) Mouse IgG Blocking Reagent (M.O.M. Immunodetection Kit, Vector, BMK-2202) for 1 h. Sections were washed 2x for 2 min in 1x PBS and incubated for 5 min in M.O.M. diluent. Sections were then incubated with Aβ antibodies aducanumab or 97 (200 nM) and NAB 228 (200x dilution) in M.O.M. diluent overnight at 4 ℃. The following day, sections were washed in 1x PBS three times for 10 min each and incubated with goat anti-mouse IgG Alexa-488 (Invitrogen; 1:500) and goat anti-human IgG Alexa-647 (1:500) for 1 h. Sections were then washed in PBS 3x for 10 min each and incubated with DAPI (Sigma) to label nuclei for 5 min at room temperature, washed 3x for 5 min each, and were mounted with Prolong Gold Antifade Reagent (Invitrogen). Slides were imaged using a Leica SP5 Confocal microscope.

Note: This chapter is adapted from manuscript titled 'Rational affinity maturation of anti-amyloid antibodies with high conformational and sequence specificity'.

Citation: Desai, A. A., Smith, M. D., Zhang, Y., Makowski, E. K., Gerson, J. E., Ionescu, E., Starr, C. G., Zupancic, J. M., Moore, S. J., Sutter, A. B., Ivanova, M. I., Murphy, G. G., Paulson, H. L., and Tessier, P. M. (2021) Rational affinity maturation of anti-amyloid antibodies with high conformational and sequence specificity. *Journal of Biological Chemistry* **296**, 100508

Data Availability: All of the data is contained within the manuscript except for the antibody sequences, which are deposited in GenBank: MT635022, MT635023, MT635024, MT635025, MT635026, MT635027, MT635028, MT635029, MT635030, MT635031, MW202274.

References

1. Tiller, K. E., and Tessier, P. M. (2015) Advances in Antibody Design. *Annu Rev Biomed Eng* **17**, 191-216

2. Kaplon, H., and Reichert, J. M. (2021) Antibodies to watch in 2021. *MAbs* **13**, 1860476

3. Rabia, L. A., Desai, A. A., Jhajj, H. S., and Tessier, P. M. (2018) Understanding and overcoming trade-offs between antibody affinity, specificity, stability and solubility. *Biochem Eng J* **137**, 365-374

4. Nelson, A. L. (2010) Antibody fragments: hope and hype. *MAbs* **2**, 77-83

5. Xenaki, K. T., Oliveira, S., and van Bergen En Henegouwen, P. M. P. (2017) Antibody or Antibody Fragments: Implications for Molecular Imaging and Targeted Therapy of Solid Tumors. *Front Immunol* **8**, 1287

6. Murphy, M. P., and LeVine, H., 3rd. (2010) Alzheimer's disease and the amyloid-beta peptide. *Journal of Alzheimer's disease : JAD* **19**, 311-323

7. Kovacs, G. G. (2015) Invited review: Neuropathology of tauopathies: principles and practice. *Neuropathol Appl Neurobiol* **41**, 3-23

8. Martí, M. J., Tolosa, E., and Campdelacreu, J. (2003) Clinical overview of the synucleinopathies. *Mov Disord* **18 Suppl 6**, S21-27

9. Long, J. M., and Holtzman, D. M. (2019) Alzheimer Disease: An Update on Pathobiology and Treatment Strategies. *Cell* **179**, 312-339

10. Haque, S. M., Ashwaq, O., Sarief, A., and Mohamed, A. K. A. J. (2020) A comprehensive review about SARS-CoV-2. *Future Virology* **15**, 625-648

11. Hu, B., Guo, H., Zhou, P., and Shi, Z. L. (2021) Characteristics of SARS-CoV-2 and COVID-19. *Nat Rev Microbiol* **19**, 141-154

12. Chiti, F., and Dobson, C. M. (2017) Protein Misfolding, Amyloid Formation, and Human Disease: A Summary of Progress Over the Last Decade. *Annu Rev Biochem* **86**, 27-68

13. Ross, C. A., and Poirier, M. A. (2004) Protein aggregation and neurodegenerative disease. *Nat Med* **10**, S10-17

14. Glabe, C. G. (2004) Conformation-dependent antibodies target diseases of protein misfolding. *Trends Biochem Sci* **29**, 542-547

15. Droste, P., Frenzel, A., Steinwand, M., Pelat, T., Thullier, P., Hust, M., Lashuel, H., and Dubel, S. (2015) Structural differences of amyloid-beta fibrils revealed by antibodies from phage display. *BMC Biotechnol* **15**, 57

16. Hatami, A., Albay, R., 3rd, Monjazeb, S., Milton, S., and Glabe, C. (2014) Monoclonal antibodies against Abeta42 fibrils distinguish multiple aggregation state polymorphisms in vitro and in Alzheimer disease brain. *J Biol Chem* **289**, 32131-32143

17. Kayed, R., Head, E., Thompson, J. L., McIntire, T. M., Milton, S. C., Cotman, C. W., and Glabe, C. G. (2003) Common Structure of Soluble Amyloid Oligomers Implies Common Mechanism of Pathogenesis. *Science* **300**, 486-489

18. Kanaan, N. M., Cox, K., Alvarez, V. E., Stein, T. D., Poncil, S., and McKee, A. C. (2016) Characterization of Early Pathological Tau Conformations and Phosphorylation in Chronic Traumatic Encephalopathy. *J Neuropathol Exp Neurol* **75**, 19-34

19. Bonito-Oliva, A., Schedin-Weiss, S., Younesi, S. S., Tiiman, A., Adura, C., Paknejad, N., Brendel, M., Romin, Y., Parchem, R. J., Graff, C., Vukojevic, V., Tjernberg, L. O., Terenius, L., Winblad, B., Sakmar, T. P., and Graham, W. V. (2019) Conformation-specific antibodies against multiple amyloid protofibril species from a single amyloid immunogen. *J Cell Mol Med* **23**, 2103-2114

20. Combs, B., Hamel, C., and Kanaan, N. M. (2016) Pathological conformations involving the amino terminus of tau occur early in Alzheimer's disease and are differentially detected by monoclonal antibodies. *Neurobiol Dis* **94**, 18-31

21. Kanaan, N. M., Morfini, G. A., LaPointe, N. E., Pigino, G. F., Patterson, K. R., Song, Y., Andreadis, A., Fu, Y., Brady, S. T., and Binder, L. I. (2011) Pathogenic forms of tau inhibit kinesin-dependent axonal transport through a mechanism involving activation of axonal phosphotransferases. *J Neurosci* **31**, 9858-9868

22. Bodani, R. U., Sengupta, U., Castillo-Carranza, D. L., Guerrero-Munoz, M. J., Gerson, J. E., Rudra, J., and Kayed, R. (2015) Antibody against Small Aggregated Peptide Specifically Recognizes Toxic Abeta-42 Oligomers in Alzheimer's Disease. *ACS Chem Neurosci* **6**, 1981-1989

23. Lasagna-Reeves, C. A., Castillo-Carranza, D. L., Sengupta, U., Sarmiento, J., Troncoso, J., Jackson, G. R., and Kayed, R. (2012) Identification of oligomers at early stages of tau aggregation in Alzheimer's disease. *FASEB J* **26**, 1946-1959

24. Weihofen, A., Liu, Y., Arndt, J. W., Huy, C., Quan, C., Smith, B. A., Baeriswyl, J. L., Cavegn, N., Senn, L., Su, L., Marsh, G., Auluck, P. K., Montrasio, F., Nitsch, R. M., Hirst, W. D., Cedarbaum, J. M., Pepinsky, R. B., Grimm, J., and Weinreb, P. H. (2019) Development of an aggregate-selective, human-derived alpha-synuclein antibody BIIB054 that ameliorates disease phenotypes in Parkinson's disease models. *Neurobiol Dis* **124**, 276-288

25. Arndt, J. W., Qian, F., Smith, B. A., Quan, C., Kilambi, K. P., Bush, M. W., Walz, T., Pepinsky, R. B., Bussiere, T., Hamann, S., Cameron, T. O., and Weinreb, P. H. (2018) Structural and kinetic basis for the selectivity of aducanumab for aggregated forms of amyloid-beta. *Sci Rep* **8**, 6412

26. Sevigny, J., Chiao, P., Bussiere, T., Weinreb, P. H., Williams, L., Maier, M., Dunstan, R., Salloway, S., Chen, T., Ling, Y., O'Gorman, J., Qian, F., Arastu, M., Li, M., Chollate, S., Brennan, M. S., Quintero-Monzon, O., Scannevin, R. H., Arnold, H. M., Engber, T., Rhodes, K., Ferrero, J., Hang, Y., Mikulskis, A., Grimm, J., Hock, C., Nitsch, R. M., and Sandrock, A. (2016) The antibody aducanumab reduces Abeta plaques in Alzheimer's disease. *Nature* **537**, 50-56

27. Castillo-Carranza, D. L., Sengupta, U., Guerrero-Munoz, M. J., Lasagna-Reeves, C. A., Gerson, J. E., Singh, G., Estes, D. M., Barrett, A. D., Dineley, K. T., Jackson, G. R., and Kayed, R. (2014) Passive immunization with Tau oligomer monoclonal antibody reverses tauopathy phenotypes without affecting hyperphosphorylated neurofibrillary tangles. *J Neurosci* **34**, 4260-4272

28. Gong, Y., Chang, L., Viola, K. L., Lacor, P. N., Lambert, M. P., Finch, C. E., Krafft, G. A., and Klein, W. L. (2003) Alzheimer's disease-affected brain: presence of oligomeric A beta ligands (ADDLs) suggests a molecular basis for reversible memory loss. *Proc Natl Acad Sci U S A* **100**, 10417-10422

29. Lambert, M. P., Velasco, P. T., Chang, L., Viola, K. L., Fernandez, S., Lacor, P. N., Khuon, D., Gong, Y., Bigio, E. H., Shaw, P., De Felice, F. G., Krafft, G. A., and Klein, W. L. (2007) Monoclonal antibodies that target pathological assemblies of Abeta. *J Neurochem* **100**, 23-35

30. Lambert, M. P., Viola, K. L., Chromy, B. A., Chang, L., Morgan, T. E., Yu, J., Venton, D. L., Krafft, G. A., Finch, C. E., and Klein, W. L. (2001) Vaccination with soluble Aβ oligomers generates toxicity-neutralizing antibodies. *Journal of Neurochemistry* **79**, 595-605

31. Kayed, R., Head, E., Sarsoza, F., Saing, T., Cotman, C. W., Necula, M., Margol, L., Wu, J., Breydo, L., Thompson, J. L., Rasool, S., Gurlo, T., Butler, P., and Glabe, C. G. (2007) Fibril specific, conformation dependent antibodies recognize a generic epitope common to amyloid fibrils and fibrillar oligomers that is absent in prefibrillar oligomers. *Mol Neurodegener* **2**, 18

32. Gibbons, G. S., Kim, S. J., Robinson, J. L., Changolkar, L., Irwin, D. J., Shaw, L. M., Lee, V. M., and Trojanowski, J. Q. (2019) Detection of Alzheimer's disease (AD) specific tau pathology with conformation-selective anti-tau monoclonal antibody in co-morbid frontotemporal lobar degeneration-tau (FTLD-tau). *Acta Neuropathol Commun* **7**, 34

33. Covell, D. J., Robinson, J. L., Akhtar, R. S., Grossman, M., Weintraub, D., Bucklin, H. M., Pitkin, R. M., Riddle, D., Yousef, A., Trojanowski, J. Q., and Lee, V. M. (2017) Novel conformation-selective alpha-synuclein antibodies raised against different in vitro fibril

forms show distinct patterns of Lewy pathology in Parkinson's disease. *Neuropathol Appl Neurobiol* **43**, 604-620

34. Julian, M. C., Rabia, L. A., Desai, A. A., Arsiwala, A., Gerson, J. E., Paulson, H. L., Kane, R. S., and Tessier, P. M. (2019) Nature-inspired design and evolution of anti-amyloid antibodies. *J Biol Chem* **294**, 8438-8451

35. Stimple, S. D., Kalyoncu, S., Desai, A. A., Mogensen, J. E., Spang, L. T., Asgreen, D. J., Staby, A., and Tessier, P. M. (2019) Sensitive detection of glucagon aggregation using amyloid fibril-specific antibodies. *Biotechnol Bioeng* **116**, 1868-1877

36. Munke, A., Persson, J., Weiffert, T., De Genst, E., Meisl, G., Arosio, P., Carnerup, A., Dobson, C. M., Vendruscolo, M., Knowles, T. P. J., and Linse, S. (2017) Phage display and kinetic selection of antibodies that specifically inhibit amyloid self-replication. *Proceedings of the National Academy of Sciences* **114**, 6444-6449

37. Sebollela, A., Cline, E. N., Popova, I., Luo, K., Sun, X., Ahn, J., Barcelos, M. A., Bezerra, V. N., Lyra, E. S. N. M., Patel, J., Pinheiro, N. R., Qin, L. A., Kamel, J. M., Weng, A., DiNunno, N., Bebenek, A. M., Velasco, P. T., Viola, K. L., Lacor, P. N., Ferreira, S. T., and Klein, W. L. (2017) A human scFv antibody that targets and neutralizes high molecular weight pathogenic amyloid-beta oligomers. *J Neurochem* **142**, 934-947

38. Lee, C. C., Julian, M. C., Tiller, K. E., Meng, F., DuConge, S. E., Akter, R., Raleigh, D. P., and Tessier, P. M. (2016) Design and Optimization of Anti-amyloid Domain Antibodies Specific for beta-Amyloid and Islet Amyloid Polypeptide. *J Biol Chem* **291**, 2858-2873

39. Silverman, J. M., Gibbs, E., Peng, X., Martens, K. M., Balducci, C., Wang, J., Yousefi, M., Cowan, C. M., Lamour, G., Louadi, S., Ban, Y., Robert, J., Stukas, S., Forloni, G., Hsiung, G. R., Plotkin, S. S., Wellington, C. L., and Cashman, N. R. (2018) A Rational Structured Epitope Defines a Distinct Subclass of Toxic Amyloid-beta Oligomers. *ACS Chem Neurosci* **9**, 1591-1606

40. Gibbs, E., Silverman, J. M., Zhao, B., Peng, X., Wang, J., Wellington, C. L., Mackenzie, I. R., Plotkin, S. S., Kaplan, J. M., and Cashman, N. R. (2019) A Rationally Designed Humanized Antibody Selective for Amyloid Beta Oligomers in Alzheimer's Disease. *Sci Rep* **9**, 9870

41. Perchiacca, J. M., Ladiwala, A. R., Bhattacharya, M., and Tessier, P. M. (2012) Structure-based design of conformation- and sequence-specific antibodies against amyloid beta. *Proc Natl Acad Sci U S A* **109**, 84-89

42. Aprile, F. A., Sormanni, P., Podpolny, M., Chhangur, S., Needham, L. M., Ruggeri, F. S., Perni, M., Limbocker, R., Heller, G. T., Sneideris, T., Scheidt, T., Mannini, B., Habchi, J., Lee, S. F., Salinas, P. C., Knowles, T. P. J., Dobson, C. M., and Vendruscolo, M. (2020) Rational design of a conformation-specific antibody for the quantification of Abeta oligomers. *Proc Natl Acad Sci U S A*, ePub June 3

43. Kulenkampff, K., Aprile, F. A., Sormanni, P., Ranasinghe, R. T., Klenerman, D., and Vendruscolo, M. (2020) Rational Design of Conformation-Specific Antibodies for Tau Oligomers. *Biophysical Journal* **118**, 370a-371a

44. Vaikath, N. N., Majbour, N. K., Paleologou, K. E., Ardah, M. T., van Dam, E., van de Berg, W. D., Forrest, S. L., Parkkinen, L., Gai, W. P., Hattori, N., Takanashi, M., Lee, S. J., Mann, D. M., Imai, Y., Halliday, G. M., Li, J. Y., and El-Agnaf, O. M. (2015) Generation and characterization of novel conformation-specific monoclonal antibodies for alpha-synuclein pathology. *Neurobiol Dis* **79**, 81-99

45. Gibbons, G. S., Banks, R. A., Kim, B., Changolkar, L., Riddle, D. M., Leight, S. N., Irwin, D. J., Trojanowski, J. Q., and Lee, V. M. Y. (2018) Detection of Alzheimer Disease (AD)-Specific Tau Pathology in AD and NonAD Tauopathies by Immunohistochemistry With Novel Conformation-Selective Tau Antibodies. *J Neuropathol Exp Neurol* **77**, 216-228

46. Tiller, K. E., Chowdhury, R., Li, T., Ludwig, S. D., Sen, S., Maranas, C. D., and Tessier, P. M. (2017) Facile Affinity Maturation of Antibody Variable Domains Using Natural Diversity Mutagenesis. *Front Immunol* **8**, 986

47. Jain, T., Sun, T., Durand, S., Hall, A., Houston, N. R., Nett, J. H., Sharkey, B., Bobrowicz, B., Caffry, I., Yu, Y., Cao, Y., Lynaugh, H., Brown, M., Baruah, H., Gray, L. T., Krauland, E. M., Xu, Y., Vasquez, M., and Wittrup, K. D. (2017) Biophysical properties of the clinical-stage antibody landscape. *Proc Natl Acad Sci U S A* **114**, 944-949

48. Swindells, M. B., Porter, C. T., Couch, M., Hurst, J., Abhinandan, K. R., Nielsen, J. H., Macindoe, G., Hetherington, J., and Martin, A. C. (2017) abYsis: Integrated Antibody Sequence and Structure-Management, Analysis, and Prediction. *J Mol Biol* **429**, 356-364

49. Rabia, L. A., Zhang, Y., Ludwig, S. D., Julian, M. C., and Tessier, P. M. (2018) Net charge of antibody complementarity-determining regions is a key predictor of specificity. *Protein Eng Des Sel* **31**, 409-418

50. Fellouse, F. A., Wiesmann, C., and Sidhu, S. S. (2004) Synthetic antibodies from a four-amino-acid code: a dominant role for tyrosine in antigen recognition. *Proc Natl Acad Sci U S A* **101**, 12467-12472

51. Tiller, K. E., Li, L., Kumar, S., Julian, M. C., Garde, S., and Tessier, P. M. (2017) Arginine mutations in antibody complementarity-determining regions display context-dependent affinity/specificity trade-offs. *J Biol Chem* **292**, 16638-16652

52. Zhang, Y., Wu, L., Gupta, P., Desai, A. A., Smith, M. D., Rabia, L. A., Ludwig, S. D., and Tessier, P. M. (2020) Physicochemical rules for identifying monoclonal antibodies with drug-like specificity. *Mol Pharm*, ePub May 26

53. Datta-Mannan, A., Thangaraju, A., Leung, D., Tang, Y., Witcher, D. R., Lu, J., and Wroblewski, V. J. (2015) Balancing charge in the complementarity-determining regions of humanized mAbs without affecting pI reduces non-specific binding and improves the pharmacokinetics. *MAbs* **7**, 483-493

54. Wardemann, H., Yurasov, S., Schaefer, A., Young, J. W., Meffre, E., and Nussenzweig, M. C. (2003) Predominant Autoantibody Production by Early Human B Cell Precursors. *Science* **301**, 1374-1377

55. Hong, G., Chappey, O., Niel, E., and Scherrmann, J. M. (2000) Enhanced cellular uptake and transport of polyclonal immunoglobulin G and fab after their cationization. *J Drug Target* **8**, 67-77

56. Datta-Mannan, A., Lu, J., Witcher, D. R., Leung, D., Tang, Y., and Wroblewski, V. J. (2015) The interplay of non-specific binding, target-mediated clearance and FcRn interactions on the pharmacokinetics of humanized antibodies. *MAbs* **7**, 1084-1093

57. Birtalan, S., Fisher, R. D., and Sidhu, S. S. (2010) The functional capacity of the natural amino acids for molecular recognition. *Mol Biosyst* **6**, 1186-1194

58. Arndt, J. W., Qian, F., Smith, B. A., Quan, C., Kilambi, K. P., Bush, M. W., Walz, T., Pepinsky, R. B., Bussière, T., Hamann, S., Cameron, T. O., and Weinreb, P. H. (2018) Structural and kinetic basis for the selectivity of aducanumab for aggregated forms of amyloid-β. *Sci Rep* **8**, 6412

59. van Dyck, C. H. (2018) Anti-Amyloid-beta Monoclonal Antibodies for Alzheimer's Disease: Pitfalls and Promise. *Biol Psychiatry* **83**, 311-319

60. Spencer, S., Bethea, D., Raju, T. S., Giles-Komar, J., and Feng, Y. (2012) Solubility evaluation of murine hybridoma antibodies. *MAbs* **4**, 319-325

61. Bradbury, A. R., Sidhu, S., Dubel, S., and McCafferty, J. (2011) Beyond natural antibodies: the power of in vitro display technologies. *Nat Biotechnol* **29**, 245-254

62. Johan, N., Peter, M. T., and Sachdev, S. S. (2016) Engineered Autonomous Human Variable Domains. *Curr Pharm Des* **22**, 6527-6537

63. Xu, Y., Roach, W., Sun, T., Jain, T., Prinz, B., Yu, T. Y., Torrey, J., Thomas, J., Bobrowicz, P., Vasquez, M., Wittrup, K. D., and Krauland, E. (2013) Addressing polyspecificity of antibodies selected from an in vitro yeast presentation system: a FACS-based, high-throughput selection and analytical tool. *Protein Eng Des Sel* **26**, 663-670

64. Kelly, R. L., Sun, T., Jain, T., Caffry, I., Yu, Y., Cao, Y., Lynaugh, H., Brown, M., Vasquez, M., Wittrup, K. D., and Xu, Y. (2015) High throughput cross-interaction measures for human IgG1 antibodies correlate with clearance rates in mice. *MAbs* **7**, 770-777

65. Alam, M. E., Slaney, T. R., Wu, L., Das, T. K., Kar, S., Barnett, G. V., Leone, A., and Tessier, P. M. (2020) Unique Impacts of Methionine Oxidation, Tryptophan Oxidation, and Asparagine Deamidation on Antibody Stability and Aggregation. *J Pharm Sci* **109**, 656-669

66. Cromwell, M. E. M., Hilario, E., and Jacobson, F. (2006) Protein aggregation and bioprocessing. *AAPS J* **8**, E572-E579

67. Hober, S., Nord, K., and Linhult, M. (2007) Protein A chromatography for antibody purification. *J Chromatogr B Analyt Technol Biomed Life Sci* **848**, 40-47

68. Shukla, A. A., Gupta, P., and Han, X. (2007) Protein aggregation kinetics during Protein A chromatography. Case study for an Fc fusion protein. *J Chromatogr A* **1171**, 22-28

69. Ejima, D., Tsumoto, K., Fukada, H., Yumioka, R., Nagase, K., Arakawa, T., and Philo, J. S. (2007) Effects of acid exposure on the conformation, stability, and aggregation of monoclonal antibodies. *Proteins* **66**, 954-962

70. Hari, S. B., Lau, H., Razinkov, V. I., Chen, S., and Latypov, R. F. (2010) Acid-induced aggregation of human monoclonal IgG1 and IgG2: molecular mechanism and the effect of solution composition. *Biochemistry* **49**, 9328-9338

71. Julian, M. C., Li, L., Garde, S., Wilen, R., and Tessier, P. M. (2017) Efficient affinity maturation of antibody variable domains requires co-selection of compensatory mutations to maintain thermodynamic stability. *Sci Rep* **7**, 45259

72. Julian, M. C., Lee, C. C., Tiller, K. E., Rabia, L. A., Day, E. K., Schick, A. J., 3rd, and Tessier, P. M. (2015) Co-evolution of affinity and stability of grafted amyloid-motif domain antibodies. *Protein Eng Des Sel* **28**, 339-350

73. Boswell, C. A., Tesar, D. B., Mukhyala, K., Theil, F.-P., Fielder, P. J., and Khawli, L. A. (2010) Effects of Charge on Antibody Tissue Distribution and Pharmacokinetics. *Bioconjug Chem* **21**, 2153-2163

74. Dobson, C. L., Devine, P. W., Phillips, J. J., Higazi, D. R., Lloyd, C., Popovic, B., Arnold, J., Buchanan, A., Lewis, A., Goodman, J., van der Walle, C. F., Thornton, P., Vinall, L., Lowne, D., Aagaard, A., Olsson, L. L., Ridderstad Wollberg, A., Welsh, F., Karamanos, T. K., Pashley, C. L., Iadanza, M. G., Ranson, N. A., Ashcroft, A. E., Kippen, A. D., Vaughan, T. J., Radford, S. E., and Lowe, D. C. (2016) Engineering the surface properties of a human monoclonal antibody prevents self-association and rapid clearance in vivo. *Sci Rep* **6**, 38644

75. Starr, C. G., and Tessier, P. M. (2019) Selecting and engineering monoclonal antibodies with drug-like specificity. *Curr Opin Biotechnol* **60**, 119-127

76. Birtalan, S., Zhang, Y., Fellouse, F. A., Shao, L., Schaefer, G., and Sidhu, S. S. (2008) The intrinsic contributions of tyrosine, serine, glycine and arginine to the affinity and specificity of antibodies. *J Mol Biol* **377**, 1518-1528

77. Pardridge, W. M. (2015) Blood-brain barrier drug delivery of IgG fusion proteins with a transferrin receptor monoclonal antibody. *Expert Opin Drug Deliv* **12**, 207-222

78. Jones, A. R., and Shusta, E. V. (2007) Blood-brain barrier transport of therapeutics via receptor-mediation. *Pharm Res* **24**, 1759-1771

79. Pardridge, W. M. (2017) Delivery of Biologics Across the Blood-Brain Barrier with Molecular Trojan Horse Technology. *BioDrugs* **31**, 503-519

80. Chung, S., Nguyen, V., Lin, Y. L., Lafrance-Vanasse, J., Scales, S. J., Lin, K., Deng, R., Williams, K., Sperinde, G., Li, J. J., Zheng, K., Sukumaran, S., Tesar, D., Ernst, J. A., Fischer, S., Lazar, G. A., Prabhu, S., and Song, A. (2019) An in vitro FcRn- dependent transcytosis assay as a screening tool for predictive assessment of nonspecific clearance of antibody therapeutics in humans. *MAbs* **11**, 942-955

81. Triguero, D., Buciak, J. B., Yang, J., and Pardridge, W. M. (1989) Blood-brain barrier transport of cationized immunoglobulin G: enhanced delivery compared to native protein. *Proceedings of the National Academy of Sciences* **86**, 4761-4765

82. Pardridge, W. M., Bickel, U., Buciak, J., Yang, J., Diagne, A., and Aepinus, C. (1994) Cationization of a monoclonal antibody to the human immunodeficiency virus REV protein enhances cellular uptake but does not impair antigen binding of the antibody. *Immunology letters* **42**, 191-195

83. Triguero, D., Buciak, J. B., Yang, J., and Pardridge, W. M. (1989) Blood-brain barrier transport of cationized immunoglobulin G: enhanced delivery compared to native protein. *Proc Natl Acad Sci U S A* **86**, 4761-4765

84. Zago, W., Schroeter, S., Guido, T., Khan, K., Seubert, P., Yednock, T., Schenk, D., Gregg, K. M., Games, D., Bard, F., and Kinney, G. G. (2013) Vascular alterations in PDAPP mice after anti-Abeta immunotherapy: Implications for amyloid-related imaging abnormalities. *Alzheimers Dement* **9**, S105-115

85. Barkhof, F., Daams, M., Scheltens, P., Brashear, H. R., Arrighi, H. M., Bechten, A., Morris, K., McGovern, M., and Wattjes, M. P. (2013) An MRI rating scale for amyloid-related imaging abnormalities with edema or effusion. *AJNR Am J Neuroradiol* **34**, 1550-1555

86. Sperling, R., Salloway, S., Brooks, D. J., Tampieri, D., Barakos, J., Fox, N. C., Raskind, M., Sabbagh, M., Honig, L. S., Porsteinsson, A. P., Lieberburg, I., Arrighi, H. M., Morris, K. A., Lu, Y., Liu, E., Gregg, K. M., Brashear, H. R., Kinney, G. G., Black, R., and Grundman, M. (2012) Amyloid-related imaging abnormalities in patients with Alzheimer's disease treated with bapineuzumab: a retrospective analysis. *Lancet Neurol* **11**, 241-249

87. Pardridge, W. M. (2016) Re-engineering therapeutic antibodies for Alzheimer's disease as blood-brain barrier penetrating bi-specific antibodies. *Expert Opin Biol Ther* **16**, 1455-1468

88. Sumbria, R. K., Hui, E. K., Lu, J. Z., Boado, R. J., and Pardridge, W. M. (2013) Disaggregation of amyloid plaque in brain of Alzheimer's disease transgenic mice with daily subcutaneous administration of a tetravalent bispecific antibody that targets the transferrin receptor and the Abeta amyloid peptide. *Mol Pharm* **10**, 3507-3513

89. Niewoehner, J., Bohrmann, B., Collin, L., Urich, E., Sade, H., Maier, P., Rueger, P., Stracke, J. O., Lau, W., Tissot, A. C., Loetscher, H., Ghosh, A., and Freskgard, P. O. (2014) Increased brain penetration and potency of a therapeutic antibody using a monovalent molecular shuttle. *Neuron* **81**, 49-60

90. Zuchero, Y. J., Chen, X., Bien-Ly, N., Bumbaca, D., Tong, R. K., Gao, X., Zhang, S., Hoyte, K., Luk, W., Huntley, M. A., Phu, L., Tan, C., Kallop, D., Weimer, R. M., Lu, Y., Kirkpatrick, D. S., Ernst, J. A., Chih, B., Dennis, M. S., and Watts, R. J. (2016) Discovery of Novel Blood-Brain Barrier Targets to Enhance Brain Uptake of Therapeutic Antibodies. *Neuron* **89**, 70-82

91. Benatuil, L., Perez, J. M., Belk, J., and Hsieh, C. M. (2010) An improved yeast transformation method for the generation of very large human antibody libraries. *Protein Eng Des Sel* **23**, 155-159

92. Bushnell, B., Rood, J., and Singer, E. (2017) BBMerge - Accurate paired shotgun read merging via overlap. *PLoS One* **12**, e0185056

93. Cock, P. J., Antao, T., Chang, J. T., Chapman, B. A., Cox, C. J., Dalke, A., Friedberg, I., Hamelryck, T., Kauff, F., Wilczynski, B., and de Hoon, M. J. (2009) Biopython: freely available Python tools for computational molecular biology and bioinformatics. *Bioinformatics* **25**, 1422-1423

Chapter 3 **Isolation Of Anti-Tau And Anti-α-Synuclein Conformational Antibodies**

Introduction

Protein misfolding and aggregation has been identified as a key event in several devastating diseases like Alzheimer's and Parkinson's disease (7-9,12). The aggregation of benign protein monomer into amyloidogenic oligomers, protofibrils and matured fibrils is linked to cellular death and disease progression in several pathologies termed as neurodegenerative diseases. Currently no cure exists for several of these neurodegenerative diseases.

Antibodies are currently the most promising class of bio therapeutics with >100 antibodies approved for treating several types of disorders like cancer, auto-immune diseases, inflammatory diseases and viral infections (2). Conformational antibodies which selectively bind to toxic conformers of proteins are important for several different applications including diagnostic, therapeutic and better understanding of disease mechanisms (14). Although it is not trivial to generate conformational antibodies, many conformational antibodies have entered clinical trials for several neurodegenerative diseases. Traditional methods for making conformational antibodies include immunization, rational design and panning (31,36-38,44,94). Antibody isolation from human B-cell have also been used lately with great success (24-26). Even though many of these methods have worked in the past, they lack robustness. Their limited success is because of complex properties of amyloid aggregates like high hydrophobicity, poor diffusion, no control over antigen presentation and lack of molecular nature (1).

We have sought to develop robust methods to develop conformational antibodies against tau and α-synuclein amyloid aggregates which are associated with several pathologies collectively

called tauopathies and synucleinopathies respectively. The aggregation of tau and α-synuclein proteins is a key event in these pathologies and fibrillar deposits are founds in brains of patients postmortem. We have developed high throughput screening methods using yeast surface display in combinations with powerful positive and negative selections to isolate antibodies with high affinity and conformational specificity (34,95). We have successfully generated antibodies whose conformational specificity are similar or better than many clinical antibodies against tau and α-synuclein fibrils. We hope such methods would speed the discovery of conformational antibodies against several different protein targets.

We have developed a novel nanoparticle-based flow cytometry-based selection technique. We first start with quantum dot (QD) functionalized with DIBO chemistry. Next, we selectively modify the glycan on a sequence specific antibody (also called capture antibody), introduce an azide group followed by covalently linking of capture antibody to QD by click chemistry. Next, we incubated the QD-antibody complex with our amyloid fibrils of interest to immobilize the fibrils on antibody (Fig. 3-1A). The QD-antibody-fibril complex is then incubated with yeast cells displaying antibody library followed by simple two color (antibody display and QD binding) FACS based selection (Fig. 3-1B).

Methods

Antibody – quantum dot conjugation and sorting

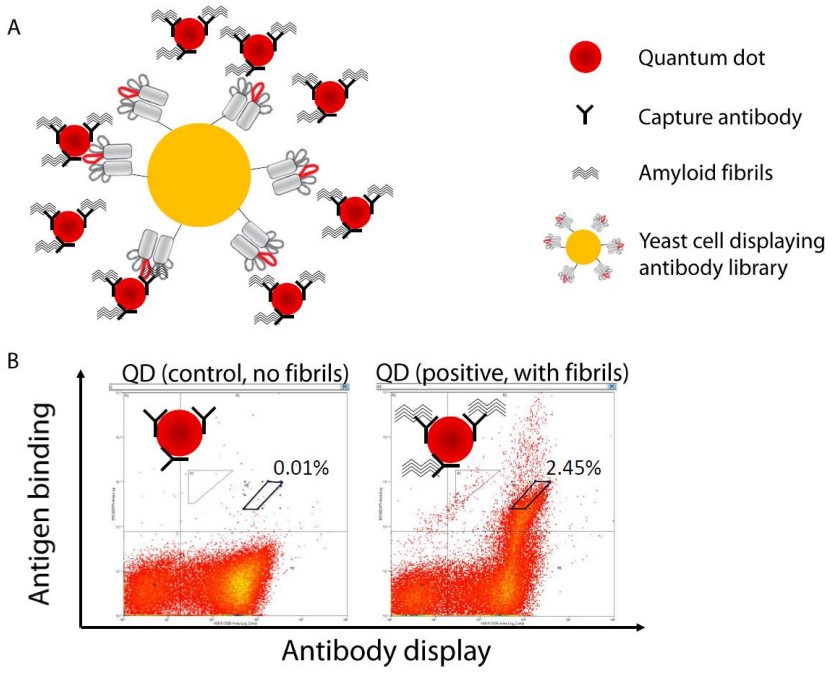

Figure 3-1: Illustration of novel QD based FACS selection for amyloid fibrils.
(A) Quantum dots (red) are covalently attached to capture antibody (black) and incubated with amyloid fibril of interest to immobilize them. (B) FACS cytograms showing control/background and (right) binding population with fibril positive samples (right).

In addition to conventional positive selection against amyloid fibrils by magnetic activated cell sorting (MACS) discussed in Chapter 2, we developed a novel florescence activated cell sorting (FACS) based selection for amyloid aggregates. SiteClick Qdot 565 antibody labeling kit was purchased from Invitrogen (S10450). Capture antibodies Tau5 (expressed and purified in-house) and MJFR1 (Abcam, ab138501) were conjugated to QD as per manufacturers' guidelines. Tau fibrils SPR-329) and α-synuclein fibrils (SPR-317) were purchased from Stressmarq. 5 µg fibrils were first sonicated (5 mins; 30 s on, 30 s off) on ice and then incubated with 5 µL QD in a final volume of 200 µL at room temperature with end-over-end mixing for 2-3 hours. Post incubation, the fibril-QD complex was incubated with yeast cells displaying antibody library in 1% milk with anti-myc antibody (1000x dilution) at room temperature with end-over-end mixing

for 2-3 hours. Post primary incubation, the cells were washed once with ice-cold PBSB and incubated with goat anti-mouse AF488 on ice for 4 mins. Following secondary incubation, the cells were washed once with ice-cold PBSB and then sorted by flow cytometry.

Antibody cloning and expression

The antibody genes from the libraries were PCR amplified, cloned and sequenced in expression plasmids as discussed above in Chapter 2. Briefly, the scFv genes were PCR amplified from yeast mini-preps with forward primer containing NheI site and reverse primer containing HindIII site. Each PCR product was purified by DNA gel electrophoresis and digested with NheI-HF and HindIII-HF. Next, it was purified by PCR clean-up, ligated into linearized Fc expression plasmid by T4 DNA ligase, transformed into competent DH5α cells, plated on LB agar plates supplemented with 100 µg/mL ampicillin and grown at 37 ^{o}C overnight. The next day, individual colonies were picked, grown into LB media supplemented with ampicillin overnight at 37 ^{o}C. Following day, the cultures were miniprepped followed by plasmid extraction and sequencing. The antibodies were expressed as Fc fusion proteins. The detailed procedure is discussed in Chapter 2. Briefly, HEK293-6E cells were transfected with antibody plasmids (15 µg) complexed with PEI (45 µg) and allowed to grow for 5-6 days. Next, the media was clarified by centrifuging the cells at 3000xg for 40 min and incubated with Protein A agarose beads overnight at 4 ^{o}C with gentle mixing. Following days, the beads were collected in filter column under vacuum and washed with ~50 mL of PBS. Next, the protein was eluted from the beads by incubating with 0.1 M glycine (pH 3.0) and buffer exchanged into 20 mM acetate (pH 5.0) by Zeba desalting columns. The proteins were filtered by 0.22 µm filters, aliquoted and stored at -80 ^{o}C. Their purity was evaluated by SEC and concentration were measured by measuring absorbance at 280 nm.

Antibody binding analysis

Antibody binding analysis including affinity, conformational specificity and PSR binding were performed as discussed in Chapter 2. Briefly, for affinity analysis, the antibodies (at different concentrations) were incubated with dynabeads immobilized with amyloid aggregates. The binding was performed in 1% milk at room temperature for 3 h with mild agitation. Next, the beads were washed once with ice-cold PBSB and incubated with goat anti-human Fc AF647 on ice for 4 mins. Following secondary incubation, the beads were washed once and analyzed by flow cytometry. For conformational specificity analysis, first the antibody (10 nM) was incubated with different concentration of soluble monomer at room temperature for 1 h. Next, beads immobilized with aggregates were added to this mixture and further incubated for 3 h at room temperature with mild agitation. Next, the beads were washed once, incubated with goat anti-human AF647, washed once again and analyzed by flow cytometry. For PSR binding, the antibodies were immobilized on Protein A beads overnight at 4 ^{o}C. The followed day, the beads were washed once and incubated with biotinylated PSR. For incubation, the beads were washed once, incubated with streptavidin AF647, washed once more, and analyzed by flow cytometry.

Results

Anti-α-synuclein antibodies

The lead clone aS2.1 was discovered in single chain variable fragment (scFv) format from non-immune library. It retained the binding to α-synuclein aggregates when we re-formatted into IgG format with human IgG1 framework. Based on this exciting result, we decided to evaluate this antibody further in IgG format only. First, we looked at binding affinity against recombinant α-synuclein fibrils and our antibody aS2.1 showed high binding (EC_{50} – 24 nM) which was comparable to clinical antibody Cinpanemab (EC_{50} of ~10 nM) (Fig. 3-2A). Following up on these

exciting results, we next evaluated conformational specificity analysis like described in Chapter 2 and encouragingly, our antibody showed superior conformational specificity than Cinpanemab (Fig. 3-2B). We next evaluated our antibody for non-specific/off-target binding. We find our antibody aS2.1 as well as Cinpanemab shows medium levels of PSR binding (Fig. 3-2C). Although, we are unsure of the exact implications of this result, we suspect this might influence the pharmacodynamics properties *in vivo*.

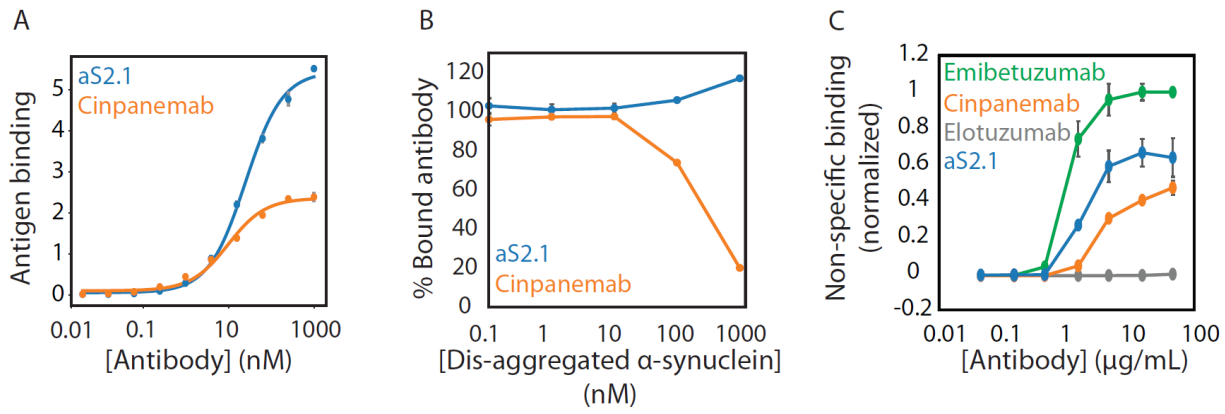

Figure 3-2: Binding analysis of α-synuclein antibodies.
Bead based affinity (A), conformational specificity (B) analysis of anti-α-synuclein antibodies aS2.1 and clinical antibody Cinpanemab. (C) Off-target/PSR binding analysis of aS2.1, Cinpanemab compared to control clinical antibody Emibetuzumab and approved drug Elotuzumab.

Anti-tau antibodies

We also isolated conformational anti-tau antibody ATA1 using the similar methods described in Chapter 2 and above. The lead clone ATA1 displayed high conformational specificity but modest affinity. Next, we designed three CDR (L1, H1 and H2) focused soft randomization sub-libraries where at specific sites, we sampled the wild-type residue (~50%) and other amino acids (~50%). Next, we went through two rounds of selection against tau aggregates. In round 1, we performed MACS where immobilized tau aggregated on dynabeads as described in Chapter 2. In round 2, we performed FACS with QD-tau conjugates as described above. Following sort 2, we

amplified individual CDR sequences from L1, H1 and H2 libraries, combined them using overlap extension PCR and made a new library where we combined the beneficial mutations from three CDR libraries. We next went through four rounds of screening with the new library. In round 1, we performed MACS with tau aggregates immobilized on dynabeads. In round 2, we performed FACS with QD-tau conjugates. In round 3, we performed a negative selection against tau monomer at 10 nM by collecting display with low monomer binding population. In round 4, we performed FACS with QD-tau conjugate but at lower QD-tau concentration (reduced by 60%). Next, we amplified the antibody genes from our library by PCR, cloned them into soluble antibody expression plasmids, expressed the antibody as Fc-fusion proteins and evaluated them. We found that several of our affinity matured antibodies show higher affinity (EC_{50} - 0.2-1 nM) than wild type antibody ATA1 (EC_{50} – 10 nM). Interestingly, our affinity matured antibodies also showed affinity similar or higher than clinical antibody Zagotanemab (EC_{50} – 0.5 nM) (Fig. 3-3A). We next evaluated our antibodies for conformational specificity in monomer competition assay as described in Chapter 2. We find that all our antibodies including the wild type and affinity matured variants retained the highest levels of conformational specificity similar to reagent antibody TNT1 and clinical antibody Zagotanemab (Fig. 3-3B). These are two of the most conformational antibodies reported for tau amyloid aggregates. Next, we evaluated off-target binding for our clones by evaluating their binding to PSR. We observed that our antibodies show low levels of PSR binding only modestly higher than Elotuzumab (Fig. 3-3C).

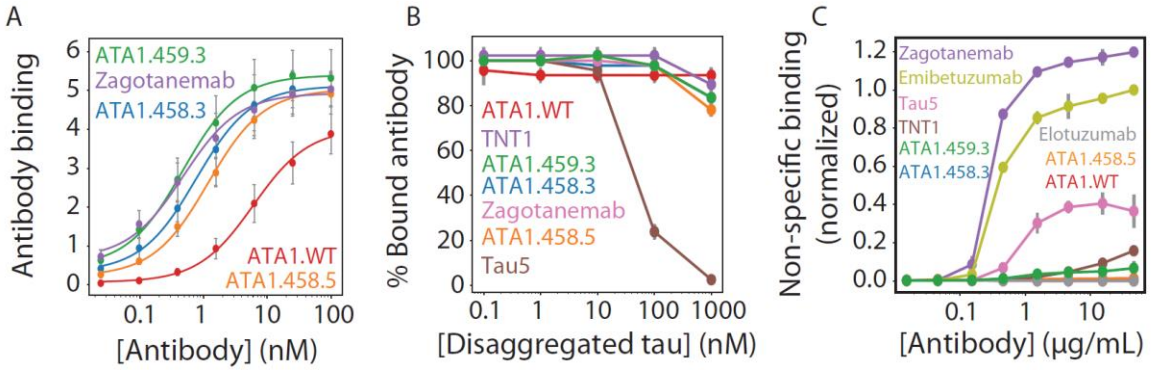

Figure 3-3: Binding analysis of tau antibodies.
Bead based affinity (A), conformational specificity (B) analysis of anti-tau antibodies; ATA1,WT (wild type), affinity matured clones ATA1.458.3, 458.5, 459.3 and clinical antibody Zagotanemab and reagent antibody TNT1. (C) Off-target/PSR binding analysis of anti-tau antibodies compared to control clinical antibody Emibetuzumab and approved drug Elotuzumab. In (B) we report the median values from two independent repeats and the error bars are standard deviation.

Discussion and future work

We were able to successfully isolate and engineer conformational antibodies against tau and α-synuclein protein aggregates. Such antibodies could be used for both therapeutic and diagnostic applications in additional to further our understanding diseases' pathology. Although, conformational antibodies are not trivial to isolate, their importance to this field seems underappreciated. We have discovered novel strategies to isolate conformational antibodies which showed sets of properties similar or better than several clinical stage antibodies. Our tau antibodies how similar affinity (EC_{50} values of ~0.5-1 nM) and conformational specificity to clinical antibody Zagotanemab. Our α-synuclein antibodies show similar affinity (EC_{50} values of ~10-20 nM) but superior conformational specificity to clinical antibody Cinpanemab. We hope such systematic selection tools would speed the screening and selection of high affinity and conformational antibodies against amyloid aggregates.

There are multiple aspects of our work which would be highly interesting to pursue. It would be very informative to evaluate the binding epitope of these antibodies since they bind to conformational epitope. It would be interesting to see if our antibodies recognize a novel epitope or ones already reported in literature. Next, it would be exciting to check if our antibodies can bind to pathological aggregates from transgenic mice. We do have some evidence for our tau and α-synuclein antibodies recognizing pathological fibrils from transgenic mice in immunodot blot assay (data not shown), these experiments would need to be repeated to make sure the results are reproducible. Ultimately, evaluating these antibodies against pathological fibrils from human brain tissue in different assay formats like immunodot blots, western blots and immunofluorescence would be the final test.as it has been shown that pathological fibrils from transgenic mice and human brains have different structures.

Antibody specificity is a poorly defined concept since it depends on the nature of non-specificity molecule being using. We define non-specificity as binding to PSR which is a complex mixture of proteins, lipids, carbohydrates from CHO cell membranes (63,96). Our conformational anti-α-synuclein antibody aS2.1 seems to have modest PSR binding. A possible reason is the Fv (variable domain) net charge which has been to be a strong determinant of an antibody's non-specificity (64). Many of clinical stage antibodies and drugs with low levels of non-specificity have Fv charge of +1.5±2.5 (52,96) and the charge of aS2.1 is +4.1. In comparison, our tau antibodies have a range of Fv charge +1-5.1 but have low levels of PSR binding. This would suggest that in addition to charge which mainly contributes to electrostatics interactions, other modes of interactions like hydrophobic, hydrogen bonding, van der Waals's might also be playing an important in governing specificity of these antibodies. Detailed animal experiments will have to be performed to determine the pharmacodynamics properties of these antibodies.

Conformational anti-α-synuclein antibody aS2.1 has high affinity, but it would be very attractive to perform affinity maturation to further improve it. Surprisingly, this antibody was isolated during initial discovery using a human non-immune library from initial discovery campaign. It would serve as a high-quality lead for further affinity maturation. It is also worth considering methods for reducing the non-specific binding for this antibody during affinity maturation. This can be potentially performed in multiple different ways but the easiest and the most effective way would be to perform negative selection again PSR reagent and incorporate it during the affinity selections. The goal would be to further improve the affinity and off-target binding for this antibody while maintaining the conformational specificity which are the some of the properties we look for in therapeutic antibodies.

Contributions

I would like to thank several members of the Tessier Lab including Jennifer M. Zupancic, Matthew D. Smith, Emily K. Makowski, Yulei Zhang, Jie Huang and Hongwei Chen for their help with this project.

References

1. Tiller, K. E., and Tessier, P. M. (2015) Advances in Antibody Design. *Annu Rev Biomed Eng* **17**, 191-216

2. Kaplon, H., and Reichert, J. M. (2021) Antibodies to watch in 2021. *MAbs* **13**, 1860476

3. Rabia, L. A., Desai, A. A., Jhajj, H. S., and Tessier, P. M. (2018) Understanding and overcoming trade-offs between antibody affinity, specificity, stability and solubility. *Biochem Eng J* **137**, 365-374

4. Nelson, A. L. (2010) Antibody fragments: hope and hype. *MAbs* **2**, 77-83

5. Xenaki, K. T., Oliveira, S., and van Bergen En Henegouwen, P. M. P. (2017) Antibody or Antibody Fragments: Implications for Molecular Imaging and Targeted Therapy of Solid Tumors. *Front Immunol* **8**, 1287

6. Murphy, M. P., and LeVine, H., 3rd. (2010) Alzheimer's disease and the amyloid-beta peptide. *Journal of Alzheimer's disease : JAD* **19**, 311-323

7. Kovacs, G. G. (2015) Invited review: Neuropathology of tauopathies: principles and practice. *Neuropathol Appl Neurobiol* **41**, 3-23

8. Martí, M. J., Tolosa, E., and Campdelacreu, J. (2003) Clinical overview of the synucleinopathies. *Mov Disord* **18 Suppl 6**, S21-27

9. Long, J. M., and Holtzman, D. M. (2019) Alzheimer Disease: An Update on Pathobiology and Treatment Strategies. *Cell* **179**, 312-339

10. Haque, S. M., Ashwaq, O., Sarief, A., and Mohamed, A. K. A. J. (2020) A comprehensive review about SARS-CoV-2. *Future Virology* **15**, 625-648

11. Hu, B., Guo, H., Zhou, P., and Shi, Z. L. (2021) Characteristics of SARS-CoV-2 and COVID-19. *Nat Rev Microbiol* **19**, 141-154

12. Chiti, F., and Dobson, C. M. (2017) Protein Misfolding, Amyloid Formation, and Human Disease: A Summary of Progress Over the Last Decade. *Annu Rev Biochem* **86**, 27-68

13. Ross, C. A., and Poirier, M. A. (2004) Protein aggregation and neurodegenerative disease. *Nat Med* **10**, S10-17

14. Glabe, C. G. (2004) Conformation-dependent antibodies target diseases of protein misfolding. *Trends Biochem Sci* **29**, 542-547

15. Droste, P., Frenzel, A., Steinwand, M., Pelat, T., Thullier, P., Hust, M., Lashuel, H., and Dubel, S. (2015) Structural differences of amyloid-beta fibrils revealed by antibodies from phage display. *BMC Biotechnol* **15**, 57

16. Hatami, A., Albay, R., 3rd, Monjazeb, S., Milton, S., and Glabe, C. (2014) Monoclonal antibodies against Abeta42 fibrils distinguish multiple aggregation state polymorphisms in vitro and in Alzheimer disease brain. *J Biol Chem* **289**, 32131-32143

17. Kayed, R., Head, E., Thompson, J. L., McIntire, T. M., Milton, S. C., Cotman, C. W., and Glabe, C. G. (2003) Common Structure of Soluble Amyloid Oligomers Implies Common Mechanism of Pathogenesis. *Science* **300**, 486-489

18. Kanaan, N. M., Cox, K., Alvarez, V. E., Stein, T. D., Poncil, S., and McKee, A. C. (2016) Characterization of Early Pathological Tau Conformations and Phosphorylation in Chronic Traumatic Encephalopathy. *J Neuropathol Exp Neurol* **75**, 19-34

19. Bonito-Oliva, A., Schedin-Weiss, S., Younesi, S. S., Tiiman, A., Adura, C., Paknejad, N., Brendel, M., Romin, Y., Parchem, R. J., Graff, C., Vukojevic, V., Tjernberg, L. O., Terenius, L., Winblad, B., Sakmar, T. P., and Graham, W. V. (2019) Conformation-specific antibodies against multiple amyloid protofibril species from a single amyloid immunogen. *J Cell Mol Med* **23**, 2103-2114

20. Combs, B., Hamel, C., and Kanaan, N. M. (2016) Pathological conformations involving the amino terminus of tau occur early in Alzheimer's disease and are differentially detected by monoclonal antibodies. *Neurobiol Dis* **94**, 18-31

21. Kanaan, N. M., Morfini, G. A., LaPointe, N. E., Pigino, G. F., Patterson, K. R., Song, Y., Andreadis, A., Fu, Y., Brady, S. T., and Binder, L. I. (2011) Pathogenic forms of tau inhibit kinesin-dependent axonal transport through a mechanism involving activation of axonal phosphotransferases. *J Neurosci* **31**, 9858-9868

22. Bodani, R. U., Sengupta, U., Castillo-Carranza, D. L., Guerrero-Munoz, M. J., Gerson, J. E., Rudra, J., and Kayed, R. (2015) Antibody against Small Aggregated Peptide Specifically Recognizes Toxic Abeta-42 Oligomers in Alzheimer's Disease. *ACS Chem Neurosci* **6**, 1981-1989

23. Lasagna-Reeves, C. A., Castillo-Carranza, D. L., Sengupta, U., Sarmiento, J., Troncoso, J., Jackson, G. R., and Kayed, R. (2012) Identification of oligomers at early stages of tau aggregation in Alzheimer's disease. *FASEB J* **26**, 1946-1959

24. Weihofen, A., Liu, Y., Arndt, J. W., Huy, C., Quan, C., Smith, B. A., Baeriswyl, J. L., Cavegn, N., Senn, L., Su, L., Marsh, G., Auluck, P. K., Montrasio, F., Nitsch, R. M., Hirst, W. D., Cedarbaum, J. M., Pepinsky, R. B., Grimm, J., and Weinreb, P. H. (2019) Development of an aggregate-selective, human-derived alpha-synuclein antibody BIIB054 that ameliorates disease phenotypes in Parkinson's disease models. *Neurobiol Dis* **124**, 276-288

25. Arndt, J. W., Qian, F., Smith, B. A., Quan, C., Kilambi, K. P., Bush, M. W., Walz, T., Pepinsky, R. B., Bussiere, T., Hamann, S., Cameron, T. O., and Weinreb, P. H. (2018) Structural and kinetic basis for the selectivity of aducanumab for aggregated forms of amyloid-beta. *Sci Rep* **8**, 6412

26. Sevigny, J., Chiao, P., Bussiere, T., Weinreb, P. H., Williams, L., Maier, M., Dunstan, R., Salloway, S., Chen, T., Ling, Y., O'Gorman, J., Qian, F., Arastu, M., Li, M., Chollate, S., Brennan, M. S., Quintero-Monzon, O., Scannevin, R. H., Arnold, H. M., Engber, T., Rhodes, K., Ferrero, J., Hang, Y., Mikulskis, A., Grimm, J., Hock, C., Nitsch, R. M., and Sandrock, A. (2016) The antibody aducanumab reduces Abeta plaques in Alzheimer's disease. *Nature* **537**, 50-56

27. Castillo-Carranza, D. L., Sengupta, U., Guerrero-Munoz, M. J., Lasagna-Reeves, C. A., Gerson, J. E., Singh, G., Estes, D. M., Barrett, A. D., Dineley, K. T., Jackson, G. R., and Kayed, R. (2014) Passive immunization with Tau oligomer monoclonal antibody reverses tauopathy phenotypes without affecting hyperphosphorylated neurofibrillary tangles. *J Neurosci* **34**, 4260-4272

28. Gong, Y., Chang, L., Viola, K. L., Lacor, P. N., Lambert, M. P., Finch, C. E., Krafft, G. A., and Klein, W. L. (2003) Alzheimer's disease-affected brain: presence of oligomeric A beta ligands (ADDLs) suggests a molecular basis for reversible memory loss. *Proc Natl Acad Sci U S A* **100**, 10417-10422

29. Lambert, M. P., Velasco, P. T., Chang, L., Viola, K. L., Fernandez, S., Lacor, P. N., Khuon, D., Gong, Y., Bigio, E. H., Shaw, P., De Felice, F. G., Krafft, G. A., and Klein, W. L. (2007) Monoclonal antibodies that target pathological assemblies of Abeta. *J Neurochem* **100**, 23-35

30. Lambert, M. P., Viola, K. L., Chromy, B. A., Chang, L., Morgan, T. E., Yu, J., Venton, D. L., Krafft, G. A., Finch, C. E., and Klein, W. L. (2001) Vaccination with soluble Aβ oligomers generates toxicity-neutralizing antibodies. *Journal of Neurochemistry* **79**, 595-605

31. Kayed, R., Head, E., Sarsoza, F., Saing, T., Cotman, C. W., Necula, M., Margol, L., Wu, J., Breydo, L., Thompson, J. L., Rasool, S., Gurlo, T., Butler, P., and Glabe, C. G. (2007) Fibril specific, conformation dependent antibodies recognize a generic epitope common to amyloid fibrils and fibrillar oligomers that is absent in prefibrillar oligomers. *Mol Neurodegener* **2**, 18

32. Gibbons, G. S., Kim, S. J., Robinson, J. L., Changolkar, L., Irwin, D. J., Shaw, L. M., Lee, V. M., and Trojanowski, J. Q. (2019) Detection of Alzheimer's disease (AD) specific tau pathology with conformation-selective anti-tau monoclonal antibody in co-morbid frontotemporal lobar degeneration-tau (FTLD-tau). *Acta Neuropathol Commun* **7**, 34

33. Covell, D. J., Robinson, J. L., Akhtar, R. S., Grossman, M., Weintraub, D., Bucklin, H. M., Pitkin, R. M., Riddle, D., Yousef, A., Trojanowski, J. Q., and Lee, V. M. (2017) Novel conformation-selective alpha-synuclein antibodies raised against different in vitro fibril

forms show distinct patterns of Lewy pathology in Parkinson's disease. *Neuropathol Appl Neurobiol* **43**, 604-620

34. Julian, M. C., Rabia, L. A., Desai, A. A., Arsiwala, A., Gerson, J. E., Paulson, H. L., Kane, R. S., and Tessier, P. M. (2019) Nature-inspired design and evolution of anti-amyloid antibodies. *J Biol Chem* **294**, 8438-8451

35. Stimple, S. D., Kalyoncu, S., Desai, A. A., Mogensen, J. E., Spang, L. T., Asgreen, D. J., Staby, A., and Tessier, P. M. (2019) Sensitive detection of glucagon aggregation using amyloid fibril-specific antibodies. *Biotechnol Bioeng* **116**, 1868-1877

36. Munke, A., Persson, J., Weiffert, T., De Genst, E., Meisl, G., Arosio, P., Carnerup, A., Dobson, C. M., Vendruscolo, M., Knowles, T. P. J., and Linse, S. (2017) Phage display and kinetic selection of antibodies that specifically inhibit amyloid self-replication. *Proceedings of the National Academy of Sciences* **114**, 6444-6449

37. Sebollela, A., Cline, E. N., Popova, I., Luo, K., Sun, X., Ahn, J., Barcelos, M. A., Bezerra, V. N., Lyra, E. S. N. M., Patel, J., Pinheiro, N. R., Qin, L. A., Kamel, J. M., Weng, A., DiNunno, N., Bebenek, A. M., Velasco, P. T., Viola, K. L., Lacor, P. N., Ferreira, S. T., and Klein, W. L. (2017) A human scFv antibody that targets and neutralizes high molecular weight pathogenic amyloid-beta oligomers. *J Neurochem* **142**, 934-947

38. Lee, C. C., Julian, M. C., Tiller, K. E., Meng, F., DuConge, S. E., Akter, R., Raleigh, D. P., and Tessier, P. M. (2016) Design and Optimization of Anti-amyloid Domain Antibodies Specific for beta-Amyloid and Islet Amyloid Polypeptide. *J Biol Chem* **291**, 2858-2873

39. Silverman, J. M., Gibbs, E., Peng, X., Martens, K. M., Balducci, C., Wang, J., Yousefi, M., Cowan, C. M., Lamour, G., Louadi, S., Ban, Y., Robert, J., Stukas, S., Forloni, G., Hsiung, G. R., Plotkin, S. S., Wellington, C. L., and Cashman, N. R. (2018) A Rational Structured Epitope Defines a Distinct Subclass of Toxic Amyloid-beta Oligomers. *ACS Chem Neurosci* **9**, 1591-1606

40. Gibbs, E., Silverman, J. M., Zhao, B., Peng, X., Wang, J., Wellington, C. L., Mackenzie, I. R., Plotkin, S. S., Kaplan, J. M., and Cashman, N. R. (2019) A Rationally Designed Humanized Antibody Selective for Amyloid Beta Oligomers in Alzheimer's Disease. *Sci Rep* **9**, 9870

41. Perchiacca, J. M., Ladiwala, A. R., Bhattacharya, M., and Tessier, P. M. (2012) Structure-based design of conformation- and sequence-specific antibodies against amyloid beta. *Proc Natl Acad Sci U S A* **109**, 84-89

42. Aprile, F. A., Sormanni, P., Podpolny, M., Chhangur, S., Needham, L. M., Ruggeri, F. S., Perni, M., Limbocker, R., Heller, G. T., Sneideris, T., Scheidt, T., Mannini, B., Habchi, J., Lee, S. F., Salinas, P. C., Knowles, T. P. J., Dobson, C. M., and Vendruscolo, M. (2020) Rational design of a conformation-specific antibody for the quantification of Abeta oligomers. *Proc Natl Acad Sci U S A*, ePub June 3

43. Kulenkampff, K., Aprile, F. A., Sormanni, P., Ranasinghe, R. T., Klenerman, D., and Vendruscolo, M. (2020) Rational Design of Conformation-Specific Antibodies for Tau Oligomers. *Biophysical Journal* **118**, 370a-371a

44. Vaikath, N. N., Majbour, N. K., Paleologou, K. E., Ardah, M. T., van Dam, E., van de Berg, W. D., Forrest, S. L., Parkkinen, L., Gai, W. P., Hattori, N., Takanashi, M., Lee, S. J., Mann, D. M., Imai, Y., Halliday, G. M., Li, J. Y., and El-Agnaf, O. M. (2015) Generation and characterization of novel conformation-specific monoclonal antibodies for alpha-synuclein pathology. *Neurobiol Dis* **79**, 81-99

45. Gibbons, G. S., Banks, R. A., Kim, B., Changolkar, L., Riddle, D. M., Leight, S. N., Irwin, D. J., Trojanowski, J. Q., and Lee, V. M. Y. (2018) Detection of Alzheimer Disease (AD)-Specific Tau Pathology in AD and NonAD Tauopathies by Immunohistochemistry With Novel Conformation-Selective Tau Antibodies. *J Neuropathol Exp Neurol* **77**, 216-228

46. Tiller, K. E., Chowdhury, R., Li, T., Ludwig, S. D., Sen, S., Maranas, C. D., and Tessier, P. M. (2017) Facile Affinity Maturation of Antibody Variable Domains Using Natural Diversity Mutagenesis. *Front Immunol* **8**, 986

47. Jain, T., Sun, T., Durand, S., Hall, A., Houston, N. R., Nett, J. H., Sharkey, B., Bobrowicz, B., Caffry, I., Yu, Y., Cao, Y., Lynaugh, H., Brown, M., Baruah, H., Gray, L. T., Krauland, E. M., Xu, Y., Vasquez, M., and Wittrup, K. D. (2017) Biophysical properties of the clinical-stage antibody landscape. *Proc Natl Acad Sci U S A* **114**, 944-949

48. Swindells, M. B., Porter, C. T., Couch, M., Hurst, J., Abhinandan, K. R., Nielsen, J. H., Macindoe, G., Hetherington, J., and Martin, A. C. (2017) abYsis: Integrated Antibody Sequence and Structure-Management, Analysis, and Prediction. *J Mol Biol* **429**, 356-364

49. Rabia, L. A., Zhang, Y., Ludwig, S. D., Julian, M. C., and Tessier, P. M. (2018) Net charge of antibody complementarity-determining regions is a key predictor of specificity. *Protein Eng Des Sel* **31**, 409-418

50. Fellouse, F. A., Wiesmann, C., and Sidhu, S. S. (2004) Synthetic antibodies from a four-amino-acid code: a dominant role for tyrosine in antigen recognition. *Proc Natl Acad Sci U S A* **101**, 12467-12472

51. Tiller, K. E., Li, L., Kumar, S., Julian, M. C., Garde, S., and Tessier, P. M. (2017) Arginine mutations in antibody complementarity-determining regions display context-dependent affinity/specificity trade-offs. *J Biol Chem* **292**, 16638-16652

52. Zhang, Y., Wu, L., Gupta, P., Desai, A. A., Smith, M. D., Rabia, L. A., Ludwig, S. D., and Tessier, P. M. (2020) Physicochemical rules for identifying monoclonal antibodies with drug-like specificity. *Mol Pharm*, ePub May 26

53. Datta-Mannan, A., Thangaraju, A., Leung, D., Tang, Y., Witcher, D. R., Lu, J., and Wroblewski, V. J. (2015) Balancing charge in the complementarity-determining regions of humanized mAbs without affecting pI reduces non-specific binding and improves the pharmacokinetics. *MAbs* **7**, 483-493

54. Wardemann, H., Yurasov, S., Schaefer, A., Young, J. W., Meffre, E., and Nussenzweig, M. C. (2003) Predominant Autoantibody Production by Early Human B Cell Precursors. *Science* **301**, 1374-1377

55. Hong, G., Chappey, O., Niel, E., and Scherrmann, J. M. (2000) Enhanced cellular uptake and transport of polyclonal immunoglobulin G and fab after their cationization. *J Drug Target* **8**, 67-77

56. Datta-Mannan, A., Lu, J., Witcher, D. R., Leung, D., Tang, Y., and Wroblewski, V. J. (2015) The interplay of non-specific binding, target-mediated clearance and FcRn interactions on the pharmacokinetics of humanized antibodies. *MAbs* **7**, 1084-1093

57. Birtalan, S., Fisher, R. D., and Sidhu, S. S. (2010) The functional capacity of the natural amino acids for molecular recognition. *Mol Biosyst* **6**, 1186-1194

58. Arndt, J. W., Qian, F., Smith, B. A., Quan, C., Kilambi, K. P., Bush, M. W., Walz, T., Pepinsky, R. B., Bussière, T., Hamann, S., Cameron, T. O., and Weinreb, P. H. (2018) Structural and kinetic basis for the selectivity of aducanumab for aggregated forms of amyloid-β. *Sci Rep* **8**, 6412

59. van Dyck, C. H. (2018) Anti-Amyloid-beta Monoclonal Antibodies for Alzheimer's Disease: Pitfalls and Promise. *Biol Psychiatry* **83**, 311-319

60. Spencer, S., Bethea, D., Raju, T. S., Giles-Komar, J., and Feng, Y. (2012) Solubility evaluation of murine hybridoma antibodies. *MAbs* **4**, 319-325

61. Bradbury, A. R., Sidhu, S., Dubel, S., and McCafferty, J. (2011) Beyond natural antibodies: the power of in vitro display technologies. *Nat Biotechnol* **29**, 245-254

62. Johan, N., Peter, M. T., and Sachdev, S. S. (2016) Engineered Autonomous Human Variable Domains. *Curr Pharm Des* **22**, 6527-6537

63. Xu, Y., Roach, W., Sun, T., Jain, T., Prinz, B., Yu, T. Y., Torrey, J., Thomas, J., Bobrowicz, P., Vasquez, M., Wittrup, K. D., and Krauland, E. (2013) Addressing polyspecificity of antibodies selected from an in vitro yeast presentation system: a FACS-based, high-throughput selection and analytical tool. *Protein Eng Des Sel* **26**, 663-670

64. Kelly, R. L., Sun, T., Jain, T., Caffry, I., Yu, Y., Cao, Y., Lynaugh, H., Brown, M., Vasquez, M., Wittrup, K. D., and Xu, Y. (2015) High throughput cross-interaction measures for human IgG1 antibodies correlate with clearance rates in mice. *MAbs* **7**, 770-777

65. Alam, M. E., Slaney, T. R., Wu, L., Das, T. K., Kar, S., Barnett, G. V., Leone, A., and Tessier, P. M. (2020) Unique Impacts of Methionine Oxidation, Tryptophan Oxidation, and Asparagine Deamidation on Antibody Stability and Aggregation. *J Pharm Sci* **109**, 656-669

66. Cromwell, M. E. M., Hilario, E., and Jacobson, F. (2006) Protein aggregation and bioprocessing. *AAPS J* **8**, E572-E579

67. Hober, S., Nord, K., and Linhult, M. (2007) Protein A chromatography for antibody purification. *J Chromatogr B Analyt Technol Biomed Life Sci* **848**, 40-47

68. Shukla, A. A., Gupta, P., and Han, X. (2007) Protein aggregation kinetics during Protein A chromatography. Case study for an Fc fusion protein. *J Chromatogr A* **1171**, 22-28

69. Ejima, D., Tsumoto, K., Fukada, H., Yumioka, R., Nagase, K., Arakawa, T., and Philo, J. S. (2007) Effects of acid exposure on the conformation, stability, and aggregation of monoclonal antibodies. *Proteins* **66**, 954-962

70. Hari, S. B., Lau, H., Razinkov, V. I., Chen, S., and Latypov, R. F. (2010) Acid-induced aggregation of human monoclonal IgG1 and IgG2: molecular mechanism and the effect of solution composition. *Biochemistry* **49**, 9328-9338

71. Julian, M. C., Li, L., Garde, S., Wilen, R., and Tessier, P. M. (2017) Efficient affinity maturation of antibody variable domains requires co-selection of compensatory mutations to maintain thermodynamic stability. *Sci Rep* **7**, 45259

72. Julian, M. C., Lee, C. C., Tiller, K. E., Rabia, L. A., Day, E. K., Schick, A. J., 3rd, and Tessier, P. M. (2015) Co-evolution of affinity and stability of grafted amyloid-motif domain antibodies. *Protein Eng Des Sel* **28**, 339-350

73. Boswell, C. A., Tesar, D. B., Mukhyala, K., Theil, F.-P., Fielder, P. J., and Khawli, L. A. (2010) Effects of Charge on Antibody Tissue Distribution and Pharmacokinetics. *Bioconjug Chem* **21**, 2153-2163

74. Dobson, C. L., Devine, P. W., Phillips, J. J., Higazi, D. R., Lloyd, C., Popovic, B., Arnold, J., Buchanan, A., Lewis, A., Goodman, J., van der Walle, C. F., Thornton, P., Vinall, L., Lowne, D., Aagaard, A., Olsson, L. L., Ridderstad Wollberg, A., Welsh, F., Karamanos, T. K., Pashley, C. L., Iadanza, M. G., Ranson, N. A., Ashcroft, A. E., Kippen, A. D., Vaughan, T. J., Radford, S. E., and Lowe, D. C. (2016) Engineering the surface properties of a human monoclonal antibody prevents self-association and rapid clearance in vivo. *Sci Rep* **6**, 38644

75. Starr, C. G., and Tessier, P. M. (2019) Selecting and engineering monoclonal antibodies with drug-like specificity. *Curr Opin Biotechnol* **60**, 119-127

76. Birtalan, S., Zhang, Y., Fellouse, F. A., Shao, L., Schaefer, G., and Sidhu, S. S. (2008) The intrinsic contributions of tyrosine, serine, glycine and arginine to the affinity and specificity of antibodies. *J Mol Biol* **377**, 1518-1528

77. Pardridge, W. M. (2015) Blood-brain barrier drug delivery of IgG fusion proteins with a transferrin receptor monoclonal antibody. *Expert Opin Drug Deliv* **12**, 207-222

78. Jones, A. R., and Shusta, E. V. (2007) Blood-brain barrier transport of therapeutics via receptor-mediation. *Pharm Res* **24**, 1759-1771

79. Pardridge, W. M. (2017) Delivery of Biologics Across the Blood-Brain Barrier with Molecular Trojan Horse Technology. *BioDrugs* **31**, 503-519

80. Chung, S., Nguyen, V., Lin, Y. L., Lafrance-Vanasse, J., Scales, S. J., Lin, K., Deng, R., Williams, K., Sperinde, G., Li, J. J., Zheng, K., Sukumaran, S., Tesar, D., Ernst, J. A., Fischer, S., Lazar, G. A., Prabhu, S., and Song, A. (2019) An in vitro FcRn- dependent transcytosis assay as a screening tool for predictive assessment of nonspecific clearance of antibody therapeutics in humans. *MAbs* **11**, 942-955

81. Triguero, D., Buciak, J. B., Yang, J., and Pardridge, W. M. (1989) Blood-brain barrier transport of cationized immunoglobulin G: enhanced delivery compared to native protein. *Proceedings of the National Academy of Sciences* **86**, 4761-4765

82. Pardridge, W. M., Bickel, U., Buciak, J., Yang, J., Diagne, A., and Aepinus, C. (1994) Cationization of a monoclonal antibody to the human immunodeficiency virus REV protein enhances cellular uptake but does not impair antigen binding of the antibody. *Immunology letters* **42**, 191-195

83. Triguero, D., Buciak, J. B., Yang, J., and Pardridge, W. M. (1989) Blood-brain barrier transport of cationized immunoglobulin G: enhanced delivery compared to native protein. *Proc Natl Acad Sci U S A* **86**, 4761-4765

84. Zago, W., Schroeter, S., Guido, T., Khan, K., Seubert, P., Yednock, T., Schenk, D., Gregg, K. M., Games, D., Bard, F., and Kinney, G. G. (2013) Vascular alterations in PDAPP mice after anti-Abeta immunotherapy: Implications for amyloid-related imaging abnormalities. *Alzheimers Dement* **9**, S105-115

85. Barkhof, F., Daams, M., Scheltens, P., Brashear, H. R., Arrighi, H. M., Bechten, A., Morris, K., McGovern, M., and Wattjes, M. P. (2013) An MRI rating scale for amyloid-related imaging abnormalities with edema or effusion. *AJNR Am J Neuroradiol* **34**, 1550-1555

86. Sperling, R., Salloway, S., Brooks, D. J., Tampieri, D., Barakos, J., Fox, N. C., Raskind, M., Sabbagh, M., Honig, L. S., Porsteinsson, A. P., Lieberburg, I., Arrighi, H. M., Morris, K. A., Lu, Y., Liu, E., Gregg, K. M., Brashear, H. R., Kinney, G. G., Black, R., and Grundman, M. (2012) Amyloid-related imaging abnormalities in patients with Alzheimer's disease treated with bapineuzumab: a retrospective analysis. *Lancet Neurol* **11**, 241-249

87. Pardridge, W. M. (2016) Re-engineering therapeutic antibodies for Alzheimer's disease as blood-brain barrier penetrating bi-specific antibodies. *Expert Opin Biol Ther* **16**, 1455-1468

88. Sumbria, R. K., Hui, E. K., Lu, J. Z., Boado, R. J., and Pardridge, W. M. (2013) Disaggregation of amyloid plaque in brain of Alzheimer's disease transgenic mice with daily subcutaneous administration of a tetravalent bispecific antibody that targets the transferrin receptor and the Abeta amyloid peptide. *Mol Pharm* **10**, 3507-3513

89. Niewoehner, J., Bohrmann, B., Collin, L., Urich, E., Sade, H., Maier, P., Rueger, P., Stracke, J. O., Lau, W., Tissot, A. C., Loetscher, H., Ghosh, A., and Freskgard, P. O. (2014) Increased brain penetration and potency of a therapeutic antibody using a monovalent molecular shuttle. *Neuron* **81**, 49-60

90. Zuchero, Y. J., Chen, X., Bien-Ly, N., Bumbaca, D., Tong, R. K., Gao, X., Zhang, S., Hoyte, K., Luk, W., Huntley, M. A., Phu, L., Tan, C., Kallop, D., Weimer, R. M., Lu, Y., Kirkpatrick, D. S., Ernst, J. A., Chih, B., Dennis, M. S., and Watts, R. J. (2016) Discovery of Novel Blood-Brain Barrier Targets to Enhance Brain Uptake of Therapeutic Antibodies. *Neuron* **89**, 70-82

91. Benatuil, L., Perez, J. M., Belk, J., and Hsieh, C. M. (2010) An improved yeast transformation method for the generation of very large human antibody libraries. *Protein Eng Des Sel* **23**, 155-159

92. Bushnell, B., Rood, J., and Singer, E. (2017) BBMerge - Accurate paired shotgun read merging via overlap. *PLoS One* **12**, e0185056

93. Cock, P. J., Antao, T., Chang, J. T., Chapman, B. A., Cox, C. J., Dalke, A., Friedberg, I., Hamelryck, T., Kauff, F., Wilczynski, B., and de Hoon, M. J. (2009) Biopython: freely available Python tools for computational molecular biology and bioinformatics. *Bioinformatics* **25**, 1422-1423

94. Yanamandra, K., Kfoury, N., Jiang, H., Mahan, T. E., Ma, S., Maloney, S. E., Wozniak, D. F., Diamond, M. I., and Holtzman, D. M. (2013) Anti-tau antibodies that block tau aggregate seeding in vitro markedly decrease pathology and improve cognition in vivo. *Neuron* **80**, 402-414

95. Desai, A. A., Smith, M. D., Zhang, Y., Makowski, E. K., Gerson, J. E., Ionescu, E., Starr, C. G., Zupancic, J. M., Moore, S. J., Sutter, A. B., Ivanova, M. I., Murphy, G. G., Paulson, H. L., and Tessier, P. M. (2021) Rational affinity maturation of anti-amyloid antibodies with high conformational and sequence specificity. *Journal of Biological Chemistry* **296**, 100508

96. Jain, T., Sun, T., Durand, S., Hall, A., Houston, N. R., Nett, J. H., Sharkey, B., Bobrowicz, B., Caffry, I., Yu, Y., Cao, Y., Lynaugh, H., Brown, M., Baruah, H., Gray, L. T., Krauland, E. M., Xu, Y., Vásquez, M., and Wittrup, K. D. (2017) Biophysical properties of the clinical-stage antibody landscape. *Proceedings of the National Academy of Sciences* **114**, 944-949

Chapter 4 **Directed Evolution Of Potent Neutralizing Nanobodies Against SARS-CoV-2 Using CDR-Swapping Mutagenesis**

Introduction

The COVID-19 pandemic has resulted in widespread interest in developing antibodies and other affinity reagents that recognize the SARS-CoV-2 virus with high affinity and specificity for diagnostic and therapeutic applications. Most antibody generation efforts against SARS-CoV-2 have involved either immunizing animals (Alsoussi et al., 2020; Hanke et al., 2020; Hansen et al., 2020) with the spike (S1) protein [or receptor-binding domain (RBD) thereof] or isolating antigen-specific antibodies from humans after infection and generation of neutralizing antibodies (Hansen et al., 2020; Shi et al., 2020; Wu et al., 2020). These approaches have yielded diverse types of antibodies for sensitive virus detection and potent inhibition of viral infection, including multiple antibodies now being used as therapeutics in humans (Baum et al., 2020a; Chen et al., 2020; Hansen et al., 2020).

Despite the many strengths of *in vivo* antibody generation methods, they possess limitations relative to *in vitro* antibody generation methods, including those that use antibody display technologies such as phage and yeast surface display. The most important limitation is that *in vivo* methods lack the ability to robustly control antigen presentation to the immune system (Boder et al., 2000; Bradbury et al., 2011; Foote and Eisen, 2000; Tiller and Tessier, 2015). This, in turn, limits the ability to use such methods to select antibodies with pre-defined affinities, specificities and functional activities that are optimal for different applications. Even antibodies generated *in*

vivo are commonly affinity matured using *in vitro* display methods to achieve ultra-high affinities and/or cross species reactivities (Jackson et al., 1995).

We have evaluated the potential of directed evolution methods for selecting high-affinity nanobodies against the SARS-CoV-2 spike protein from a nonimmune library (McMahon et al., 2018). In particular, we tested if nanobody variants could be identified that would possess similar or superior affinities and neutralizing activities relative to a potent SARS-CoV-2 neutralizing nanobody (Ty1) generated via immunization [Ty1 (Hanke et al., 2020)] and a potent neutralizing SARS-CoV-2 human antibody isolated after infection [CB6 (Shi et al., 2020)]. Herein, we report an unexpected finding that high-affinity nanobodies can be isolated from nonimmune libraries by complementarity-determining region (CDR) swapping between low-affinity lead clones without additional mutagenesis. We demonstrate that this surprising finding, which was initially discovered by accident due to inadvertent recombination of two low-affinity lead clones, can be easily employed in a systematic manner during initial library sorting to identify high-affinity nanobodies without the need for subsequent affinity maturation.

Results

In vitro discovery and affinity maturation of potent neutralizing nanobodies

A synthetic nanobody library was first systematically sorted to isolate nanobodies that bind to the RBD of the SARS-CoV-2 spike protein S1 subunit (residues V16-R685; GenBank ID QHD43416; Fig. 4-1). This library has been previously reported for use in isolating nanobodies that bind to a diverse range of antigens (McMahon et al., 2018). For use in this study, the library was transferred to a yeast surface display system in which the nanobody N-terminus is linked to Aga2. We found that this Aga2 display system increased the percentage of yeast cells within the library that display nanobodies on the cell surface compared to a GPI anchor display system. The naïve library was first sorted against a soluble biotinylated SARS-CoV-2 RBD via magnetic-activated cell sorting (MACS) to initially enrich the library and reduce the diversity to a level that could be feasibly processed by fluorescence-activated cell sorting (FACS). The enriched library was then sorted by FACS five times against RBD-Fc, biotinylated RBD or spike protein trimer. We found that the use of a bivalent antigen, RBD-Fc, was necessary for the first three rounds of FACS in order to distinguish a clear binding population within the library. Biotinylated RBD or spike protein trimer was used in later rounds of sorting after greater enrichment of a binding population was achieved.

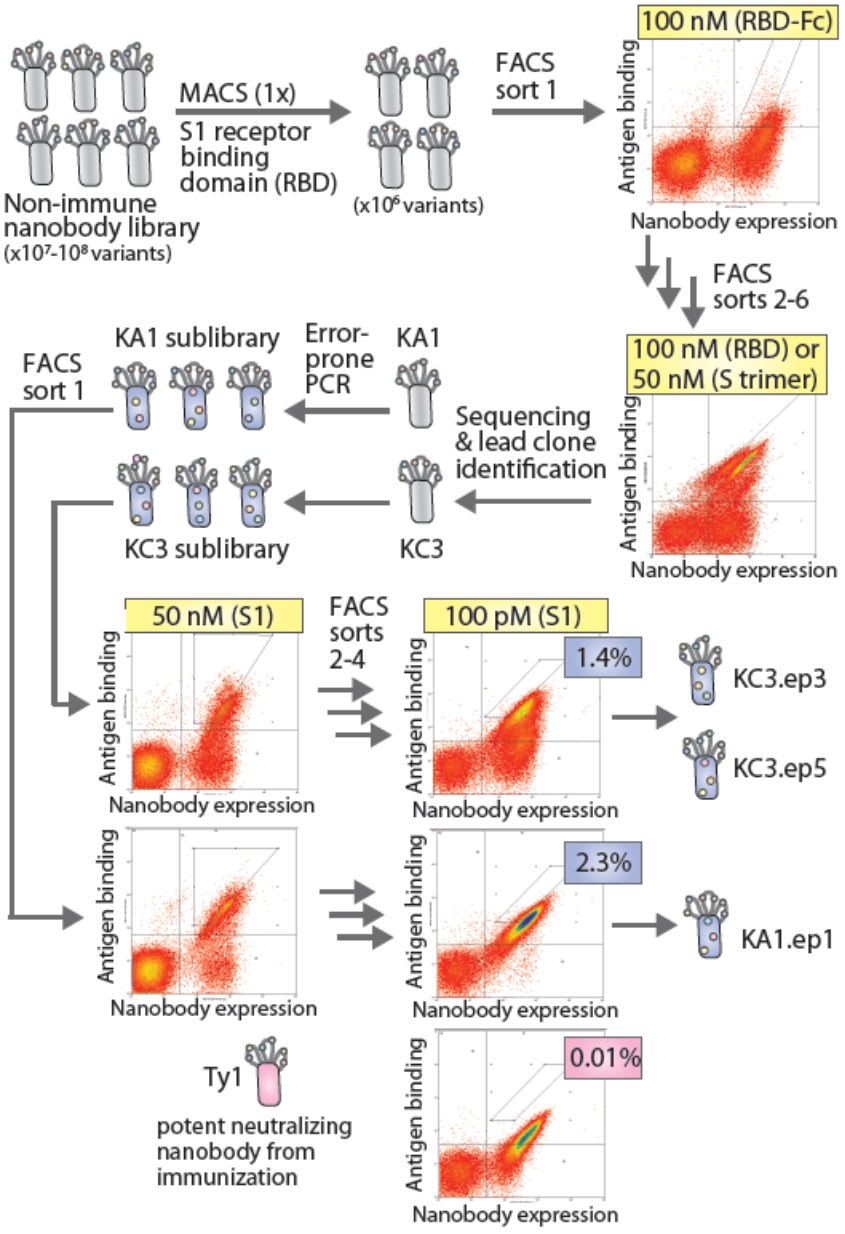

Figure 4-1: Summary of the discovery and affinity maturation of nanobodies against the spike protein of SARS-CoV-2.
A synthetic nanobody library displayed on yeast was screened against the receptor-binding domain (RBD), spike (S1) protein and spike protein trimer of SARS-CoV-2 by MACS and FACS. Two lead clones (KA1 and KC3) were identified, and affinity matured using error-prone PCR. The sub-libraries were screened against the S1 protein by FACS to isolate nanobody variants (KA1.ep1, KC3.ep3 and KC3.ep5) with superior binding activity relative to a potent neutralizing nanobody generated via immunization (Ty1).

Next, unique nanobody sequences that were enriched due to library sorting were identified via Sanger sequencing, expressed on the yeast surface, and tested for binding to biotinylated S1 protein

(50 nM). Two lead clones were selected from a sort against the RBD (KA1) and spike protein trimer (KC3) for further examination and affinity maturation. A third lead clone was also observed in sequencing from the spike protein trimer sort (KC1) which possessed more modest affinity compared to the two selected lead clones. The lead clones have the same frameworks because the library consists of nanobody variants with a common framework and diversity only in all three of the CDRs (McMahon et al., 2018). The two selected lead nanobodies have similar sequences for CDR1 with only one residue difference between them (Fig. 4-2). However, the sequences of CDR2 differ by five residues, and the sequences of HCDR3 differ by eight residues as well as minor differences in length (13 residues for KA1 and 11 residues for KC3).

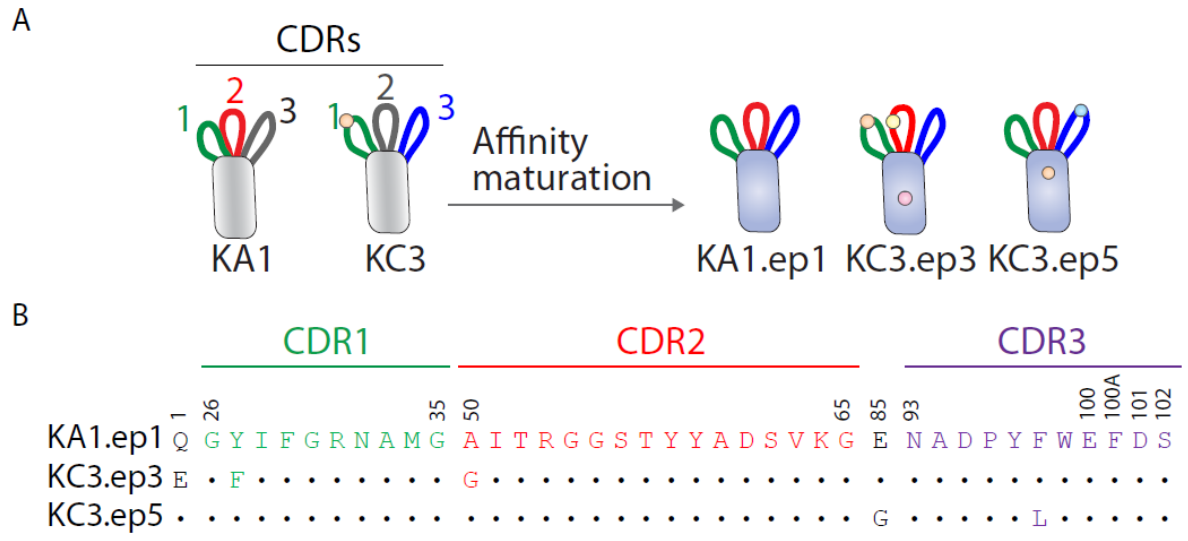

Figure 4-2: Affinity-matured nanobodies possess a combination of CDRs from the two lead clones.
(A) Affinity maturation of lead nanobodies KA1 and KC3 via error-prone PCR results in nanobody variants that possess one CDR from each lead nanobody [CDR2 (red) from KA1 and CDR3 (blue) from KC3] in addition to one CDR [CDR1 (green)] that only differs by a single mutation. (B) Nanobody sequences (Kabat numbering) for the three affinity-matured variants. Residues that are different than KA1.ep1 are indicated with an amino acid letter.

KA1 and KC3 were then affinity matured using error-prone PCR at a low mutational frequency of approximately 1.2-1.5 mutations per nanobody on average (Fig. 4-1). Four rounds of FACS were performed to select for clones with improved affinity for the S1 protein. The concentration

of S1 antigen was decreased in each subsequent round until the library was enriched for superior binding relative to that of a leading SARS-CoV-2 nanobody (Ty1) with potent neutralization activity that was generated via immunization (Hanke et al., 2020). In the final round of sorting, the enriched nanobodies displayed clear binding at 100 pM S1, and the observed binding was stronger than Ty1. Only cells which bound at levels higher than that observed for Ty1 were collected. Clones were isolated from these terminal sorts for analysis and Sanger sequenced. Unexpectedly, all nine unique clones contained CDR2 from KA1 and CDR3 from KC3 (Fig. 4-2), including one clone (KA1.ep1) without any additional mutations in the CDRs or framework regions. KC3.ep3 and KC3.ep5 both contained a few (2-3) additional mutations in their CDRs and frameworks resulting from error-prone PCR (Fig. 4-2). Herein, we refer to the replacement of one or more CDRs in a given nanobody (e.g., CDR2 in nanobody #1) with one or more CDRs from another nanobody (e.g., CDR2 from nanobody #2) as CDR swapping.

CDR-swapped nanobodies display large increases in neutralization activity and affinity

Both lead and affinity-matured clones were next analyzed for their ability to neutralize SARS-CoV-2 infection as nanobody-Fc fusion proteins using a lentivirus-based SARS-CoV-2 pseudovirus assay (Fig. 4-3A). The nanobody-Fc fusion proteins were produced in HEK 293-6E cells and isolated at high purity via Protein A chromatography. Their neutralization activity was directly compared to that of two previously published neutralizers, namely a nanobody [Ty1 (Hanke et al., 2020)] and an antibody [CB6 (Shi et al., 2020)]. Strikingly, the three affinity-matured clones demonstrated dramatic (>300-fold) improvement in neutralization activity relative to their parental nanobodies (Fig. 4-3A). Moreover, the affinity-matured variants displayed complete neutralization at concentrations lower than for Ty1 and CB6. KA1.ep1 (IC_{50} of 4.8±2.6 ng/mL), KC3.ep3 (IC_{50} of 1.9±1.2 ng/mL), and KC3.ep5 (IC_{50} of 2.3±1.3 ng/mL) displayed the lowest IC_{50}

values, with KC3.ep3 being the most potent neutralizer (Fig. 3-3A). The IC_{50} values determined for Ty1 (IC_{50} of 16±7 ng/mL) and CB6 (IC_{50} of 23±6 ng/mL) were comparable to those previously reported for these antibodies (Hanke et al., 2020; Shi et al., 2020).

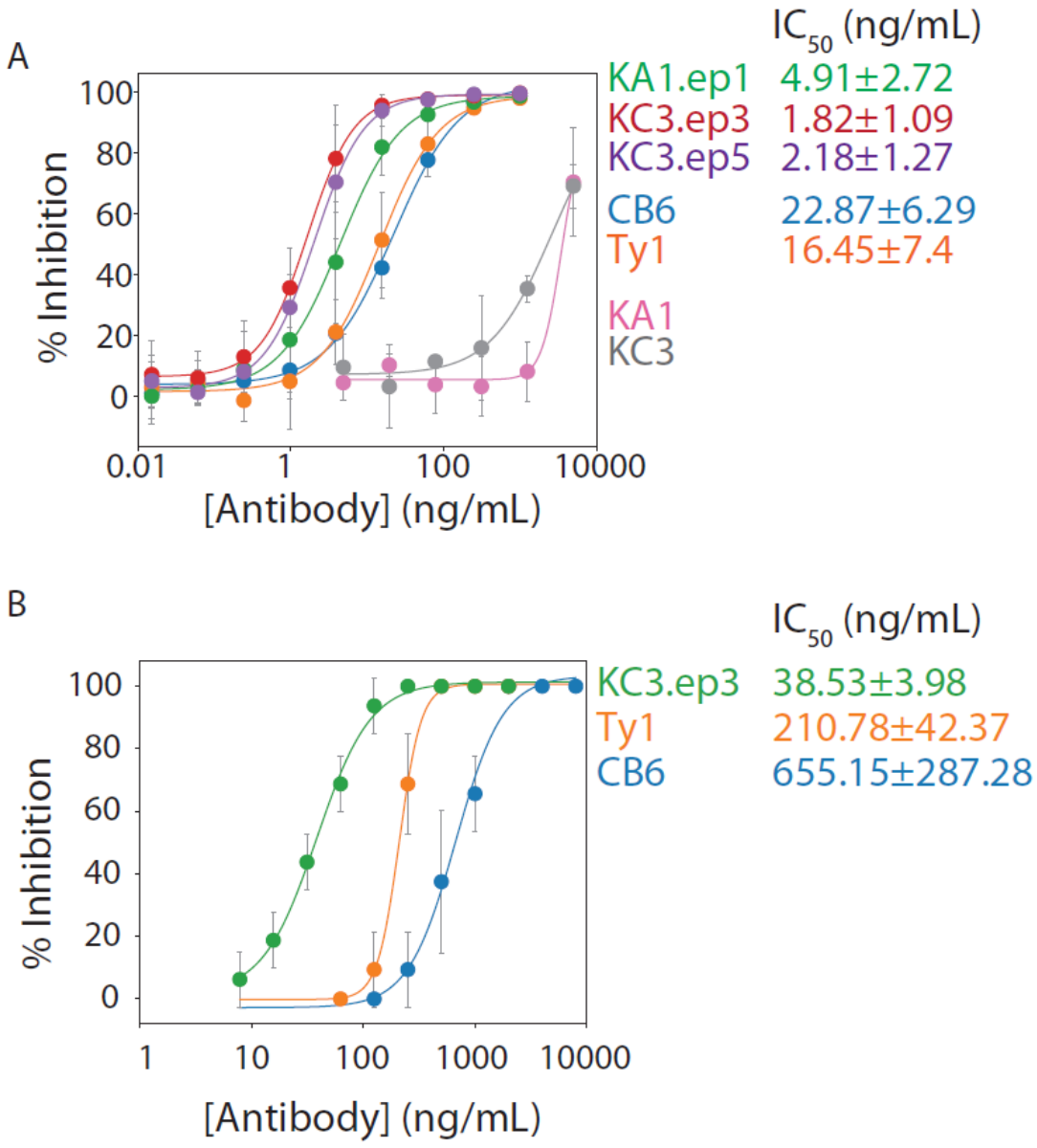

Figure 4-3: Affinity-matured nanobodies potently neutralize SARS-CoV-2 pseudovirus and live virus.
(A) Neutralization results for nanobodies as bivalent Fc-fusion proteins (KA1, KC3, KA1.ep1, KC3.ep3, KC3.ep5 and Ty1) and antibodies (CB6) for inhibiting pseudovirus infectivity in a luciferase-based, HEK293T reporter cell line. Pseudovirus particles were pre-incubated with antibodies, added to reporter cells, and luciferase signal was measured after 48 h. (B) Neutralization results for nanobodies as bivalent Fc-fusion proteins (KC3.ep3, Ty1) and antibodies (CB6) for inhibiting live virus infection of VeroE6 cells. Nanobody and antibody dilutions were tested in eight replicate wells each. After cells were incubated with virus and nanobodies or antibody for 3 d, the cells were examined microscopically for visible cytopathic effect. Wells with any degree of visible, virus-induced cytopathic effect were scored as positive for infection. In (A), the data are averages of 4-5 repeats and the error bars are standard deviations. In (B), the data are averages of 2-4 repeats, and the error bars are standard deviations.

Based on the promising results from the pseudovirus assay, we further examined the neutralization activity of KC3.ep3 and Ty1 (as Fc-fusion proteins) and CB6 (IgG) against live SARS-CoV-2 virus (Fig. 4-3B). Neutralization of the live virus was determined by observing the cytopathic effect of the virus on VeroE6 cells. Measurement of neutralization activity using cytopathic effect has been previously observed to result in higher IC_{50} values than those reported using other detection methods for both live virus and pseudovirus (Shi et al., 2020). Nevertheless, our best affinity-matured variant (KC3.ep3) was significantly more potent at inhibiting the live virus (IC_{50} of 39±4 ng/mL) than Ty1 (IC_{50} of 211±42 ng/mL) and CB6 (IC_{50} of 655±287 ng/mL). These results are consistent with the pseudovirus assay and demonstrate the potent neutralization activity of our CDR-swapped nanobody.

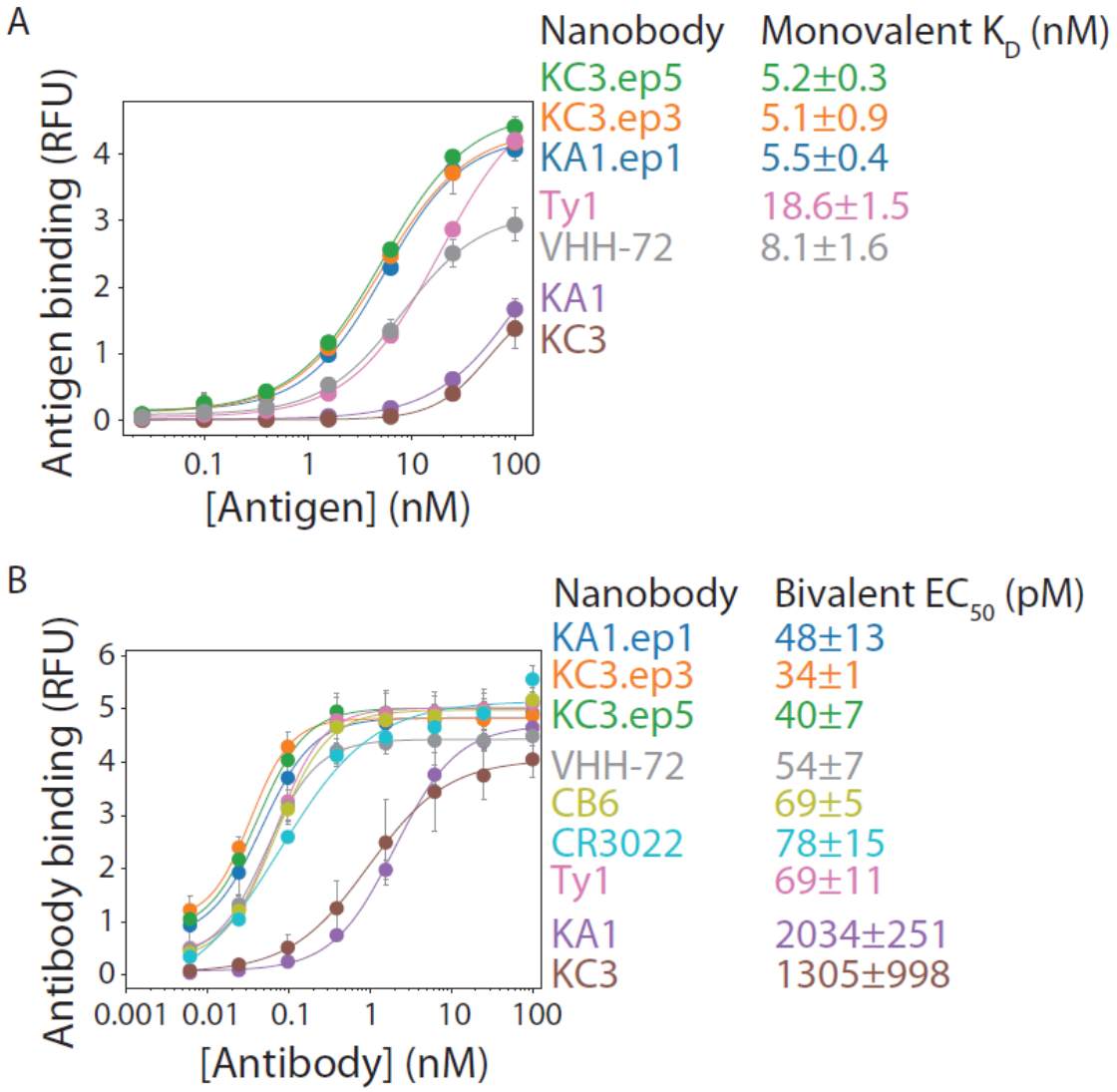

Figure 4-4: Potent neutralizing nanobodies display high monovalent and bivalent affinities for the SARS-CoV-2 receptor-binding domain.
(A) Monovalent binding of nanobodies displayed on the surface of yeast to biotinylated SARS-CoV-2 receptor-binding domain.
(B) Bivalent binding of nanobodies (Fc-fusion proteins) and antibodies to biotinylated SARS-CoV-2 receptor-binding domain immobilized on magnetic beads. The results are averages from three independent experiments and the error bars are standard deviations.

We also characterized the affinities for our matured nanobodies relative to their parental nanobodies in the monovalent and bivalent formats (Fig. 4-4). Monovalent affinities of the nanobodies for the SARS-CoV-2 RBD were examined using yeast surface display (Figs. 4-4A). The different monovalent nanobodies expressed on the yeast surface (as Aga2-nanobody fusions)

at similar levels. Notably, the monovalent affinities of the affinity-matured nanobodies (K_Ds of 5.1-5.5 nM) were superior to leading nanobodies generated *in vivo* (K_Ds of 8-19 nM), and much higher than the parental nanobodies (K_Ds >100 nM). We also observed similar differences for the apparent affinities (EC_{50}s) of bivalent nanobodies (Fig. 4-4B). These latter experiments were performed using nanobodies formatted as soluble Fc-fusion proteins and RBD immobilized on magnetic Dynabeads. The affinity-matured nanobodies displayed stronger binding (EC_{50}s of 34-48 pM) than the previously reported nanobodies (EC_{50}s of 55-69 pM for Ty1 and VHH-72) and antibodies (69-78 pM for CB6 and CR3022), and much stronger binding (>20-fold improved affinity) than the parental nanobodies (>1000 pM for KA1 and KC3). In summary, the affinity-matured nanobodies demonstrate improved monovalent and bivalent affinities compared to leading nanobodies and antibodies generated *in vivo*, which is consistent with their superior neutralization activities.

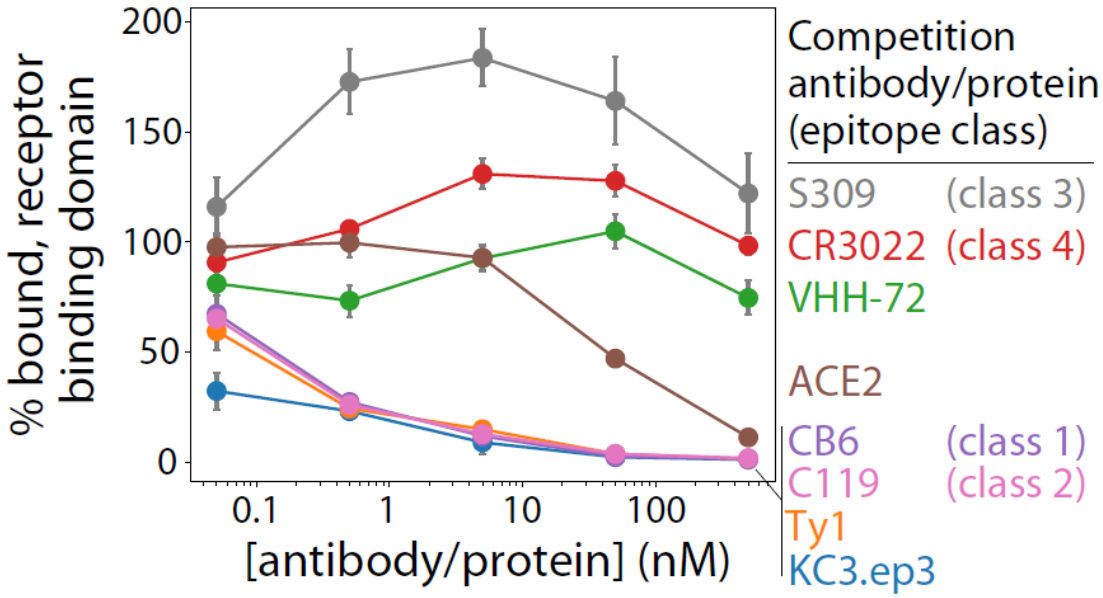

Figure 4-5: Affinity-matured nanobody recognizes an epitope in the receptor-binding domain that overlaps with epitopes recognized by ACE2 and other potent SARS-CoV-2 neutralizing nanobodies and antibodies.
Bivalent nanobodies (KC3.ep3, VHH-72 and Ty1), antibodies (S309, CR3022, CB6 and C119) and ACE2 were pre-incubated with biotinylated receptor-binding domain of SARS-CoV-2 (5 nM) over a range of nanobody, antibody and ACE2 concentrations, and then the mixtures were added to yeast cells displaying monovalent KC3.ep3. The % bound receptor-binding domain is reported relative to the % bound in the absence of pre-blocking. The results are averages from three independent repeats and the error bars are standard deviations.

KC3.ep3 recognizes an epitope in the receptor-binding domain common to other potent neutralizers

The RBDs from the SARS-CoV-2 and SARS-CoV viruses share >70% sequence similarity (Tian et al., 2020). It has been observed that some antibodies, including VHH-72, CR3022 and S309, bind to the RBDs of both viruses (Pinto et al., 2020; Tian et al., 2020; Wrapp et al., 2020). Therefore, we evaluated the affinity of monovalent KC3.ep3 to the RBDs of SARS-CoV and SARS-CoV-2 to compare its specificity relative to VHH-72. Both KC3.ep3 and VHH-72 demonstrated strong binding to the SARS-CoV-2 RBD, but KC3.ep3 did not show detectable binding to the RBD of SARS-CoV, indicating that KC3.ep3 recognizes an epitope that is unique

in SARS-CoV-2 RBD, while VHH-72 strongly recognizes the SARS-CoV RBD (K_D of 1.6±0.6 nM), indicating that VHH-72 and KC3.ep3 recognize distinct RBD epitopes.

We further probed the epitope of KC3.ep3 by examining its competition for binding to the RBD of SARS-CoV-2 with the ACE2 receptor, previously reported nanobodies (Ty1 and VHH-72), and antibodies which recognize distinct epitopes on the SARS-CoV-2 RBD [CB6 with class 1 epitope (Shi et al., 2020), C119 with class 2 epitope (Barnes et al., 2020), S309 with class 3 epitope (Pinto et al., 2020), and CR3022 with class 4 RBD epitope (Yuan et al., 2020); Fig. 3-5]. Soluble biotinylated RBD (5 nM) was preincubated with soluble ACE2 receptor or bivalent antibodies (nanobody-Fc fusions or IgGs) at a range of antibody concentrations (0.05-500 nM), and then these receptor-antigen or antibody-antigen complexes were incubated with yeast-surface displayed monovalent KC3.ep3.

Notably, the binding of monovalent KC3.ep3 to RBD was inhibited by preincubation of ACE2 with RBD, suggesting that the KC3.ep3 and ACE2 binding sites on RBD overlap and explain the ability of KC3.ep3 to potently neutralize the virus (Fig. 3-5). Moreover, the binding of monovalent KC3.ep3 to RBD was strongly inhibited by preincubation of RBD with bivalent KC3.ep3, as expected. KC3.ep3 binding to RBD was also inhibited by bivalent Ty1, CB6 or C119, although not as strongly as for bivalent KC3.ep3. Thus, the epitope of KC3.ep3 appears to overlap with that of Ty1, CB6 (class 1 epitope) and C119 (class 2 epitope).

Conversely, monovalent KC3.ep3 binding was weakly impacted or even enhanced when the RBD was preincubated with bivalent VHH-72, S309 (class 3 epitope) and CR3022 (class 4 epitope; Fig. 4-5), revealing that the epitope of KC3.ep3 does not overlap with these antibodies. The fact that KC3.ep3 and VHH-72 do not compete for binding is in agreement with our finding that KC3.ep3 recognizes an epitope in SARS-CoV-2 RBD that is absent in SARS-CoV RBD while

VHH-72 recognizes an epitope that is present in both RBDs. Likewise, CR3022 has been previously demonstrated to cross-react with both viruses (Tian et al., 2020), and most residues in its class 4 epitope are conserved between both viruses (Yuan et al., 2020), indicating that its epitope would also be expected to be distinct from that of KC3.ep3. Likewise, S309 has been observed to cross-react with SARS-CoV, and the absence of competition between KC3.ep3 and S309 also agrees with our observation that KC3.ep3 competes with ACE2 and previous observations that S309 does not compete with ACE2 (Pinto et al., 2020).

Neutralizing nanobodies display drug-like biophysical properties

For use in therapeutic and diagnostic applications, nanobodies need to be easily produced and possess favorable biophysical and biomanufacturing properties, including high stability, high solubility, low levels of aggregation, low non-specific binding and high expression levels. Therefore, we first quantified the expression yields of nanobodies in this study via transient transfection of HEK293 cells. It has been previously shown that this expression system can be used to express nanobody Fc-fusion proteins at yields ranging from ~20-140 mg/L (Zhang et al., 2009). We observed similar high purification yields for the affinity-matured nanobodies obtained via directed evolution (~27-110 mg/L), which were also comparable to the purification yields for the nanobodies obtained via immunization (Ty1 and VHH-72; 52-85 mg/L). The purity (SDS-PAGE) and homogeneity (size-exclusion chromatography) of the affinity-matured nanobodies were also excellent (e.g., >95% monomer), and similar to the nanobodies generated via immunization.

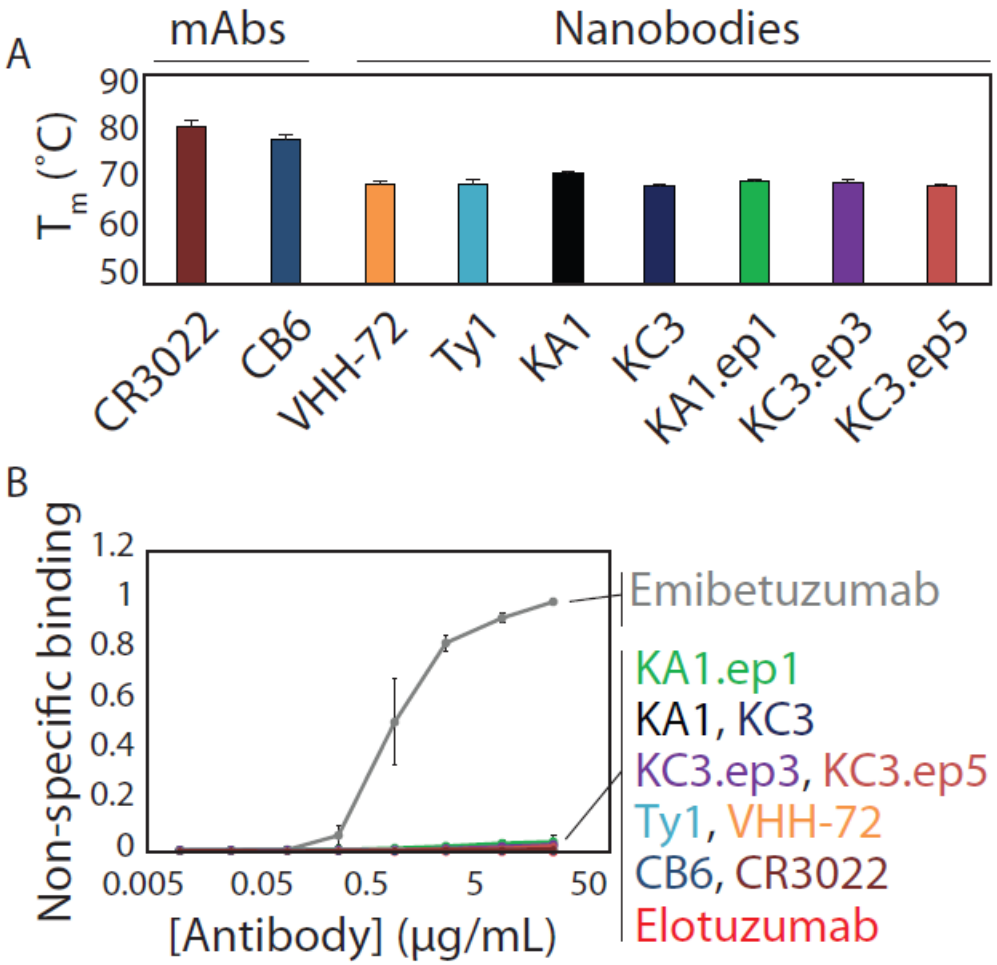

Figure 4-6: Affinity-matured nanobodies display high stability and specificity.
(A) Melting temperatures of bivalent nanobodies and antibodies evaluated via differential scanning fluorimetry. (B) Non-specific binding of bivalent nanobodies and antibodies (immobilized on magnetic beads) was evaluated via incubation with biotinylated soluble membrane proteins from CHO cells and detection of non-specific binding via flow cytometry. Control antibodies with high (emibetuzumab) and low (elotuzumab) non-specific binding were also evaluated for comparison. The two control antibodies are not identical to the actual drugs, as they have the variable regions of the actual drugs and a common IgG1 framework. In (A) and (B), the results are averages from three independent repeats and the error bars are standard deviations.

The stability of the affinity-matured nanobodies was also examined (Fig. 3-6A). It is a concern that mutations accumulated by nanobodies, and antibodies in general, during affinity maturation have an increased risk for reducing stability (Julian et al., 2017; Rabia et al., 2018; Shehata et al., 2019). This is even more concerning for CDR-swapped variants with CDRs of different lengths, as observed for the CDR3-swapped variant KA1.ep1, because these changes could impact the local

structure of the nanobody. Therefore, we analyzed the folding stability (melting temperature, T_m) of the lead nanobody clones and their affinity-matured variants relative to previously reported SARS-CoV-2 nanobodies and mAbs. The lead nanobodies displayed high stabilities, as both KA1 and KC3 displayed melting temperatures >68 °C (KA1 T_m of 71.3±0.4 °C and KC3 T_m of 68.3±1.0 °C). Notably, the affinity-matured variants displayed similar stabilities (KA1.ep1 T_m of 69.5±0.8 °C, KC3.ep3 T_m of 69.6±0.8 °C and KC3.ep5 T_m of 68.6±0.6 °C), suggesting that the affinity-enhancing CDR swaps maintained high stability. Moreover, the stabilities of the affinity-matured nanobodies were similar to those for nanobodies generated via immunization (Ty1 T_m of 69.3±1.0 °C and VHH-72 T_m of 69.1±0.6 °C). As expected, the stability of the mAbs (CB6 and CR3022) were higher (T_m values >77 °C) because of their stabilizing constant regions (C_H1 and C_L).

Finally, the specificity (non-specific binding) of the affinity-matured variants was examined by testing their ability to bind complex mixtures of soluble membrane proteins obtained from HEK293 cells (Fig. 4-6B) (Xu et al., 2013). It has been previously reported that approved antibody drugs typically display lower levels of non-specific binding, including to soluble membrane proteins, than antibodies that either failed in clinical development or are still in development (Jain et al., 2017). Further, low antibody specificity has also been shown to correlate with poor pharmacokinetic properties (Hötzel et al., 2012). Notably, the lead nanobodies and affinity-matured variants in this work displayed extremely low binding to soluble membrane proteins. The levels of binding observed were comparable to other SARS-CoV-2 nanobodies and antibodies generated *in vivo* and similar to a clinical-stage mAb with low levels of non-specific binding (elotuzumab), and much lower than a clinical-stage antibody with high levels of non-specific binding (emibetuzumab). These results collectively demonstrate that the potent neutralizing

nanobodies reported in this work have drug-like biophysical properties that are similar to SARS-CoV-2 nanobodies and antibodies generated by the natural immune system.

Systematic CDR-swapping mutagenesis for identifying high-affinity nanobodies without affinity maturation

Given that unintentional CDR swapping between low-affinity lead nanobodies led to unexpectedly large increases in affinity, we next asked whether the introduction of intentional CDR swapping during the initial library sorting process would enable identification of high-affinity nanobodies without the need for lead clone evaluation and affinity maturation. Therefore, we isolated the enriched library of nanobody plasmids prior to the terminal sort of our original sorting efforts (after five rounds of sorting against RBD and related reagents; Fig. 4-1), shuffled their three CDRs via standard PCR methods (see Methods for details), and sorted the CDR-swapped library for two additions times against RBD.

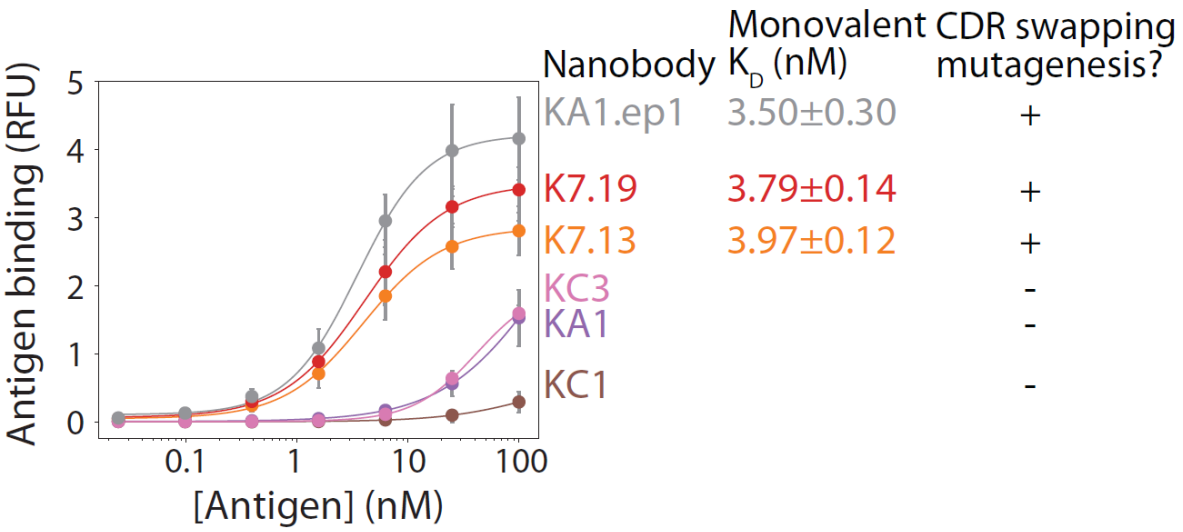

Figure 4-7: Nanobodies with nanomolar monovalent affinities can be generated via CDR-swapping mutagenesis without the need for lead clone identification and subsequent affinity maturation.
Nanobodies were selected from a nonimmune library with (KA1.ep1, K7.13, K7.19) or without (KC3, KA1, KC1) CDR-swapping mutagenesis, and the selected clones were evaluated in terms of their monovalent binding affinities for the SARS-CoV-2 receptor-binding domain. The results are averages from two independent experiments and the error bars are standard deviations.

Encouragingly, Sanger sequencing revealed that this simple mutagenesis method is able to identify multiple known or promising high-affinity nanobodies. These include a high-affinity nanobody that we discovered in our initial two-step library sorting and affinity maturation process (KA1.ep1) as well as nanobodies not observed previously (K7.13 and K7.19). The most common nanobody identified was KA1.ep1, which is logical because this high-affinity nanobody is a CDR-swapped version of KA1 and KC3 without any additional mutations. We also identified a nanobody (K7.19) that was a variant of KA1.ep1 with one mutation. Notably, we also identified a nanobody (K7.13) with a unique CDR3, which is particularly interesting because we originally identified a low-affinity lead clone (KC1) with the same CDR3 but with different CDR1 and CDR2 loops. Our initial observations of CDR swapping in KA1.ep1, KC3.ep3 and KC3.ep5 resulted from

a combination of CDRs from KA1 and KC3. Similarly, K7.13 contains CDR1 and CDR2 from KA1 and CDR3 from KC1.

Finally, we evaluated the monovalent affinities of the nanobodies generated by CDR-swapping mutagenesis (Fig. 4-7). Notably, the nanobodies identified from intentional CDR-swapping mutagenesis displayed single digit monovalent binding affinities (K_D of 3-4 nM) that were similar to KA1.ep1. These binding affinities were much stronger than the lead clones identified in our original sorting efforts (KA1, KC1 and KC3) despite that the CDRs of the high-affinity clones are identical to or closely related to the low-affinity lead clones. In summary, these results indicate that CDR swapping between common framework nanobodies has great potential to enable the facile isolation of high-affinity nanobodies, and this mutagenesis strategy can be easily incorporated during the initial sorting process to avoid the need for lead clone evaluation and subsequent affinity maturation.

Discussion

We have demonstrated that common framework, nonimmune nanobody libraries can be used in a surprisingly simple manner to generate high-affinity nanobodies without the need for lead clone identification or additional mutagenesis in the framework or CDRs. Some previous reports of antibodies against unrelated targets have optimized individual CDRs separately, and then combined the optimized CDRs to further increase affinity (Steidl et al., 2008; Yang et al., 1995). However, these studies are for antibodies that already have relatively high affinity and, thus, address a simpler challenge of affinity maturation and result in much lower synergistic improvements in affinity after CDR swapping than we observed in our studies. In contrast, our work addresses a more challenging problem of how to identify high-affinity clones without the need to first identify lead clones with modest affinity and select individual clones for affinity

maturation. We expect that this approach of combining multiple low affinity clones via CDR and/or framework swapping holds great potential for rapidly generating nanobodies and, more generally, antibodies with high affinity with much less effort than is typically required. Despite that this discovery was unintentional, we demonstrate that it is simple to perform CDR swapping using standard PCR methods, and it could be used as a facile method for identifying high-affinity clones, even without additional mutagenesis.

Compared to CDR swapping, we observed much smaller improvements in affinity from additional CDR and framework mutations (KC3.ep3 and KC3.ep5) due to error-prone PCR. Nevertheless, the average number of mutations incorporated by this error-prone PCR (1.2-1.5 mutations per nanobody) was low in comparison to the changes incorporated though CDR swapping. A higher error rate could have the potential to introduce a greater number of beneficial mutations in combination with or following CDR swapping.

The epitopes of our neutralizing nanobodies relative to previously reported neutralizing nanobodies and antibodies also deserve further consideration. The epitope is of particular interest in order to identify pairs of nanobodies or antibodies which bind to different sites and can therefore aid in the prevention of infection by SARS-CoV-2 escape mutants (Baum et al., 2020b; Greaney et al., 2020; Weisblum et al., 2020). Like KC3.ep3, the epitopes of several other potent neutralizing antibodies in the RBD have also been reported to overlap with the ACE2 binding site (Barnes et al., 2020). It is notable that KC3.ep3 competes with a class 1 antibody (CB6), indicating that CB6 binds the RBD only in the “up” conformation and competes with ACE2. CB6 has been shown to sterically hinder ACE2 binding to RBD, and the epitope recognized by CB6 overlaps with the region bound by ACE2 (Shi et al., 2020). Further, class 1 antibodies have been observed to have

short (<15 residue) HCDR3 loops (Barnes et al., 2020). KC3.ep3 similarly has a CDR3 which consists of only 11 residues.

The fact that KC3.ep3 also competes with a class 2 antibody (C119) indicates that C119 binds to the RBD in both the “up” and “down” conformations and also competes with ACE2. Consistent with its competition with class 1 and class 2 antibodies, the binding of KC3.ep3 was also reduced when the RBD was preincubated with ACE2 (Fig. 4-5). Thus, KC3.ep3 appears to recognize an epitope that overlaps with the ACE2 binding site and is common to potent neutralizing antibodies that also block ACE2 binding. KC3.ep3 competes similarly with a potent neutralizing nanobody, Ty1. Like class 2 antibodies, Ty1 has previously been demonstrated to reduce the ability of RBD to bind ACE2, and structural analysis indicates that Ty1 sterically hinders this binding when the RBD is in both the "up" and "down" conformations (Hanke et al., 2020). Moreover, preincubation of RBD with ACE2 did not reduce the ability of KC3.ep3 to bind RBD as strongly as preincubation with the class 1 and class 2 antibodies, indicating that the KC3.ep3 epitope does not completely overlap with the ACE2 binding site.

However, KC3.ep3 does not compete for binding with antibodies that cross-react with both SARS-CoV and SARS-CoV-2, namely VHH-72, CR3022 and S309. CR3022 has been reported to be a class 4 antibody, indicating that it binds the RBD in the “up” conformation but does not compete with ACE2 (Barnes et al., 2020). Structural analysis has further shown that CR3022 binds to the SARS-CoV-2 RBD but does not compete for binding with ACE2, and CR3022 weakly neutralizes the SARS-CoV-2 virus (Yuan et al., 2020). Interestingly, the epitopes for CR3022 and VHH-72 overlap, but due to different angles of binding, VHH-72 indirectly hinders RBD binding to ACE2 while CR3022 does not (Wrapp et al., 2020). As both VHH-72 and CR3022 cross-react with the SARS-CoV RBD while KC3.ep3 does not, it would be expected that KC3.ep3 does not

recognize an overlapping epitope. Therefore, the reported epitopes are consistent with the lack of competition observed between KC3.ep3 and both CR3022 and VHH-72.

The fact that KC3.ep3 also does not compete with a class 3 antibody (S309) also deserves further consideration. Class 3 antibodies can bind to the RBD in both the “up” and “down” conformations but do not compete with ACE2. Interestingly, the binding of KC3.ep3 was enhanced when RBD was incubated with S309 (Fig. 4-5). Given that KC3.ep3 competes with ACE2, its epitope would be expected to be distinct from that of a class 3 antibody, such as S309. Enhancement of neutralization activity has previously been reported for antibody cocktails composed of S309 and an antibody targeting as distinct epitope (Pinto et al., 2020). A pair of class 1 and class 3 antibodies (Barnes et al., 2020), REGEN10933 and REGN10967, have previously been examined for combination as a cocktail (Baum et al., 2020b, 2020a). This analysis of the epitope of KC3.ep3 indicates that it is likely to compete with binding the SARS-CoV-2 RBD with class 1 and class 2 antibodies, but the observed enhancement of KC3.ep3 binding in the presence of S309 suggests that the combination of KC3.ep3 with a class three antibody could be beneficial in terms of affinity and potentially neutralization activity as well.

The identification of neutralizing nanobodies and antibodies which target SARS-CoV-2 represents a rapidly evolving area of research. As such, consideration should also be given to the affinity and neutralization activities of the nanobodies that we report in context of previously reported nanobodies and antibodies in addition to the targeted epitope. In terms of nanobody affinity and neutralization activity, a broad range of these properties has been reported in the literature. Several recent studies have reported nanobodies that bind to the SARS-CoV-2 virus (Chi et al.; Hanke et al., 2020; Huo et al., 2020; Schoof et al., 2020; Wrapp et al., 2020; Xiang et al., 2020). Multiple studies have reported nanobodies isolated from naïve and synthetic libraries

using various *in vitro* panning and sorting strategies (Chi et al.; Custódio et al., 2020; Huo et al., 2020; Schoof et al., 2020). Similar to the strategy that we have reported here, some of these studies have incorporated affinity maturation in order to further improve the properties of the isolated lead candidates (Huo et al., 2020; Schoof et al., 2020). Direct comparison between various studies and comparison with the results reported here are complicated by the use of different experimental methodologies and nanobody constructs (e.g., monovalent vs bivalent). Nevertheless, the nanobodies that we report appear to compare favorably in terms of affinity and neutralization activity to those reported previously. Similar to several nanobodies previously isolated using *in vitro* methods (Chi et al.; Custódio et al., 2020; Huo et al., 2020), the nanobodies we report here demonstrate nanomolar monovalent affinities (Fig. 4-4A). Direct comparison to nanobodies and antibodies isolated in three previous studies also indicates that the nanobodies reported here have comparable or improved affinities (Fig. 4-4) and neutralization activities (Fig. 4-3) to multiple leading nanobodies isolated from immunization [VHH-72 (Wrapp et al., 2020) and Ty1 (Hanke et al., 2020)] and an antibody isolated from infected humans [CB6 (Shi et al., 2020)]. While recent studies also demonstrate that extensive, large-scale efforts can identify nanobodies with higher affinities and increased neutralization activities (Xiang et al., 2020), it would be simple to further affinity mature our nanobodies to achieve even higher affinities. More generally, our findings demonstrate the power of directed evolution methods to rapidly generate high-affinity nanobodies with epitopes that overlap with leading neutralizing nanobodies and antibodies, and which result in highly potent neutralization activities.

Using the simple method of CDR swapping, we were able to improve the affinity of our lead clones (K_D - 1-5 nM). This would further the make the process of affinity maturation more efficient and faster.

Experimental Procedures

Lead nanobody isolation and maturation

The original nanobody library (McMahon et al., 2018) was cloned into an Aga2-based yeast surface display plasmid (Julian et al., 2019). The nanobodies were expressed on the yeast surface as C-terminal fusion proteins to Aga2 (Aga2-nanobody). In the first round, MACS was performed against biotinylated RBD (bRBD) of SARS-CoV-2 (Acro, SPD-C82E9). 10^9 cells were incubated with 300 nM biotinylated RBD in PBS supplemented with 1 g/L BSA (PBSB) and 1% milk at room temperature for 3 h. Post incubation, the cells were washed once and incubated with streptavidin microbeads (Miltenyi, 130-048-141) with gentle rocking for 30 mins at 4 ^{o}C. Following incubation, the cells were washed once with ice-cold PBSB and passed through a MACS column under magnetic field to isolate cells bound to beads. The captured beads were washed once with ice-cold PBSB while employing the magnetic field. After washing, the beads were eluted into low pH SDCAA (20 g/L of dextrose, 6.7 g/L of yeast nitrogen base without amino acids, 5 g/L of casamino acids, 16.75 g/L of sodium citrate and 4 g/L of citric acid) liquid media and grown at 30 ^{o}C for 2 d. All subsequent sorting was performed by FACS. In rounds 2, 3 and 4, a selection was performed against RBD-Fc (Acro, SPD-C5255; 100 nM for rounds 2 and 3 and 50 nM for round 4 respectively). In round 5, a selection against bRBD was performed at 100 nM followed by selection against 100 nM bRBD, 100 nM bS1 (S1 domain of SARS-CoV-2; Acro, S1N-C82E8) or 50 nM S protein trimer (Acro, SPN-C52H8).

Three lead nanobodies (KA1, KC3 and KC1) from the initial discovery campaign were isolated with modest affinities. Two of these clones (KA1 and KC3) were affinity matured by first preparing error-prone PCR libraries as previously described (Chao et al., 2006). Briefly, the DNA region encoding only KA1 or KC3 was amplified using *Taq* DNA Polymerase with Standard *Taq*

Buffer (New England Biolabs, M0273L) in the presence of non-natural nucleotides, 8-Oxo-2'-deoxyguanosine-5'-Triphosphate (TriLink Biotechnologies, N-2034-1) and 2'-Deoxy-P-nucleoside-5'-Triphosphate (TriLink Biotechnologies, N-2037). Ten PCR cycles were used to amplify the DNA, and nanobody DNA was gel purified in a 1% agarose gel. To increase the number of mutations, DNA was amplified using Q5 High-Fidelity DNA Polymerase (New England Biolabs, M0491L), gel purified, and a second error-prone PCR with *Taq* DNA polymerase (New England Biolabs, M0320L) was performed under identical conditions. DNA encoding the region of plasmid surrounding KA1 or KC3 was added by overlap PCR. Total insert DNA was then amplified, and DNA was transformed into EBY100 as previously described (Benatuil et al., 2010). Four rounds of FACS selections were performed for each library, and the antigen concentration was progressively reduced, including 50 nM biotinylated S1 in round 1, 10 nM biotinylated S1 in round 2, 2 nM biotinylated S1 in round 3, and 100 pM biotinylated S1 in round 4.

CDR-swapping mutagenesis and clone evaluation

We also intentionally introduced CDR-swapping mutagenesis after sort 5 of the initial discovery campaign. DNA was isolated from yeast cells that were collected after the fifth sort of the initial synthetic library. DNA segments of the nanobody gene comprising CDR1 (framework 1 to framework 2), CDR2 (framework 2 to framework 3) and CDR3 (framework 3 to framework 4) were PCR amplified to facilitate overlap PCR. The DNA encoding each CDR was then mixed at an equal mass ratio, and overlap PCR was used to reassemble and amplify DNA encoding the entire nanobody. The CDR-swapped nanobody DNA library was inserted into the yeast display plasmid by homologous recombination. The transformation efficiency for this CDR-swapped nanobody library was ~5 x 10^7. Next, two rounds of sorting were performed by FACS using

biotinylated RBD (100 nM in sort 1 and 10 nM in sort 2). Yeast cells collected from the terminal sort were miniprepped and Sanger sequenced.

Nanobody-Fc expression and purification

Yeast cells from the terminal rounds of sorting were mini-prepped (Zymo Research, D2004) and plasmids were recovered. Nanobody genes were amplified by performing PCR on yeast mini-prepped DNA with forward and reverse primers containing NheI and HindIII restriction sites, respectively. The PCR products were purified via a 1% agarose gel and extracted with DNA purification kit (Qiagen, 28704). The nanobody genes were then digested with NheI-HF (New England Biolabs, R3131L) and HindIII-HF (New England Biolabs, R3104L), as instructed by the manufacturer's protocol, followed by purification (Qiagen, 28104). Nanobody-Fc expression plasmid was digested with NheI-HF and HindIII-HF, as instructed by the manufacturer's protocol, followed by treatment with calf intestinal alkaline phosphatase (New England Biolabs, M0525L). The digested vector was purified by 1% agarose gel electrophoresis and followed by DNA extraction. The digested vector and inserts were ligated with T4 ligase (New England Biolabs, M0202L) followed by transformation into competent DH5α cells. Transformed cells were plated on LB plates supplemented with ampicillin (100 ug/mL) overnight at 37 ^{o}C. Individual colonies were picked and grown in LB media (with ampicillin) overnight followed by mini-prepping (Qiagen, 27106). Plasmids from colonies were sequenced using Sanger sequencing.

HEK 293-6E cells (National Research Council of Canada) were grown, maintained and passaged at a density of 1.5-2 million cells per mL in F17 media (Thermo Fisher Scientific, A1383502) supplemented with Glutamine (Invitrogen, 25030081), Kolliphor (Thermo Fisher Scientific, NC0917244) and G418 (Thermo Fisher Scientific, 10131035). Nanobody-Fc plasmid (15 μg) was mixed with PEI (45 μg) at room temperature with F17 media (without supplements)

for 10-15 min and added to cells at a density of 1.5-1.8 million cells per mL. Cells were fed with 20% w/v yeastolate (BD Sciences, 292804) 24-48 h post transfection and were grown for an additional 2-4 d at 37 ^{o}C. Post expression, media was harvested by centrifuging cells at 4000 xg for 40 min. Media was collected, transferred to new tubes and 0.5-1 mL Protein A bead (Thermo Fisher Scientific, 20333) slurry was added followed by gently rocking at 4 ^{o}C overnight. Protein A beads were collected from media with filter columns (Thermo Fisher Scientific, 89898) under vacuum followed by washing with 50-100 mL of PBS. Protein was eluted from Protein A beads using 0.1 M glycine buffer (pH 3.0) followed by 1x buffer exchange into 20 mM acetate (pH 5.0) using Zeba desalting columns (Thermo Fisher Scientific, 89894). Proteins were then filtered using 0.2 µm filters, aliquoted and stored at -80 ^{o}C. Nanobody concentrations were evaluated by measuring absorbance at 280 nm and purity was evaluated by SDS-PAGE (Thermo Fisher Scientific, WG1203BOX).

Pseudovirus neutralization analysis

SARS-CoV-2 pseudovirus neutralization assay was adapted from a previous report (Crawford et al., 2020). To prepare SARS-CoV-2 pseudovirus particles, Lenti-X 293T cells (Takara, 632180) were seeded at $5x10^5$ per well in 6-well plates in RPMI media supplemented with 10% Fetal Bovine Serum (FBS), 1% penicillin/streptomycin (P/S) and cultured at 37 °C with 5% CO_2. Upon reaching a target confluency of 50-70%, cells were transfected with third generation lentivirus 5 plasmid system (0.22, 0.22, 0.22, 1, or 0.34 µg respectively): HDM-Hgpm2 plasmid (BEI catalog number NR-52517) encoding HIV Gag-Pol under CMV promoter, HDM-tat1b plasmid (BEI catalog number NR-52518) encoding HIV Tat under CMV promoter, pRC-CMV-Rev1b plasmid (BEI catalog number NR-52519) encoding HIV Rev, pHAGE-CMV-Luc2-IRES-ZsGreen-W (BEI catalog number NR-52516) lentiviral transfer plasmid encoding co-expression of luciferase

and ZsGreen, pCMV3 SARS-CoV2 S Untagged Delta 19AA C-term plasmid encoding the SARS-CoV-2 spike (S) protein with a 19-amino acid deletion at the C-terminus.

At 24 h post-transfection, cell media was changed to fresh RPMI with 10% FBS and 1% P/S. At 72 h post-transfection, cell supernatant was collected and passed through a 0.45 µm filter to remove cellular debris. SARS-CoV-2 pseudovirus was then concentrated via Lenti-X Concentrator (Takara, 631232) without ultracentrifugation. Briefly, Lenti-X Concentrator was added to cell culture supernatant at a volume ratio of 1:3 and incubated overnight at 4 °C. The mixture was then centrifuged at 1500 xg for 45 min. Supernatant was discarded, and the pseudovirus pellet was resuspended in Opti-MEM media in a volume of 50 µL Opti-MEM per well of virus harvest.

To determine virus titer, 293T-ACE2 cells (BEI resources catalog NR-52511) were seeded at 8,000 cells per well in a 96-well plate in DMEM with 10% FBS and 1% P/S and cultured at 37 °C with 5% CO_2. At 24 h post-seeding, cells were infected with varying dilutions of virus, diluted in DMEM media in the presence of 5 µg/mL polybrene, 10% FBS, and 1% P/S. At 48 h post-infection, the percentage of ZsGreen-expressing cells was determined via flow cytometry using a Bio-Rad ZE5 cell analyzer and further corroborated via fluorescence microscopy. Tissue culture infectious units (TCIU) per mL of virus was then calculated.

For neutralization assays, 293T-ACE2 cells were seeded at 8,000 cells per well in white bottom 96-well plates (Corning, 3917) in DMEM (10% FBS and 1% P/S) and cultured at 37 °C with 5% CO_2. At 24 h post-seeding, 293T-ACE2 cells were infected with 350 TCIU SARS-CoV-2 pseudovirus per well in the presence of antibody treatments. Briefly, 4-fold serial dilutions of antibody were prepared, mixed with SARS-CoV-2 pseudovirus, and incubated for 1 h at 37 °C. Following this incubation, 293T-ACE2 cells were treated with SARS-CoV-2 pseudovirus-antibody mixtures in the presence of 5 µg/mL polybrene. At 48 h post-infection, neutralization activity was determined via bioluminescence detection using a microplate reader. Briefly, 96-well

plates were equilibrated to room temperature for 15 min. Media volume in each well was then reduced to 80 µL via micropipette. Luciferase substrate (80 µL; Promega ONE-Glo, E6110) was added to each well, the plate was incubated at room temperature for 10 min, and bioluminescence was detected using Molecular Devices SpectraMax microplate reader with 500 millisecond integration/well.

Live virus neutralization analysis

For antibody neutralization assays, 96-well plates were seeded with VeroE6 (ATCC CRL1586) cells at 10,000 cells per well and incubated at 37 ˚C and 5% CO_2 for 24 h. Antibodies were diluted in DMEM with 2% FBS in 96-well plates at a 2x final concentration in a volume of 50 µL. Cell culture plates and antibody dilution plates were then transferred to a BSL3 facility. 50 µL of diluted SARS-CoV-2 (2000 pfu/mL or 100 pfu/well) was added to each well containing 50 µL of diluted antibodies. The antibody-virus mixtures were incubated at 37˚C for 1 h. Growth media was then aspirated from cell culture plates and replaced with 100 µL of the virus-antibody solution. Antibody dilutions were tested in eight replicate wells each. Plates were incubated at 37 ˚C and 5% CO_2 for 3 days, then examined microscopically for visible cytopathic effect (CPE). Wells with any degree of visible, virus-induced CPE were scored as positive. All antibody neutralization screening experiments were conducted following standard operating procedures of an approved Biosafety Level 3 Facility.

Nanobody affinity and specificity analysis

The monovalent affinities for the nanobodies were evaluated in yeast surface display format. The nanobodies were expressed on the yeast surface as C-terminus fusion proteins (Aga2-nanobody). For affinity measurements, 10^5 yeast cells per sample that express each nanobody were washed twice with PBSB and incubated with mouse anti-Myc antibody (1000x dilution) and

biotinylated RBD over a range of concentration in 1% milk at room temperature for 3 h. Post incubation, the cells were centrifuged at 2500 xg for 5 min followed by washing once with ice-cold PBSB. Next, the cells were then incubated with goat anti-mouse IgG AF488 (200x dilution; Invitrogen, A11001) and streptavidin AF647 (1000x dilution; Invitrogen, S32357) on ice for 4 min. Post-secondary antibodies incubation, cells were centrifuged and washed once with ice-cold PBSB, re-suspended in PBSB and evaluated on Bio-Rad ZE5 analyzer.

For specificity analysis, the binding was evaluated for antibodies KC3.ep3 and VHH-72 to receptor-binding domain (RBD) of SARS-CoV (Acro, SPD-S52H6) and SARS-CoV-2 virus. The antigen binding was performed in similar way as described above. Post antigen binding, the cells were washed once with ice-cold PBSB and incubated with mouse anti-Myc (1000x dilution) and chicken anti-His (1000x dilution; Invitrogen, PA1-9531) antibodies on ice for 20 min. Post primary incubation, the cells were washed with ice-cold PBSB and incubated with goat anti-mouse IgG AF488 (200x dilution) and donkey anti-chicken IgY $F(ab')_2$ fragment AF647 (500x dilution; Jackson ImmunoResearch, 703-606-155) antibodies on ice for 4 min. Post-secondary incubation, the cells were washed once with ice-cold PBSB and evaluated by flow cytometry.

For affinity measurements of soluble antibodies in the bivalent format, biotinylated RBD was first immobilized on streptavidin Dynabeads (Invitrogen, 11047). Antigen loading was 0.1 μg protein for 10^7 beads in a final volume of 400 μL. Beads were washed twice with PBSB and blocked with 10% milk in PBSB by end-over-end mixing at room temperature for 1 h. Post blocking, the beads were washed once with PBSB and incubated with varying concentrations of antibodies (10^5 beads per sample) in PBSB with 1% milk at room temperature for 3 h. After antibody incubation, the beads were centrifuged and washed once with ice-cold PBSB followed by incubation with goat anti-human IgG AF647 (Jackson ImmunoResearch, 109-605-098) on ice

for 4 min. Post labeling, the beads were washed once with ice-cold PBSB and evaluated by flow cytometry.

Nanobody competition analysis

To evaluate the epitope of KC3.ep3, competitive binding analysis was performed with other SARS-CoV-2 antibodies and nanobodies. Biotinylated RBD (5 nM) was first pre-incubated with soluble nanobodies/antibodies in the bivalent format or ACE2 (RayBiotech, 230-30165) over a range of concentrations (0.05, 0.5, 5, 50 and 500 nM) for 2 h at room temperature with mild agitation. Next, the antibody-antigen complexes were incubated with yeast cells expressing monovalent KC3.ep3, along with anti-Myc antibody (1000x dilution), in PBSB with 1% milk at room temperature for 3 h. Post incubation, cells were washed once with ice-cold PBSB and incubated with streptavidin AF647 (1000x dilution) and goat anti-mouse IgG AF488 (200x dilution) on ice for 4 min. Following secondary incubation, cells were washed once with ice-cold PBSB and analyzed by flow cytometry.

Nanobody biophysical characterization

Melting temperature analysis

The melting temperatures of the proteins in this work were determined using differential scanning fluorimetry. Proteins were prepared at 0.12 mg/mL and mixed with Protein Thermal Shift Dye (Applied Biosystems, 4461146) at a volume ratio of 7:1 protein:dye to reach a final concentration of 1x dye. The protein-dye mixture was added to individual wells of a clear 384-well plate. Background signals were determined from 2-3 wells of 1x PBS mixed with dye. Samples were submitted to the University of Michigan Advanced Genomics core for analysis. Samples were centrifuged in the 384-well plate at 1000-2000 rpm for 1 min. The plates were then inserted into an ABI Prism 7900HT Sequence Detection System (Applied Biosystems), and

thermal cycle conditions were set to examine increasing temperatures between 25-98 °C over a period of 45 min. Background signals were subtracted from samples, and melting temperatures were determined from the temperatures at which the maximum signals (first derivative equals zero) were observed.

Analytical size-exclusion chromatography

The purity of the proteins after the Protein A purification was evaluated using size-exclusion chromatography with a Shimadzu Prominence HPLC System outfitted with a LC-20AT pump, SIL-20AC autosampler and FRC-10A fraction collector. Proteins in 20 mM acetate (pH 5) were buffer exchanged into PBS (pH 7.4). For analytical SEC, 100 µL of protein sample (diluted to 0.1 mg/mL) was loaded onto the column (Superdex 200 Increase 10/300 GL column; GE, 28990944) and analyzed at 0.75 mL/min using a PBS running buffer supplemented with 200 mM arginine (pH 7.4). Absorbance was monitored at 220 and 280 nm, and the 280 nm signal was primarily used for analysis. The percentage of protein monomer was evaluated by analyzing the area under the peak between 8 and 22 min (exclusion volume to solvent elution times). Proteins with less than 90% monomer were further purified via size-exclusion chromatography. Protein fractions were collected, buffer exchanged into PBS (pH 7.4), filtered, aliquoted and stored at -80 °C.

Polyspecificity analysis

The polyspecificity reagent (PSR) was prepared as previously (Xu et al., 2013). CHO cells (10^9, Gibco, A29133) were pelleted, the cell pellets were washed separately with PBSB and Buffer B (50 mM HEPES, 0.15 M NaCl, 2 mM $CaCl_2$, 5 mM KCl, 5 mM $MgCl_2$, 10% Glycerol, pH 7.2), and then pelleted again. The pellets were resuspended in 5 mL of Buffer B supplemented with a protease inhibitor (Sigma Aldrich, 4693159001). Next, the resuspended cells were homogenized

for 90 s (three cycles of 30 s) followed by sonication for 90 s (three cycles of 30 s). The cell suspension was then spun down at 40,000 xg for 1 h and the supernatant was discarded.

The pellet, comprising the enriched membrane fraction, was resuspended in Buffer B with a Dounce homogenizer for 30 strokes. The protein concentration was determined using a detergent compatible protein assay kit (BioRad, 5000116). The enriched membrane fraction was diluted to a theoretical concentration of 1 mg/mL in solubilization buffer (pH 7.2), the latter of which contained 50 mM HEPES, 0.15 M NaCl, 2 mM $CaCl_2$, 5 mM KCl, 5 mM $MgCl_2$, 1% n-dodecyl-b-D-maltopyranoside (Sigma Aldrich, D4641), and a protease inhibitor (Sigma Aldrich, 11873580001). The solution was then mixed overnight (end-over-end) at 4 ^{o}C. The soluble membrane protein fraction was centrifuged at 40,000 xg for 1 h and the supernatant was collected. The final concentration of supernatant was ~0.8-0.9 mg/mL.

Sulfo-NHS-LC-biotin (Thermo Fisher Scientific, PI21335) was dissolved in distilled water at ~11.5 mg/mL. Stock solution of Sulfo-NHS-LC-biotin (150 mL) and the PSR reagent (4.5 mL at 0.8-0.9 mg/mL) were mixed via end-over-end mixing at room temperature (45 min). The reaction was quenched (10 mL of 1.5 M hydroxylamine at pH 7.2), and biotinylated PSR was aliquoted and stored at -80 ^{o}C.

Protein A magnetic beads (Invitrogen, 88846) were washed three times with PBSB and incubated with antibodies at a range of concentrations in 96-well plates (VWR, 650261) overnight at 4 ^{o}C. The antibodies were purified either via one-step (Protein A) or two-step (Protein A followed by size-exclusion chromatography) purification methods. Protein immobilization concentrations ranged from 0.03x to 10x of saturation of reported bead binding capacity for IgGs. Protein concentrations were normalized by molarity to maintain the same Fc concentration and bead saturation. Next, the protein-coated beads were washed by centrifuging the 96-well plates at

2500 xg for 4 min and washed twice with PBSB. Afterward, the beads were resuspended with a 10x diluted solution of biotinylated PSR and incubated on ice for 20 min. Beads were washed once with PBSB and incubated with 1000x diluted solution of streptavidin AF-647 (Invitrogen, S32357) and 1000x diluted solution of goat anti-human Fc $F(ab')_2$ AF-488 (Invitrogen, H10120) on ice (4 min). Beads were washed once, resuspended in PBSB, and analyzed via flow cytometry. The antibody binding steps were performed in PBSB, and three independent repeats were performed. The control antibodies used were the variable regions of elotuzumab (specific control) and emibetuzumab (polyspecific control) grafted onto a common IgG1 framework, which results in differences in the antibodies we have evaluated and the actual clinical-stage drugs. The control antibodies were two-step purified (Protein A and SEC) and were used to normalize results from all replicates between 0 and 1.

QUANTIFICATION AND STATISTICAL ANALYSIS

The number replicates performed for each experiment can be found in the figure caption. The average and standard deviation of the IC_{50}, K_D, and EC_{50} values are given in the figures. Curve fitting was performed in Python. The average and standard deviation of melting temperatures are given in the Results.

Acknowledgements

We thank Andrew Kruse for providing the nanobody library used in this work. We also thank Michel Nussenzweig, Pamela Bjorkman, Christopher Barnes, and Anna Gazumyan for providing class 2 and 3 SARS-CoV-2 antibodies. Moreover, we thank Adam Lauring for providing reagents and advice related to the pseudovirus neutralization assay. We acknowledge BEI Resources (NIAID, NIH) for providing SARS-Related Coronavirus 2, Wuhan-Hu-1 Spike-Pseudotyped

Lentiviral Kit (NR-5294) and SARS-Related Coronavirus 2, Isolate USA-WA1/2020 (NR-52281; originally deposited by the Centers for Disease Control and Prevention).

Note

This chapter is adapted from manuscript titled ‘Directed evolution of potent neutralizing nanobodies against SARS-CoV-2 using CDR-swapping mutagenesis’ which is currently in press.

References

Alsoussi, W.B., Turner, J.S., Case, J.B., Zhao, H., Schmitz, A.J., Zhou, J.Q., Rita, E., Lei, T., Rizk, A.A., Mcintire, K.M., et al. (2020). A Potently Neutralizing Antibody Protects Mice against SARS-CoV-2 Infection. J. Immunol. *205*, 915–922.

Barnes, C.O., Jette, C.A., Abernathy, M.E., Dam, K.M.A., Esswein, S.R., Gristick, H.B., Malyutin, A.G., Sharaf, N.G., Huey-Tubman, K.E., Lee, Y.E., et al. (2020). SARS-CoV-2 neutralizing antibody structures inform therapeutic strategies. Nature. *588*, 682–687.

Baum, A., Ajithdoss, D., Copin, R., Zhou, A., Lanza, K., Negron, N., Ni, M., Wei, Y., Mohammadi, K., Musser, B., et al. (2020a). REGN-COV2 antibodies prevent and treat SARS-CoV-2 infection in rhesus macaques and hamsters. Science. *370*, 1110–1115.

Baum, A., Fulton, B.O., Wloga, E., Copin, R., Pascal, K.E., Russo, V., Giordano, S., Lanza, K., Negron, N., Ni, M., et al. (2020b). Antibody cocktail to SARS-CoV-2 spike protein prevents rapid mutational escape seen with individual antibodies. Science. *369*, 1014–1018.

Benatuil, L., Perez, J.M., Belk, J., and Hsieh, C.-M. (2010). An improved yeast transformation method for the generation of very large human antibody libraries. Protein Eng. Des. Sel. *23*, 155–159.

Boder, E.T., Midelfort, K.S., and Wittrup, K.D. (2000). Directed evolution of antibody fragments with monovalent femtomolar antigen-binding affinity. Proc. Natl. Acad. Sci. U. S. A. *97*, 10701–10705.

Bradbury, A.R.M., Sidhu, S., Dübel, S., and McCafferty, J. (2011). Beyond natural antibodies: The power of in vitro display technologies. Nat. Biotechnol. *29*, 245–254.

Chao, G., Lau, W.L., Hackel, B.J., Sazinsky, S.L., Lippow, S.M., and Wittrup, K.D. (2006). Isolating and engineering human antibodies using yeast surface display. Nat. Protoc. *1*, 755–768.

Chen, P., Nirula, A., Heller, B., Gottlieb, R.L., Boscia, J., Morris, J., Huhn, G., Cardona, J., Mocherla, B., Stosor, V., et al. (2020). SARS-CoV-2 Neutralizing Antibody LY-CoV555 in Outpatients with Covid-19. N. Engl. J. Med.

Chi, X., Liu, X., Wang, C., Zhang, X., Li, X., Hou, J., Ren, L., Jin, Q., Wang, J., and Yang, W. Humanized single domain antibodies neutralize SARS-CoV-2 by targeting the spike receptor binding domain. Nat. Commun. 2–8.

Crawford, K.H.D., Eguia, R., Dingens, A.S., Loes, A.N., Malone, K.D., Wolf, C.R., Chu, H.Y., Tortorici, M.A., Veesler, D., Murphy, M., et al. (2020). Protocol and reagents for pseudotyping lentiviral particles with SARS-CoV-2 spike protein for neutralization assays. Viruses *12*, 13–15.

Custódio, T.F., Das, H., Sheward, D.J., Hanke, L., Pazicky, S., Pieprzyk, J., Sorgenfrei, M., Schroer, M.A., Gruzinov, A.Y., Jeffries, C.M., et al. (2020). Selection, biophysical and structural analysis of synthetic nanobodies that effectively neutralize SARS-CoV-2. Nat. Commun. *11*, 5588.

Foote, J., and Eisen, H.N. (2000). Breaking the affinity ceiling for antibodies and T cell receptors. Proc. Natl. Acad. Sci. U. S. A. *97*, 10679–10681.

Greaney, A.J., Starr, T.N., Gilchuk, P., Zost, S.J., Binshtein, E., Loes, A.N., Hilton, S.K., Huddleston, J., Eguia, R., Crawford, K.H.D., et al. (2020). Complete Mapping of Mutations to the SARS-CoV-2 Spike Receptor-Binding Domain that Escape Antibody Recognition. Cell Host Microbe *29*, 1–14.

Hanke, L., Vidakovics Perez, L., Sheward, D.J., Das, H., Schulte, T., Moliner-Morro, A., Corcoran, M., Achour, A., Karlsson Hedestam, G.B., Hällberg, B.M., et al. (2020). An alpaca nanobody neutralizes SARS-CoV-2 by blocking receptor interaction. Nat. Commun. *11*, 1–9.

Hansen, J., Baum, A., Pascal, K.E., Russo, V., Giordano, S., Wloga, E., Fulton, B.O., Yan, Y., Koon, K., Patel, K., et al. (2020). Studies in humanized mice and convalescent humans yield a SARS-CoV-2 antibody cocktail. Science. *369*, 1010–1014.

Hötzel, I., Theil, F.P., Bernstein, L.J., Prabhu, S., Deng, R., Quintana, L., Lutman, J., Sibia, R., Chan, P., Bumbaca, D., et al. (2012). A strategy for risk mitigation of antibodies with fast clearance. mAbs *4*, 753–760.

Huo, J., Bas, A. Le, Ruza, R.R., Duyvesteyn, H.M.E., Mikolajek, H., Malinauskas, T., Tan, T.K., Rijal, P., Dumoux, M., Ward, P.N., et al. (2020). Neutralizing nanobodies bind SARS-CoV-2 spike RBD and block interaction with ACE2. Nat. Struct. Mol. Biol. *27*, 846–854.

Jackson, J.R., Sathe, G., Rosenberg, M., and Sweet, R. (1995). In vitro antibody maturation. Improvement of a high affinity, neutralizing antibody against IL-1 beta. J. Immunol. *154*, 3310–3319.

Jain, T., Sun, T., Durand, S., Hall, A., Houston, N.R., Nett, J.H., Sharkey, B., Bobrowicz, B., Caffry, I., Yu, Y., et al. (2017). Biophysical properties of the clinical-stage antibody landscape. Proc. Natl. Acad. Sci. U. S. A. *114*, 944–949.

Julian, M.C., Li, L., Garde, S., Wilen, R., and Tessier, P.M. (2017). Efficient affinity maturation of antibody variable domains requires co-selection of compensatory mutations to maintain thermodynamic stability. Sci. Rep. *7*, 1–13.

Julian, M.C., Rabia, L.A., Desai, A.A., Arsiwala, A., Gerson, J.E., Paulson, H.L., Kane, R.S., and Tessier, P.M. (2019). Nature-inspired design and evolution of anti-amyloid antibodies. J. Biol. Chem. *294*, 8438–8451.

McMahon, C., Baier, A.S., Pascolutti, R., Wegrecki, M., Zheng, S., Ong, J.X., Erlandson, S.C., Hilger, D., Rasmussen, S.G.F., Ring, A.M., et al. (2018). Yeast surface display platform for rapid discovery of conformationally selective nanobodies. Nat. Struct. Mol. Biol. *25*, 289–296.

Pinto, D., Park, Y.J., Beltramello, M., Walls, A.C., Tortorici, M.A., Bianchi, S., Jaconi, S., Culap, K., Zatta, F., De Marco, A., et al. (2020). Cross-neutralization of SARS-CoV-2 by a human monoclonal SARS-CoV antibody. Nature. *583*, 290–295.

Rabia, L.A., Desai, A.A., Jhajj, H.S., and Tessier, P.M. (2018). Understanding and overcoming trade-offs between antibody affinity, specificity, stability and solubility. Biochem. Eng. J. *137*, 365–374.

Schoof, M., Faust, B., Saunders, R.A., Sangwan, S., Rezelj, V., Hoppe, N., Boone, M., Billesbølle, C.B., Puchades, C., Azumaya, C.M., et al. (2020). An ultrapotent synthetic nanobody neutralizes SARS-CoV-2 by stabilizing inactive Spike. Science. *3255*, 1473–1479.

Shehata, L., Maurer, D.P., Wec, A.Z., Lilov, A., Champney, E., Sun, T., Archambault, K., Burnina, I., Lynaugh, H., Zhi, X., et al. (2019). Affinity Maturation Enhances Antibody Specificity but Compromises Conformational Stability. Cell Rep. *28*, 3300-3308.e4.

Shi, R., Shan, C., Duan, X., Chen, Z., Liu, P., Song, J., Song, T., Bi, X., Han, C., Wu, L., et al. (2020). A human neutralizing antibody targets the receptor-binding site of SARS-CoV-2. Nature. *584*, 120–124.

Steidl, S., Ratsch, O., Brocks, B., Dürr, M., and Thomassen-Wolf, E. (2008). In vitro affinity maturation of human GM-CSF antibodies by targeted CDR-diversification. Mol. Immunol. *46*, 135–144.

Tian, X., Li, C., Huang, A., Xia, S., Lu, S., Shi, Z., Lu, L., Jiang, S., Yang, Z., Wu, Y., et al. (2020). Potent binding of 2019 novel coronavirus spike protein by a SARS coronavirus-specific human monoclonal antibody. Emerg. Microbes Infect. *9*, 382–385.

Tiller, K.E., and Tessier, P.M. (2015). Advances in Antibody Design. Annu. Rev. Biomed. Eng. *17*, 191–216.

Weisblum, Y., Schmidt, F., Zhang, F., DaSilva, J., Poston, D., Lorenzi, J.C.C., Muecksch, F., Rutkowska, M., Hoffmann, H.H., Michailidis, E., et al. (2020). Escape from neutralizing antibodies by SARS-CoV-2 spike protein variants. eLife *9*, e61312.

Wrapp, D., De Vlieger, D., Corbett, K.S., Torres, G.M., Wang, N., Van Breedam, W., Roose, K., van Schie, L., Hoffmann, M., Pöhlmann, S., et al. (2020). Structural Basis for Potent Neutralization of Betacoronaviruses by Single-Domain Camelid Antibodies. Cell. *181*, 1004-1015.e15.

Wu, Y., Wang, F., Shen, C., Peng, W., Li, D., Zhao, C., Li, Z., Li, S., Bi, Y., Yang, Y., et al. (2020). A noncompeting pair of human neutralizing antibodies block COVID-19 virus binding to its receptor ACE2. Science. *368*, 1274–1278.

Xiang, Y., Nambulli, S., Xiao, Z., Liu, H., Sang, Z., Duprex, W.P., Schneidman-Duhovny, D., Zhang, C., and Shi, Y. (2020). Versatile and multivalent nanobodies efficiently neutralize SARS-CoV-2. Science. *370*, 1479–1484.

Xu, Y., Roach, W., Sun, T., Jain, T., Prinz, B., Yu, T.-Y., Torrey, J., Thomas, J., Bobrowicz, P., Vasquez, M., et al. (2013). Addressing polyspecificity of antibodies selected from an in vitro yeast presentation system: a FACS-based, high-throughput selection and analytical tool. Protein Eng. Des. Sel. *26*, 663–670.

Yang, W.P., Green, K., Pinz-Sweeney, S., Briones, A.T., Burton, D.R., and Barbas, C.F. (1995). CDR walking mutagenesis for the affinity maturation of a potent human anti-HIV-1 antibody into the picomolar range. J. Mol. Biol. *254*, 392–403.

Yuan, M., Wu, N.C., Zhu, X., Lee, C.C.D., So, R.T.Y., Lv, H., Mok, C.K.P., and Wilson, I.A. (2020). A highly conserved cryptic epitope in the receptor binding domains of SARS-CoV-2 and SARS-CoV. Science. *368*, 630–633.

Zhang, J., Liu, X., Bell, A., To, R., Baral, T.N., Azizi, A., Li, J., Cass, B., and Durocher, Y. (2009). Transient expression and purification of chimeric heavy chain antibodies. Protein Expr. Purif. *65*, 77–82.

Chapter 5 **Conclusion**

Antibodies are currently used for a variety of applications including diagnostic and therapeutic tools as well as reagents for several diseases and proteins. This has developed a lot of interest in designing, discovering and engineering antibodies for a wide range of applications. An antibody discovery campaign has three parts: discovery platform or methodology, antibody library design and antigen design and preparation. We think for a successful discovery campaign, it is imperative to have as much control as possible over all three parts.

Traditionally, antibodies were isolated by immunization and to date it still remains as one of the most preferred techniques. Although immunization has a high success rate, it has multiple limitations like lack of control over antigen presentation and specificity for complex antigens, inability to perform counter-selections, targeting proteins with post translational-modifications and the need for humanizing antibodies for therapeutic and diagnostic applications.

In vitro selection methods like phage, yeast, mammalian antibody display can used to overcome some of the limitations of immunizations. These techniques have been used successfully to isolate and further engineer several types of proteins including peptides, antibodies, antibody-like fragments and enzymes. We have focused solely on *in vitro* selection technique of yeast surface display for our antibody isolation and engineering. Yeast is easily to work with compared to phase and mammalian systems. Further, yeast being eukaryotic, they have sophisticated machinery to make and display high quality proteins compared to phage. Also, co-selection of different properties simultaneously makes yeast surface display very attractive.

Yeast surface display mainly uses two methods for antibody selection: MACS (magnetic-activated cell sorting) and FACS (florescence-activated cell sorting). Both the sorting methods have their advantages and drawbacks. FACS allows visualization and co-selection of two or more properties simultaneously whereas this is not possible for MACS. It is challenging to process large number of cells ($>10^8$) and perform selections against insoluble antigens like amyloid aggregates by FACS. Although MACS can be used for such an application, the overall efficiency of the selection process is low because of lack of control of selection process. Also, MACS offers highly avid surface for selection which might make selections for intrinsic affinity tricky. This problem is further aggravated since amyloid fibrils are multivalent in nature. Many of the above challenges motivated us to design a novel nanoparticle-based selection technique where amyloid aggregates can be used with flow cytometry and/or FACS. Such a selection technique is reported here for the first time (at least to our understanding) and used successfully. But we do suspect this selection technique can be further improved by optimization.

Antibody library design is very crucial for a successful discovery campaign. Although, a library can be designed in several different ways, some methods might be more attractive than others in terms of library designs and constructions. We have successfully used multiple different design strategies like directed mutagenesis using natural diversity and NNK codons, error-prone PCR, naïve non-immune libraries, CDR swapping mutagenesis and so on. Many times, we have used combinations of different strategies to engineer high performance antibodies.

One of our goals was to design robust methods to isolate conformational antibodies against amyloid aggregates. Although conformational antibodies have been isolated successfully by immunization, we preferred yeast surface display for several reasons discussed above. Using our novel library designs and selection methods, we were successfully able to isolate and engineered

conformational antibodies whose properties rival or are better than several clinical stage antibodies and approved drug for disorders like Alzheimer's and Parkinson's disease. Our conformational Aβ antibodies have affinity (EC_{50} – 2-12 nM) and conformational specificity similar to drug Aducanumab but substantially lower non-specific binding. Our conformational tau antibodies have affinity (EC_{50} – 0.5-1 nM) and conformational specificity similar to clinical antibody Zagotanemab. Our conformational α-synuclein antibody have similar affinity (EC_{50} - 10-20 nM) but superior conformational specificity compared to clinical antibody Cinpanemab. Our antibodies work well against aggregates formed *in vitro* and *in vivo* from transgenic mice and human brains. We think this is remarkable since the antibodies were generated strictly using *in vitro* aggregates but show similar activity against pathological *in vivo* formed aggregates. Further, our antibodies can be used in variety of formats like ELISA, immunodot and western blots and immunofluorescence assays. Also, all our antibodies and antibody fragments are very stable and can be easily expressed in mammalian cells with high quality and quantity. All the data we generated and presented is either with *in vitro* assays or using biological samples in *in vitro* assays. It would be highly interesting and informative to see how our conformational antibodies work in *in vivo* studies. It would be attractive to test our antibodies in mouse models for Alzheimer's or Parkinson's disease to see if they can help reduce the plaque loads in brains and help with delay or reversal of symptoms. This is particularly interesting since the conformational antibodies were made with therapeutic applications in mind. Also, since our antibodies have a range of properties which are different from clinical antibodies and approved drugs, it would be informative to see how their affect *in vivo* properties.

We also successfully isolated and engineered antibody fragments against SARS-CoV-2 using yeast surface display. All our engineered nanobodies show high affinity, high specificity and

neutralization activity in pseudovirus assay. Further, our best nanobody can neutralize live SARS-CoV-2 potently. Although the discovery of our affinity matured clones which showed CDR swapping was unintentional, we intentionally performed CDR swapping mutagenesis, isolated more antibodies and evaluated them. We demonstrated that antibodies where CDRs were swapped showed large increase in affinity and neutralization potency compared to lead parent antibodies. This result is particularly exciting since we can generate high quality lead antibodies without affinity maturation. To further test the robustness of this approach, we exploited this idea of CDR loop swapping for our tau conformational antibodies where we combined beneficial mutations from three binding loops and generated antibodies with high affinity and conformational specificity. It would also be very interesting to evaluate if our antibodies can bind and neutralize the different strains of SARS-CoV-2 including the U.K, Brazilian and South African strains. The mutation of SARS-CoV-2 has rendered many monoclonal antibodies useless and also decreased the efficiency of the vaccination. This is mainly because of the mutations in RBD and other regions of the spike protein which knocked-out the binding. It would be very attractive to make broadly neutralizing class of antibodies which would bind to conserved regions in SARS-CoV-2 so the neutralizing activity is retained against different strains. Also, this would help guide the design of next generation of vaccines and help us get ready for future pandemics.

Lastly, therapies are direly needed for several disorders like Alzheimer's and Parkinson's disease. We do hope that the above work on isolating and engineering conformational antibodies could lay the foundations for more robust selection methods which would further accelerate the discovery and engineering of conformational antibodies against several different protein aggregates.